

**POLITECNICO DI MILANO**

**Facoltà di Ingegneria dei Processi Industriali**

**Corso di Laurea Specialistica in Ingegneria dei Materiali**



**Bendability of DUAL PHASE (DP)  
STEELS and V Bend Test  
Parameter Optimization**

Relatore: Prof. Massimiliano BESTETTI

Correlatore: Ing. Edip Ozer ARMAN

Tesi di Laurea Specialistica di:

A. Uygur TUNA

Matr. 748811

Anno Accademico 2011 / 2012

## **Acknowledgements**

First of all, I would like to thank and express my deepest gratitude to Toyota Motor Europe for welcoming me into the Toyota family, making me feel as a part of it and giving me the opportunity to work on this research project. It has been a great professional and life experience that will surely have tremendous contributions to my future career and you were always there for me when I needed you to be.

I also would like to thank my university and especially my promoter Professor Massimiliano Bestetti for supporting me by any means throughout my stay in Toyota.

I wish to express my love and gratitude to my beloved family; for their understanding & endless love, through the duration of my studies and my life journey in general.

My team members in Toyota; Mr. Bekir Gündüz, Mr. Kazuhiro Tanahashi and Mr. Edip Özer Arman and all my colleagues who became also my dear friends deserve special thanks for both their continuous professional support and their pleasant company.

Last but not least, I would like to express my sincerest gratitude to my mentor, Mr. Edip Özer Arman, for not only enlightening me with his professional knowledge and guidance at all times but also for his friendship which, when I look back to 9 beautiful months spent in Belgium, has been the greatest earning of all.

## Abstract

Technical centre of Toyota Motor Europe is responsible, among many others, for approval procedures regarding the materials which are subject to take part in the production processes along Europe. TME R&D deals with the concepts and investigations that are brought to attention in this study.

Nowadays, with ever increasing necessity to come up with innovative body design of an average vehicle up to 80% of which is made of dual phase steel, preserving the desired characteristic material properties has great importance by means of obtaining and maintaining a high quality product under complex geometrical shapes that are foreseen and applied by a wide range of decision making organs such as designers and associated lower, middle and upper management.

It is undoubtedly a challenging procedure to ensure the well-being of future use of the vehicle, in terms of resistance to customer and environmental based problems that are to be faced throughout the standard life cycle.

In this sense, the crucial need for such materials to undergo testing and approval processes which would have to be compatible with the industrial bending applications in order to accomplish a stable and reliable primary control mechanism is a must and it is favoured and supported by any means.

As to be mentioned in more detail later on, this study concerns developing and optimizing existing test parameters, for the so called V bend test, which are explained together with other relevant aspects throughout this investigation and results obtained will be supported by current technical awareness, as well as educated suggestions to ensure ultimate design is presented together with maximum quality.

**Keywords:** Dual Phase Steel, Bendability, V Bend, X-ray Diffraction, Residual Stress, Electrochemical Corrosion

## List of Symbols

E	Applied potential (Electrochemical corrosion)	V
M	Atomic weight	g/mol
a	Bending radius	mm
n	Charge number which indicates the number of electrons excited in a dissolution reaction	-
$i_{\text{corr}}$	Corrosion current	$i / \text{A cm}^{-2}$
$\rho$	Density	$\text{g/m}^3$
F	Faraday constant	Coulomb
d	Interplanar spacing (X.R.D.)	$\mu$
b	Length of longitudinal direction of test piece	mm
i	Measured current density	$i / \text{A cm}^{-2}$
$R_M$	Metal dissolution rate	mol/s
$\sigma_x$	Normal stress acting in the x direction	Pa
$E_{\text{corr}}$	Open circuit potential of corroding metal	V
$\eta$	Overpotential	V
$\nu$	Poisson's ratio	-
$\tau_{zx}$	Shear stress on the plane perpendicular to the z-axis in the direction of the x-axis	MPa
$\epsilon$	Strain	%
$\beta_a, \beta_b, \beta_c$	Tafel constant	-
x	Thickness of effective layer (X-ray penetration)	$\mu$
c	V shaped block opening interval	mm
E	Young's modulus (X.R.D.)	-
d	Width of upper die (V bend)	mm
$\lambda$	Wavelength of incident radiation	nm

# Table of Contents

## Acknowledgements

## Abstract

## List of Symbols

<b>Chapter 1</b>	<b>General Introduction.....</b>	<b>1</b>
<b>Chapter 2</b>	<b>State of Art.....</b>	<b>6</b>
2.1	Dual Phase Steels.....	6
2.1.1	Basic Information.....	6
2.1.2	Characteristics.....	8
2.2	V Bend Test.....	9
2.3	X-ray Diffraction Residual Stress Techniques.....	12
2.3.1	Introduction.....	12
2.3.2	Normal Stress.....	12
2.3.3	Shear Stress.....	13
2.3.4	Principal Stress.....	14
2.3.5	Principles.....	14
2.3.6	Bragg's Law.....	14
2.3.7	Strain Measurement.....	16
2.3.8	Stress Determination.....	18
2.3.9	Depth Penetration.....	21
2.4	Electrochemical Corrosion.....	23
2.4.1	Basic Concepts.....	23
2.4.2	Electrochemical Basis of Corrosion.....	23
2.4.3	Calculation of Corrosion Rates.....	24
2.4.4	Calculation of Corrosion Current.....	24
2.5	Electrochemical Corrosion Techniques.....	26
2.5.1	A new microcell for material surface investigations at large current densities .....	26
<b>Chapter 3</b>	<b>Experiments.....</b>	<b>31</b>
3.1	Surface Crack Investigation.....	31
3.1.1	V Bend Test.....	31

3.1.2	Sample Preparation and Criteria Judgement.....	32
3.1.3	Sample Dimensions 100 mm X 35 mm .....	36
3.1.4	Sample Dimensions 100 mm X 35 mm; Burr Upside Down .....	43
3.1.5	Sample Dimensions 100 mm X 35 mm; Grinded .....	44
3.1.6	Sample Dimensions 100 mm X 100 mm.....	46
3.1.7	Dimension Variations.....	46
3.1.8	Load vs. Extension Curves.....	49
3.2	Hardness Measurements.....	50
3.3	XRD Residual Stress Measurements.....	54
3.4	Electrochemical Corrosion Measurements.....	58
<b>Chapter 4</b>	<b>Results.....</b>	<b>59</b>
<b>Chapter 5</b>	<b>Conclusion.....</b>	<b>63</b>
<b>Chapter 6</b>	<b>Future Suggestions.....</b>	<b>64</b>
<b>References</b>		

# Chapter 1 General Introduction

The end of the twentieth century and the beginning of the twenty first have been characterized by an increasing environmental awareness and concern about sustainable energy supplies. Indeed, the rapidly diminishing world oil reserves have led to spikes in oil prices and alleged scarcity in the market (REUTERS, 2011). Developing countries such as China and India with annual economic growth rates of up to ten percent<sup>1</sup> demonstrate an increasing appetite for energy. Millions of people are adopting the western way of life, entailing the need for all kinds of new commodities. One of the most important aspects regarding this attitude is the climbing desire for personal transportation. Apart from the energy craving, this issue brings along a second problem, which is the emission of green house gases and other pollutants, to which the continuously growing number of cars populating our planet's roads are a big contributor (DILLIEN, 2010).

Governments and global corporations are becoming sensitive to such problems and significant efforts are shown in order to find a sustainable solution to transportation needs of mankind. Remarkable progress is seen in the fields of aerodynamics, fuel efficiency of combustion engines and even in the field of alternative energy sources for road vehicle powering (DILLIEN, 2010). However, no matter how efficient the conversion of stored energy into propulsion is, a certain amount of energy will always be required to accelerate a vehicle, to keep it in motion and to stop it again. Figure 1.1 shows energy requirements for combined city/highway driving. An important factor which determines the required amount of energy is the weight of the vehicle. Keeping this as low as possible will thus undoubtedly be a crucial factor when efficient energy use is in question.

Mild steels are the most commonly used steels in the automotive industry when present conjecture is taken into consideration (TSIPOURIDIS, 2006). Such steels are low carbon steels associated by a yield strength level of 140 MPa, a relatively low tensile strength and outstanding deep draw ability. Despite some advantages such steels possess by means of forming and cost, their ultimate strength level remains at unsatisfactorily low levels meaning that the crash performance of the vehicle is mainly dependent on the sheet thickness. By establishing a consistent control mechanism on the alloy chemistry and taking the presence of interstitial carbon

---

<sup>1</sup> NKUNDE M., "Determinants and Development Financing Flows from Brazil, Russia, India, and China to Low-Income Countries", International Monetary Fund, November 01 2011

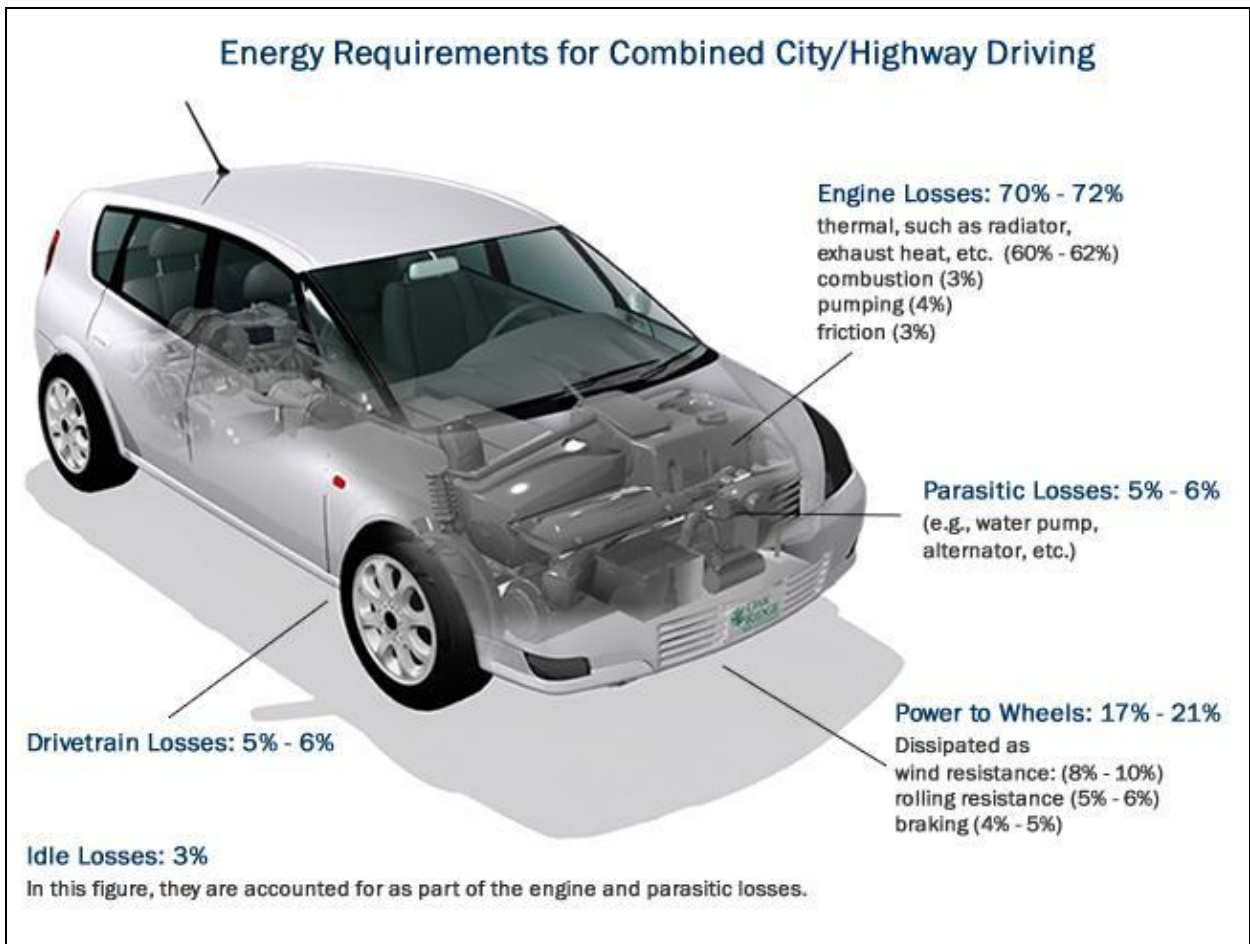


**Figure 1.1 Energy requirements for combined city/highway driving<sup>2</sup>**

in ferrite into consideration, interstitial free grades (IF) of ultra low carbon alloy were able to be produced. Conventional strengthening mechanisms such as solid solution hardening, precipitation hardening and grain refinement by carbides and/or nitrides were applied to increase the strength of such metals, while maintaining their excellent formability behaviours at the same time. Micro alloying with vanadium, niobium or titanium accompanied by fine carbide precipitation and grain refinement leads to an even higher strength level and increases the ratio of yield strength to tensile strength (YS/TS). Bake hardening steels (BH) offer a combination of good stamping formability and ensure increased yield strength after the paint baking process. In order to be able to take advantage of such an effect, some specific solute carbon content and an appropriate aging heat treatment are to be applied, which would result in a supersaturating carbon within ferrite.

<sup>2</sup> BANDIVADEKAR A., BODEK K., CHEAH L., EVANS C., GROODE T., HEYWOOD J., KASSERIS H., KROMER M., WEISS M., "On the Road in 2035: Reducing Transportation's Petroleum Consumption and GHG Emissions", MIT Laboratory for Energy and the Environment Report No. LFEE 2008-05 RP, Cambridge, Massachusetts, July 2008



Due to their sharp upper yield point, BH steels exhibit a high dent resistance, which would make them promising candidates for applications regarding outer body panels. As for the formability phenomenon, it is an inevitable consequence to encounter reduced formability for the steels mentioned above, especially when relatively high strength levels have to be chosen (AISI, 2011).

Searching for opportunities to overcome such complications and reduce the weight of existing designs, various new and relatively new materials have been developed and brought to attention. Together with alternative materials such as aluminium and fibre reinforced polymers, some new steel grades with promising properties were developed (AISI, 2011). Among these are dual phase (DP) steels and transformation induced plasticity (TRIP) steels. Figure 1.2 shows the mechanical properties of conventional and AHSS (Advanced High Strength Steels) thin sheet steels with respect to ductility and ultimate tensile strength.

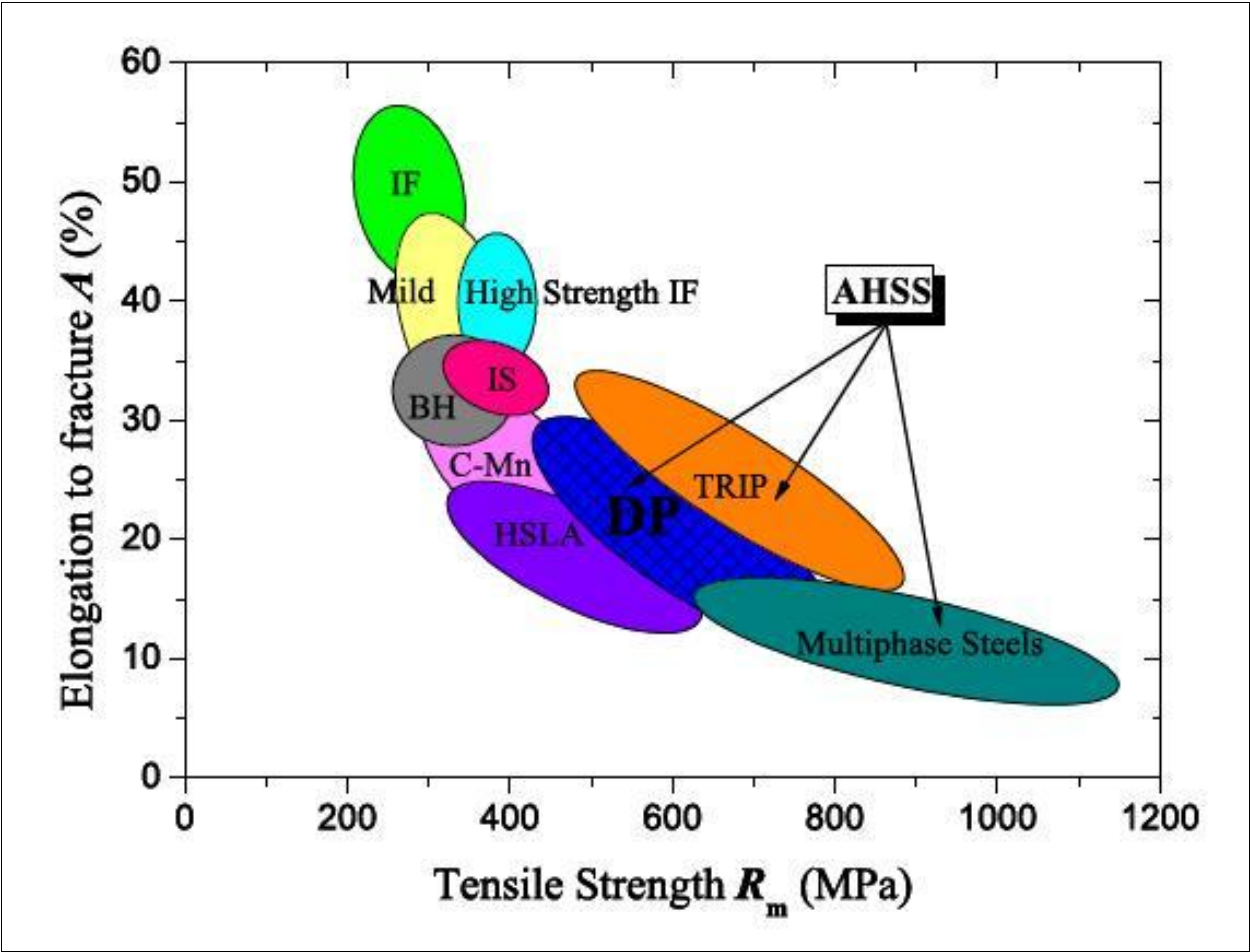


Figure 1.2 Strength formability relationships of thin sheet steels (TSIPOURIDIS, 2006)

According to the results of the ULSAB-AVC Program (Ultra Light Steel Auto Body-Advanced Vehicle Concepts, 2005), an automotive body may as well be constructed by utilizing approximately 85% of AHSS, achieving a weight reduction of around 25% with respect to a bench-marked “average base model”. Throughout the process manufacturing costs are kept constant and outcomes are much more satisfying.

Demonstrating a more through insight in our main concern in this study, it may finally be revealed that the major components of an auto body are designed using dual phase steels as clearly seen in Figure 1.3. Different criteria such as formability, weldability, spring back behaviour and of course static and dynamic properties have a significant effect on the material selection process, even though for some body parts, more than one steel grade fulfil the standards and therefore are also applicable.

For dual phase steels, which have been known for about forty years now, car manufacturing has become the single most important application domain. In particular, for a number of components that both DP and TRIP steels are applicable, DP grades are preferable due to their cost-effectiveness advantages. It would be beneficial, at this point, to further focus on some of the aspects contributing to this particular interest.

The excellent mechanical properties of dual phase steels were first discovered in the nineteen seventies. At that time, processing was primarily done in batch<sup>3</sup>, where one or more coils of low carbon steel were given a discrete heat treatment to give the steel its typical microstructure, consisting of a ferritic matrix with hard martensitic islands distributed in it. This composite structure provides the steel with its high strength and work hardening capacity and causes continuous yielding. The batch processing implies a slow cooling rate, however, and thus the steels had to be relatively high alloyed in order to obtain a sufficient hardening ability. This in turn leads to a relatively high cost of the steel and prevented widespread industrial adoption. Dual phase steels were an area of interest until the beginning of the nineteen eighties (KOT and BRAMFITT, 1981). Looking at the volume of publications, it may be concluded that they were put back on the shelf and remained there for about two decades.

---

<sup>3</sup> BATCH-ANNEALED DUAL-PHASE STEEL, United States Patent Number: 4437902, Filing Date: Oct 19, 1981, Issue Date: Mar 20, 1984

The fact that studies on such type of steels and attempts to integrate them to new designs and products have accelerated starting from the beginning of this century has created the need for a broader insight.

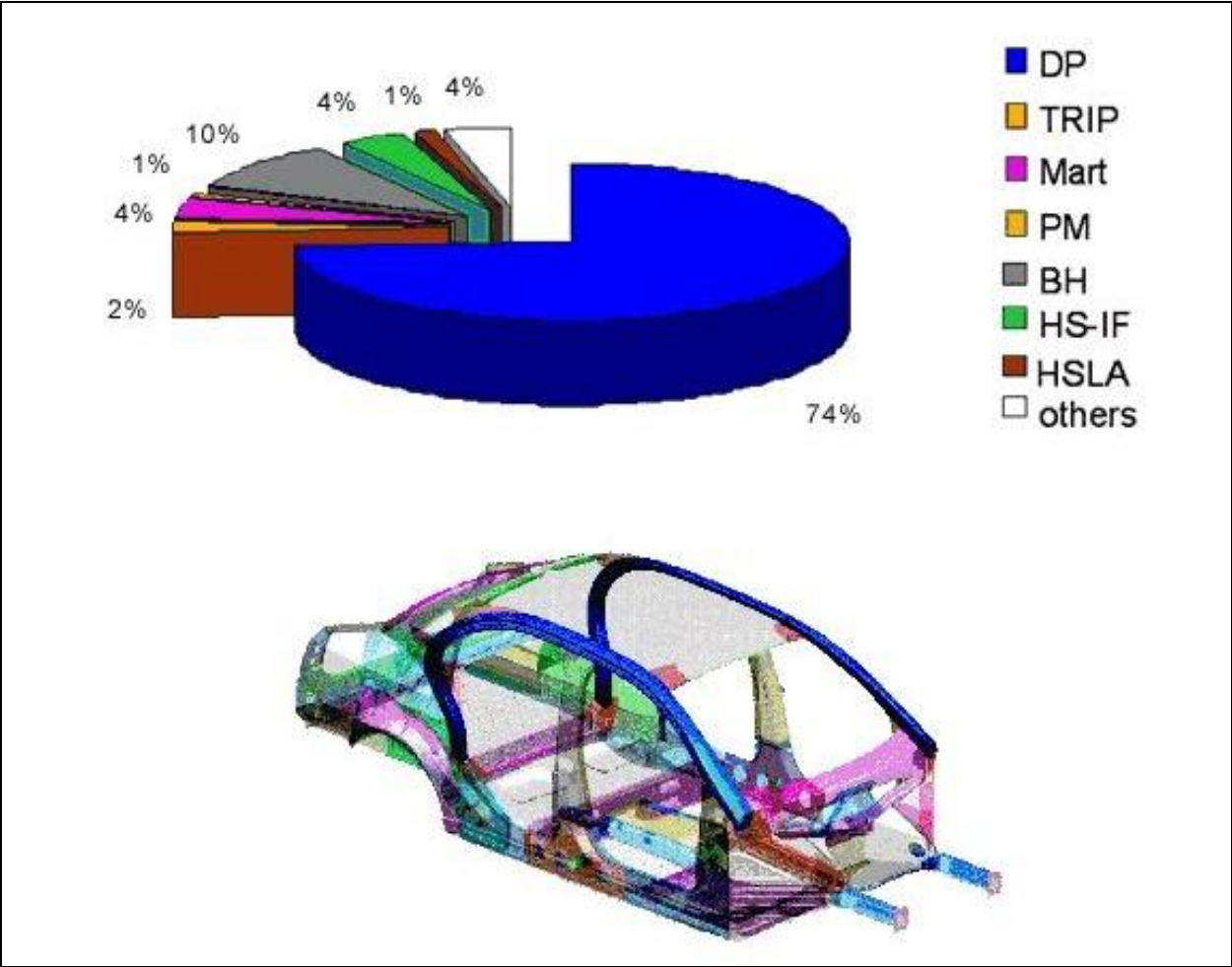


**Figure 1.3 ULSAB auto body structure steel grade distributions (ULSAB, 2005)**

## Chapter 2 State of Art

### 2.1 Dual Phase Steels and V Bend Test

#### 2.1.1 Basic Information

Steel production, in general, can be broken down into 6 stages which are represented in Figure 2.1. The main difference between low-carbon steels should be found in its composition and the heat treatment cycle, which will give it its particular microstructure as in Figure 2.2. For more information on steel processing you are kindly asked to consult relevant sources such as [steeluniversity.org](http://steeluniversity.org).

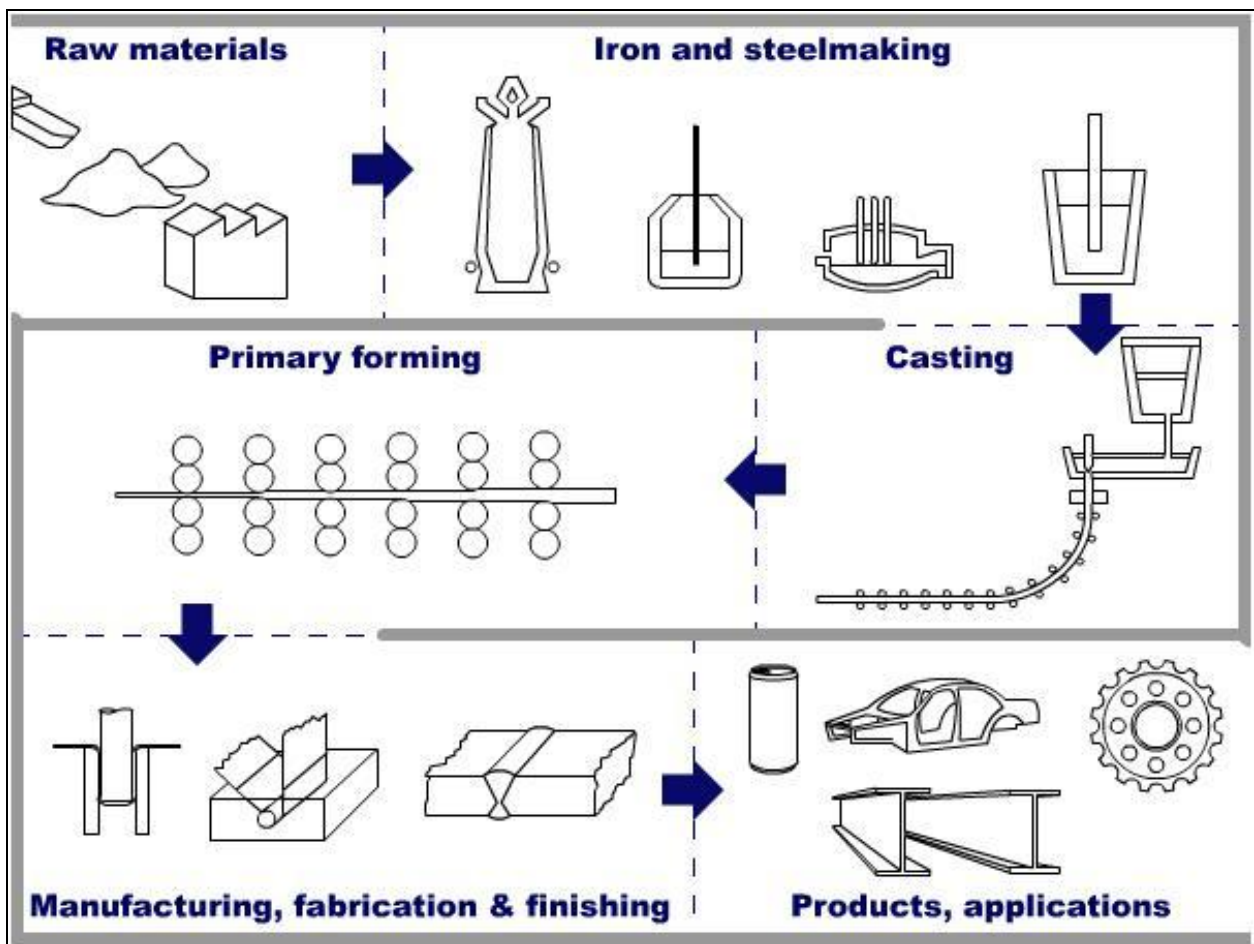
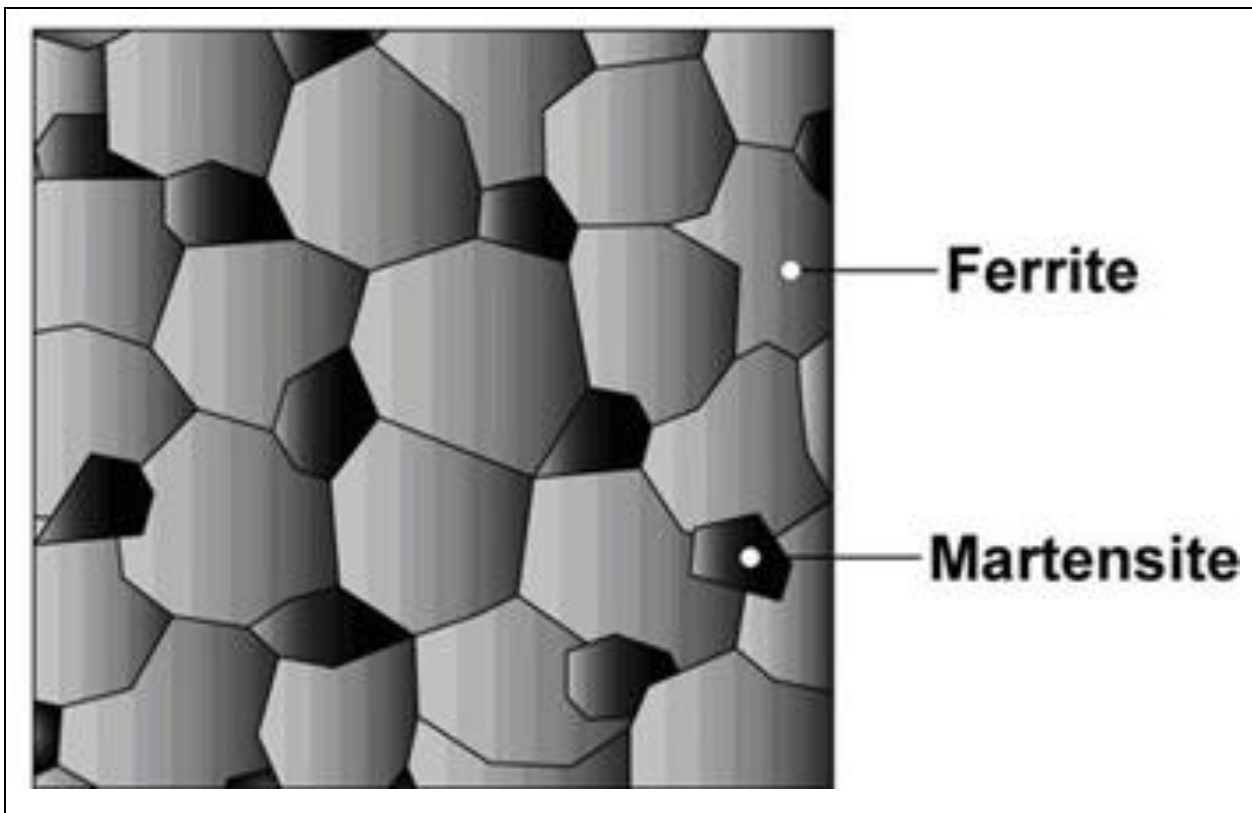


Figure 2.1 6 stages of steel production (WorldAutoSteel, 2011)



**Figure 2.2 A schematic microstructure of DP steel containing ferrite among islands of martensite (WorldAutoSteel, 2011)**

In the above figure it is shown that the soft ferrite is generally continuous, giving these steels excellent ductility. When these steels deform, strain is concentrated in the lower-strength ferrite phase surrounding the islands of martensite, creating the unique high work hardening rate exhibited by these steels.

Dual Phase steels are produced by controlled cooling from the austenite phase (in hot rolled products) or from two phase ferrite plus austenite phase (for continuously annealed cold-rolled and hot-dip coated products) to transform some austenite to ferrite before a rapid cooling transforms the remaining austenite to martensite (WorldAutoSteel, 2011).

Since millennium, dual phase steels have been rediscovered, now widely used in car manufacturing (United States Steel Corporation, 2011). The batch process is no longer variant, instead, the continuously annealed, lower alloyed type of dual phase that has attracted the attentions of design engineers, particularly, is in use (RASHID, 1981). A very low content of silicon makes sure that no severe problems with galvanization are faced and their excellent

combination of strength, ductility and price make them a very promising candidate for weight reduction. The urge to pay closer attention to the matter has increased in the last 10 years resulting with the fact that every major metallurgy institute has at least a small research project involving dual phase steels and their behaviours (DILLIEN, 2010).

### **2.1.2 Characteristics**

Dual phase steels possess some unique material properties which makes these kinds of steels to be considered superior than its competitors.

Some of the important characteristics of dual phase steels are as follows (U. S. Steel, 2011):

- Work hardening - Dual phase steels display a high and rapid initial work hardening rate. Even at low forming strain levels (2% - 3%), yield strength increases approximately 145-214 MPa.
- Yield Point Elongation - Dual phase steels show no yield point elongation.
- Formability - Due to higher work hardening rate and absence of YPE, dual phase steels behave predictably in stamping processes (i.e. resistance to necking, plastic instability, and kinking).
- FLD curves - For the needs of forming feasibility analysis, FLD can be approximated with sufficient accuracy by the conventional ASM-FLD calculated from n-value and thickness.
- Bake hardening - Dual phase steels have relatively excellent bake hardening capacity. The increase in the yield strength resulting from a typical paint baking cycle is approximately 35-70 MPa.
- In-part strength - Dual phase steels have relatively high ultimate tensile strength (UTS). UTS ranges from 500 – 1200 MPa for available grades.
- Shelf life - Dual phase steels display no room temperature aging.
- Mass reduction capability - Such steels have high potential for part downgaging and weight reduction (up to 25% with respect to equivalent conventional HSLA steels).
- Crash Energy management - Dual phase steels have a higher yield tensile ratio as compared to conventional HSLA steels (0.5 - 0.6). This results in a higher capacity to manage vehicle crash energy.
- Fatigue performance - Dual phase steels have higher fatigue strength than equivalent conventional HSLA steels.

## 2.2 V Bend Test

In this study, Dual Phase 980 Steel, which is produced by one of world's leading steel companies, has the particular attention. Ultra-High-Strength steel materials of the new Dual Phase 980 have already been introduced in EU production.

Bending of a metal is a process by which the metal is plastically deformed. Bent material is stressed beyond its tensile stress but not its ultimate tensile strength. There occur some changes in the surface area, depending on the extent of bending.

One of the most important tests regarding the above mentioned issues and especially bendability is so called V Bend Testing. V bend tests are carried out to ensure that a metal has sufficient ductility to stand bending without fracturing. A standard specimen is bent through a specified arc as schematized below in Figure 2.1.

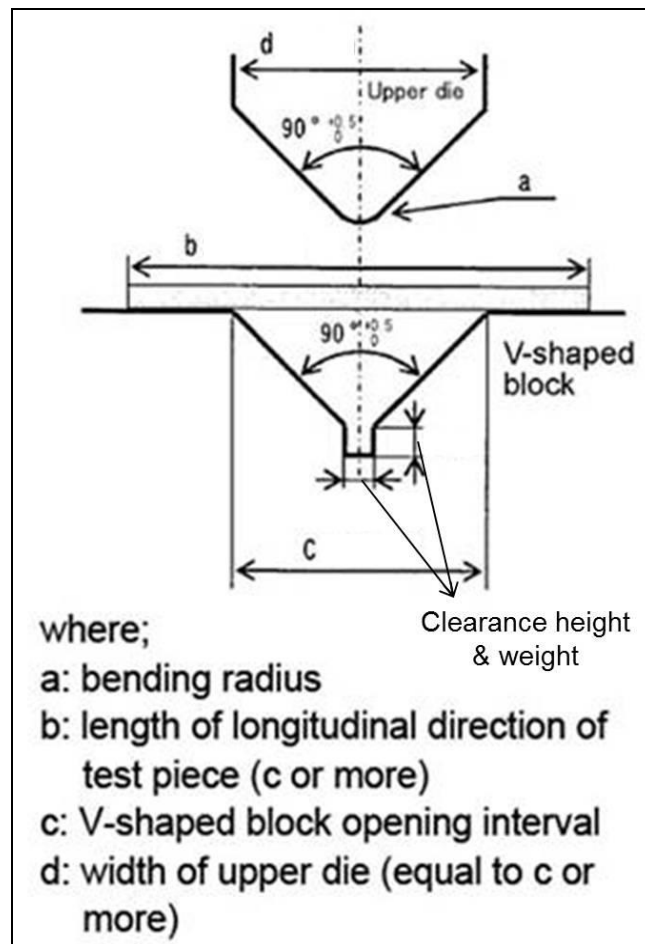
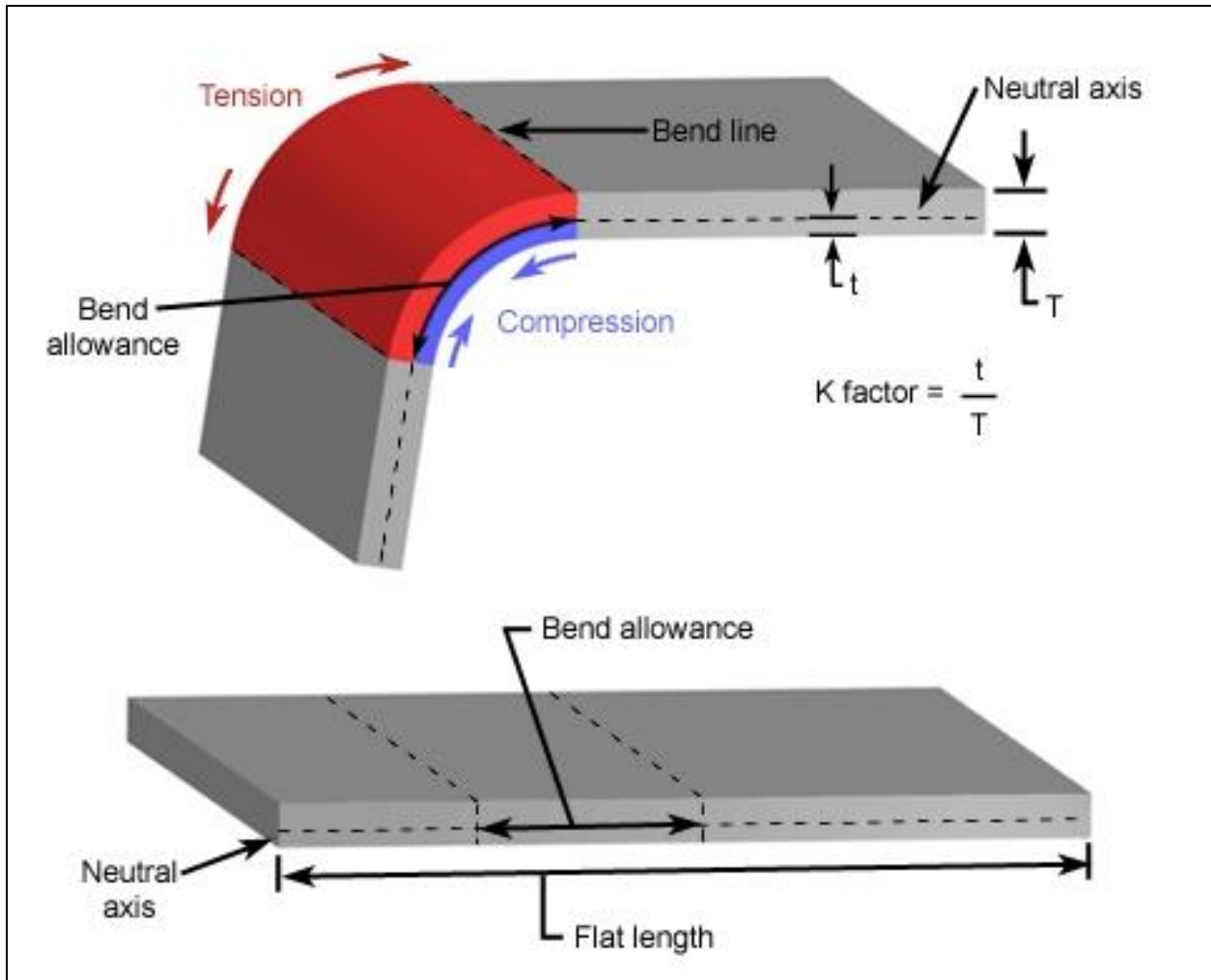


Figure 2.1 V Bend Testing experimental apparatus

Different complex shapes can be achieved as a result of metal bending. When a sheet metal, such as the subject of our investigation, is bent the inside surface is compressed whereas the outer one is stretched. In between there lies a so called neutral axis, which neither compressed nor stretched. The phenomenon occurring is represented in Figure 2.2.



**Figure 2.2 Stresses occurring on a bent metal surface (CustomPartNet, 2009)**

When a piece of sheet metal is bent, the residual stresses within the material will cause the sheet to springback. Due to this elastic recovery and it is essential to overbend the material so that desired design is ensured. The springback factor  $K_s$  is defined as the ratio of the final bend angle to the initial bend angle. Figure 2.3 schematizes this phenomenon.

It is extremely crucial to understand the changes occurring by means of microstructural variations and residual stresses introduced to the material. When different testing parameters are taken into



consideration, investigating the residual stress phenomenon would reveal important information regarding the behaviours such as crack resistance of dual phase steels.

Next section concerns and brings an insight on to the subject up to the theory extent. For through information on V bend testing related concepts, further literature survey is suggested.

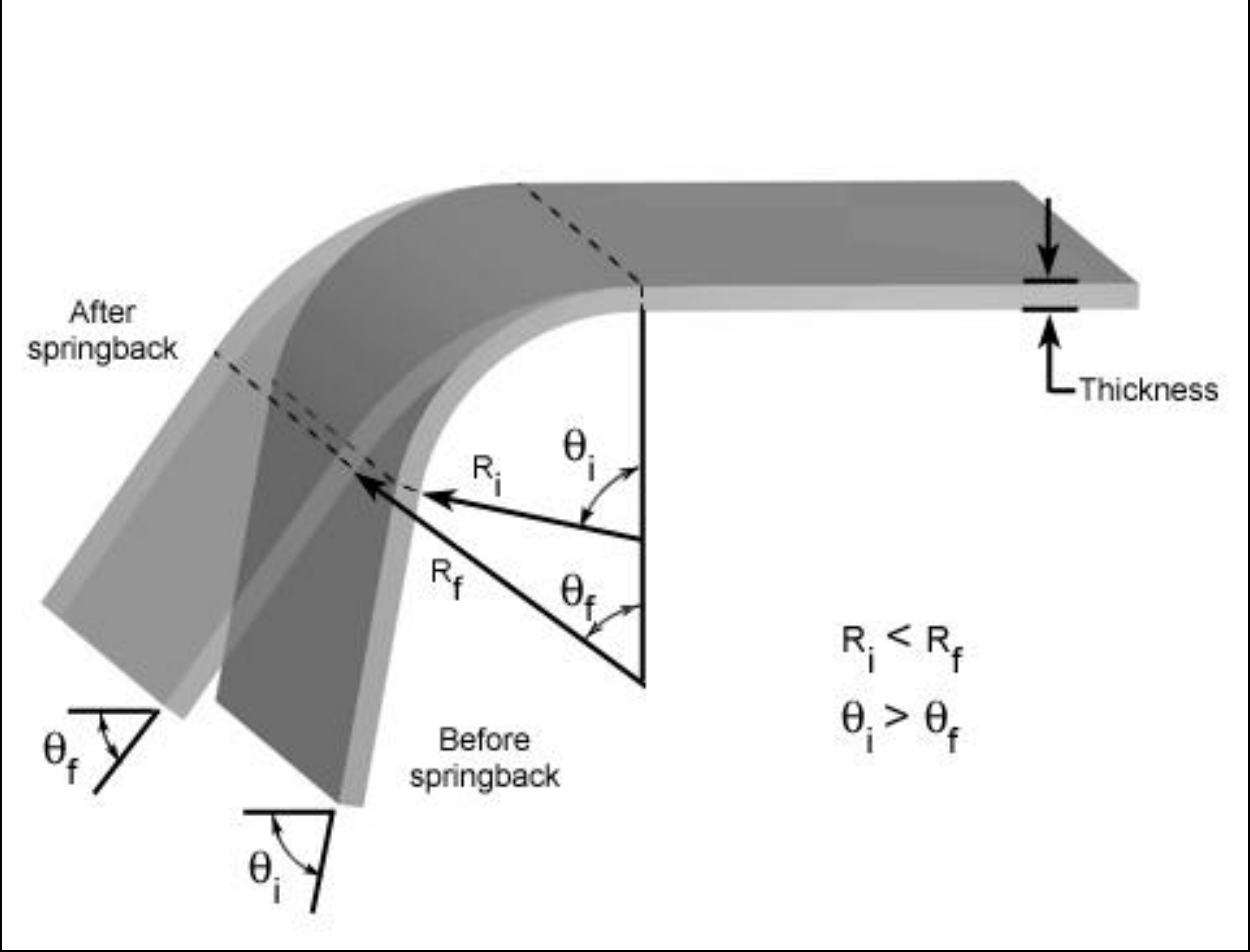


Figure 2.3 Springback phenomenon (CustomPartNet, 2009)

## 2.3 X-ray Diffraction Residual Stress Techniques

### 2.3.1 Introduction

In x-ray measurement, the strain in the crystal lattice is subject to measurement and the associated residual stress is determined from the elastic constants under the assumption that a linear elastic distortion of the appropriate crystal lattice plane is present. Since X-rays cover a relevantly high portion of the sample, measurements will include many grains and crystals. The exact number is controversial and directly depends on the grain size and beam geometry. Despite the fact that the measurement occurs on the surface, X-rays, due to their nature, are capable of penetrating up to 10 microns through the material surface. Among the factors that may affect the penetration depth are the anode, angle of incidence and the material itself. Frankly, strain measurement is the average over the depth under the surface until the specific distance the rays reach at the end.

The method is a non-destructive material testing method and it is applicable to crystalline materials of relevantly small and fine grain sizes. The material may be metallic – as in this study – or ceramic, ensuring that a diffraction peak of appropriate intensity and lack of interference of neighbouring peaks are provided.

Material evaluations performed on macro level are aimed to be supported by residual stress measurements to be able to combine and support the initial findings with micro level analysis.

### 2.3.2 Normal Stress

Normal stress may as well be defined as the stress acting normal to the surface of the plane on which such stresses are acting is quite often denoted by subscripts as schematized below in Figure 2.4.

For instance,  $\sigma_x$  is the normal stress acting in the x direction. Since  $\sigma_x$  is a normal stress, it would obviously be expected to act on the plane perpendicular to the x direction. One important point to be taken into consideration is that positive values of normal stress indicate tensile stress, whereas negative values indicate a compressive stress.

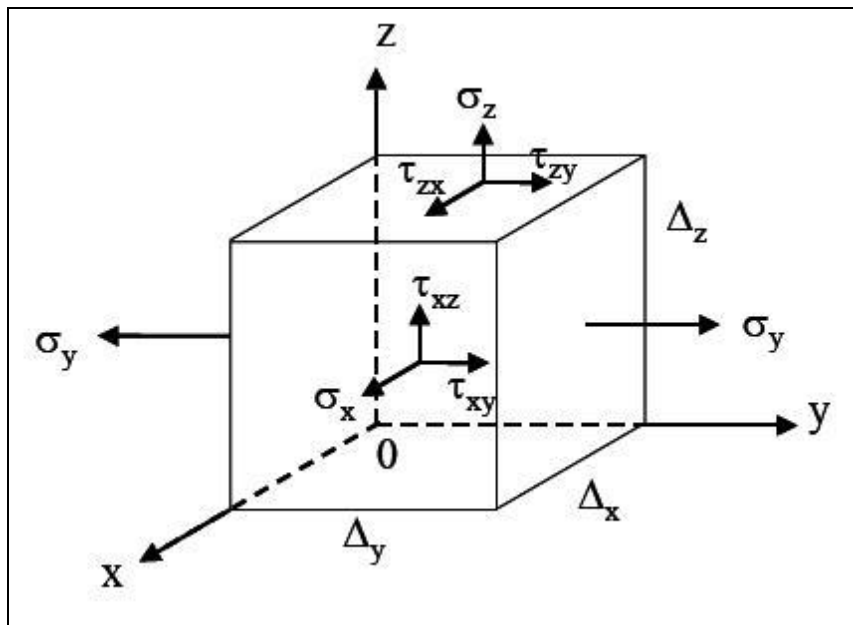


Figure 2.4 Stresses acting on an elemental unit cube (NPL, 2005)

### 2.3.3 Shear Stress

A shear stress is a stress which acts perpendicular to the plane which is also subject to a normal stress of the kind mentioned above. Two subscripts are used to define this kind of stress in a way that first one indicates the plane on which the shear stress is acting and the latter indicates the direction along which the shear stress is acting. Since a plane is most conveniently defined by its normal, the first subscript refers to this meaning that, for instance,  $\tau_{zx}$  is the shear stress on the plane perpendicular to the z-axis in the direction of the x-axis. The sign convention is given in Figure 2.5 which follows Timoshenko's notation meaning that a shear stress is positive if it points in the following direction on the positive face of a unit cube and wise versa.

### 2.3.4 Principal Stress

Principal stresses are the stresses that act on the so called "principal planes". For a given state of stress, it is possible to define a coordinate system, which has axes perpendicular to the planes on which only normal stresses act. Such planes are called principal planes. In the case of 2D plane stress there are two principal stress  $\sigma_1$  and  $\sigma_2$  which are perpendicular to each other and the directions along which the stresses act are named as 1, 2 and 3. The specification of the principal

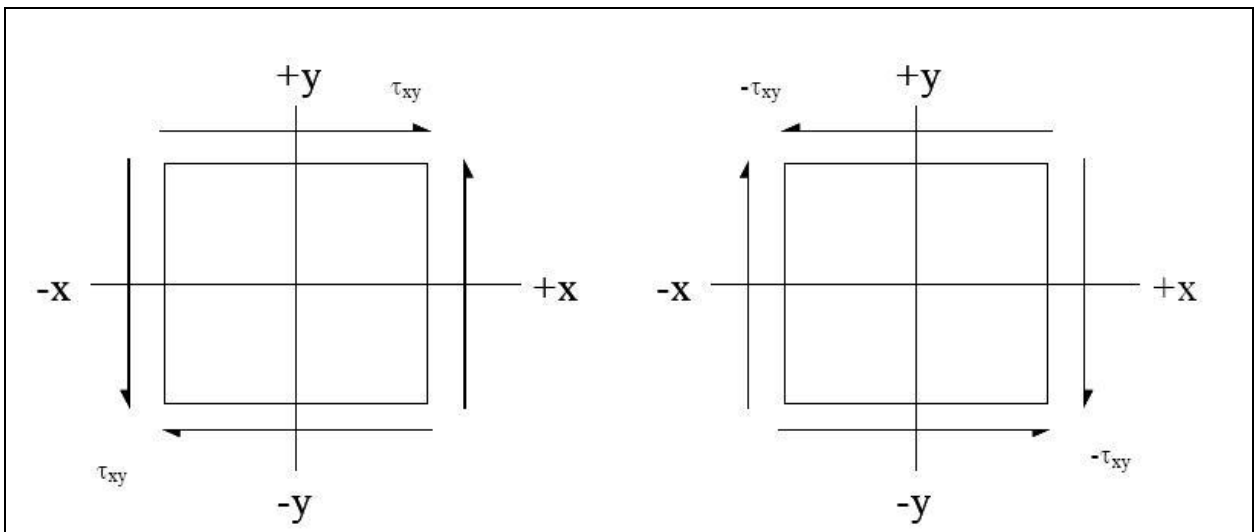


**Figure 2.5 Sign convention for shear stress - positive and negative, respectively (NPL, 2005)**

stresses and their direction are capable of providing a convenient and reliable way of describing the stress state at a specific point.

### 2.3.5 Principles

XRD Residual stress measurement takes advantage of the interactions between the wave front of the X-ray beam and the crystal lattice of the sample that is subject to such measurement. In order to be able to understand the basis that lies beneath the phenomenon Bragg's Law has to be well understood and assimilated.

### 2.3.6 Bragg's Law

A crystalline material is composed of many crystals in a way that each crystal possesses atoms that are periodically patterned in three directions. Such periodic planes of atoms cause either constructive and destructive interference patterns or one of the two where ongoing mechanism is diffraction. Among factors affecting the behaviour of the interference are the inter-planar spacing  $d$  and the wavelength of the incident radiation  $\lambda$ .

Briefly explaining Bragg's Law, a single plane of atoms should be considered as in row A in Figure 2.6. Ray 1 and 1a strike atoms K and P in the first plane of atoms and are scattered in all directions. Only in directions 1' and 1a' are the scattered beams in phase with each other, and

hence interfere constructively. A constructive interference is observed since the difference in their path length between the wave fronts  $XX'$  and  $YY'$  is equal to zero.

$$QK - PR = PK\cos\theta - Pk\cos\theta = 0$$

1

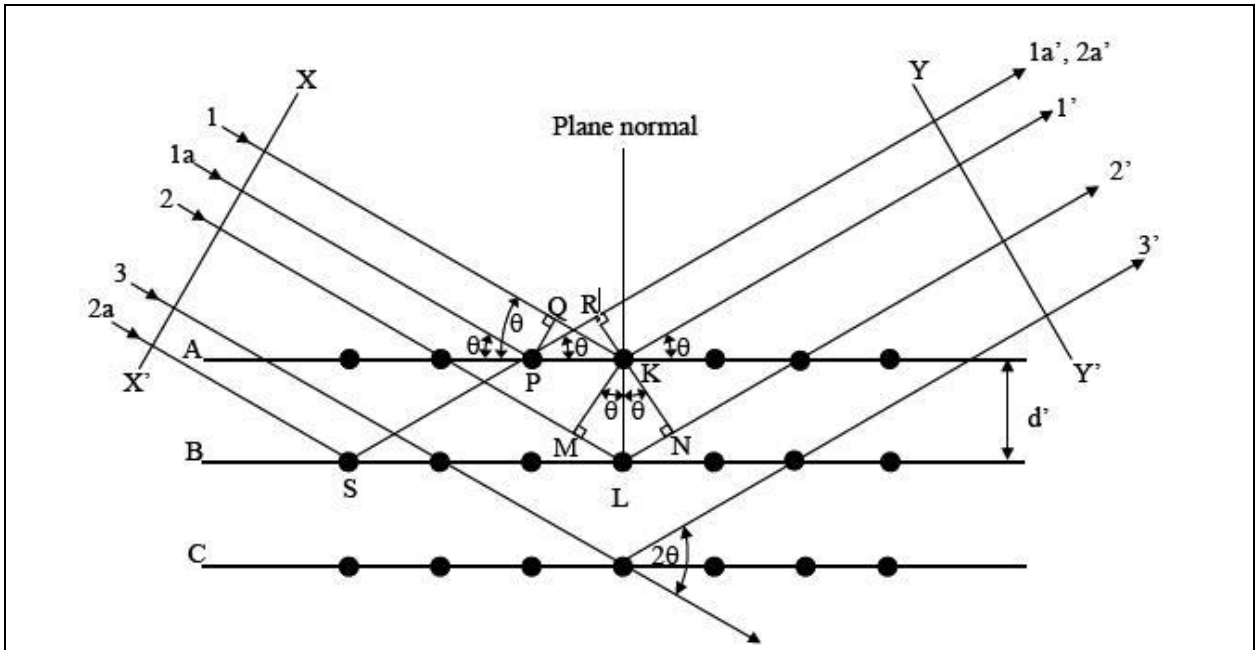


**Figure 2.6 Diffraction of x-rays by a crystal lattice**

Rays that are scattered by other atoms in the plane parallel to  $1'$  will also be in phase and thus add their contributions to the diffracted beam, therefore increasing the intensity. If we take into consideration the condition regarding constructive interference of rays scattered by atoms in different planes, it is observed that rays 1 and 2 are scattered by atoms K and L. The path difference for rays  $1K1'$  and  $2L2'$  can be expressed as

$$ML + LN + d'\sin\theta + d'\sin\theta$$

2

The above term defines also the path difference for reinforcing rays scattered from atoms S and P in the direction shown in Figure 2.6, since in this direction there is no path difference between rays scattered by atoms S and L or P and K. Scattered rays  $1'$  and  $2'$  will be in phase only if the path difference is equal to a whole number  $n$  of wavelengths, that is if

Phenomenon together with related correlations is the so called Bragg's Law and it is the fundamental basis of the X-ray diffraction theory.

### 2.3.7 Strain Measurement

In order to perform relevant stress measurements the specimen is placed in the X-ray diffractometer, and it is exposed to an X-ray beam that interacts with the crystal lattice to cause diffraction patterns. Scanning through an arc of radius about the specimen the diffraction peaks can be located and calculations can be made, as will be explained in detail, shortly.

It had been previously stressed out that there is an obvious relationship between the diffraction pattern that is observed when X-rays are diffracted through crystal lattices and inter – planar spacing within the material. Altering inter planar spacing, as well as the wavelength of the X-ray beam, will result in various diffraction patterns which are different from each other. Inter – planar spacing of a strain free material is associated with a characteristic diffraction pattern which is unique for that material. When a material is strained, elongations and contractions occur within the crystal lattice which change inter – planar spacing of the {hkl} lattice planes. Such induced change in  $d$  will result in a shift in the diffraction pattern. Precise measurement of this shift makes it possible to evaluate the change in inter – planar spacing and, therefore, the strain within the material deduced. Figure 2.7 defines the orthogonal coordinate systems used in the following explanations which reveal the mathematical relationship between inter – planar spacing and strain.

It is assumed that, since the measurement is made along the surface,  $\sigma_3$  is equal to 0. The strain  $\varepsilon_z$  however will not be equal to 0 and it can be measured experimentally by measuring the peak position  $2\theta$ , and solving equation 3 for a given value of  $d_n$ . If we know the unstrained inter-planar spacing  $d_o$  then;

$$\varepsilon_z = (d_n - d_o) / (d_o)$$

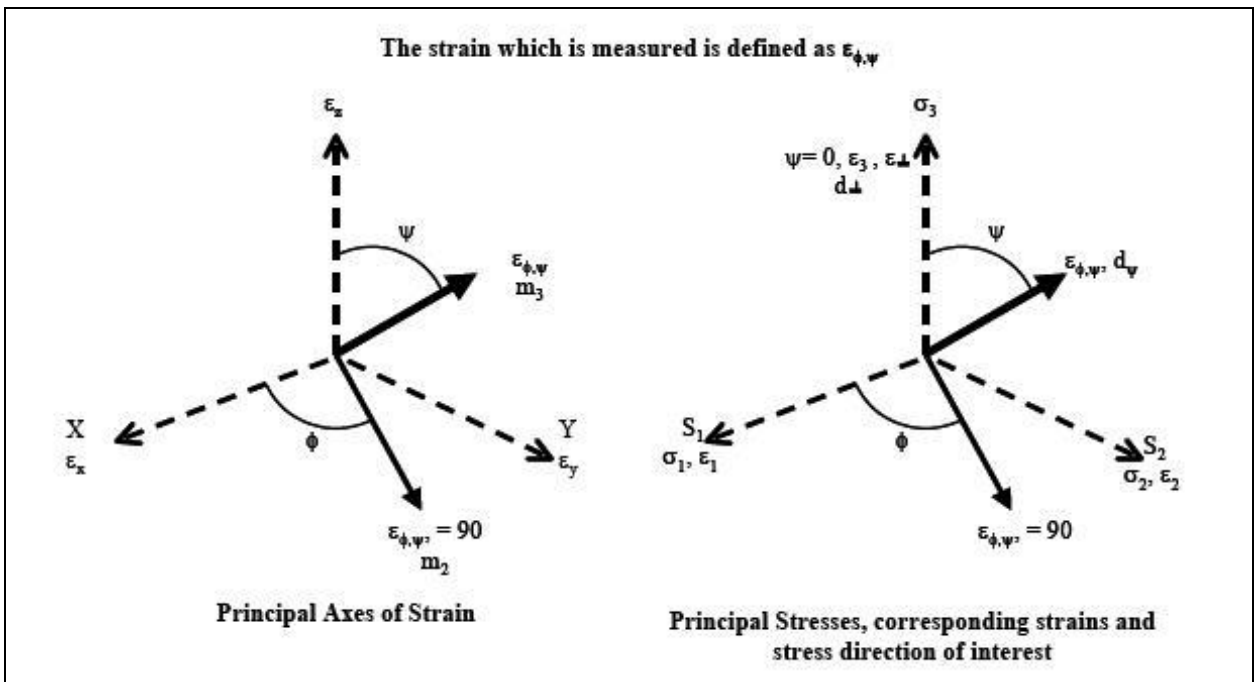


Figure 2.7 Coordinate systems used for calculating surface strain and stresses (NPL, 2005)

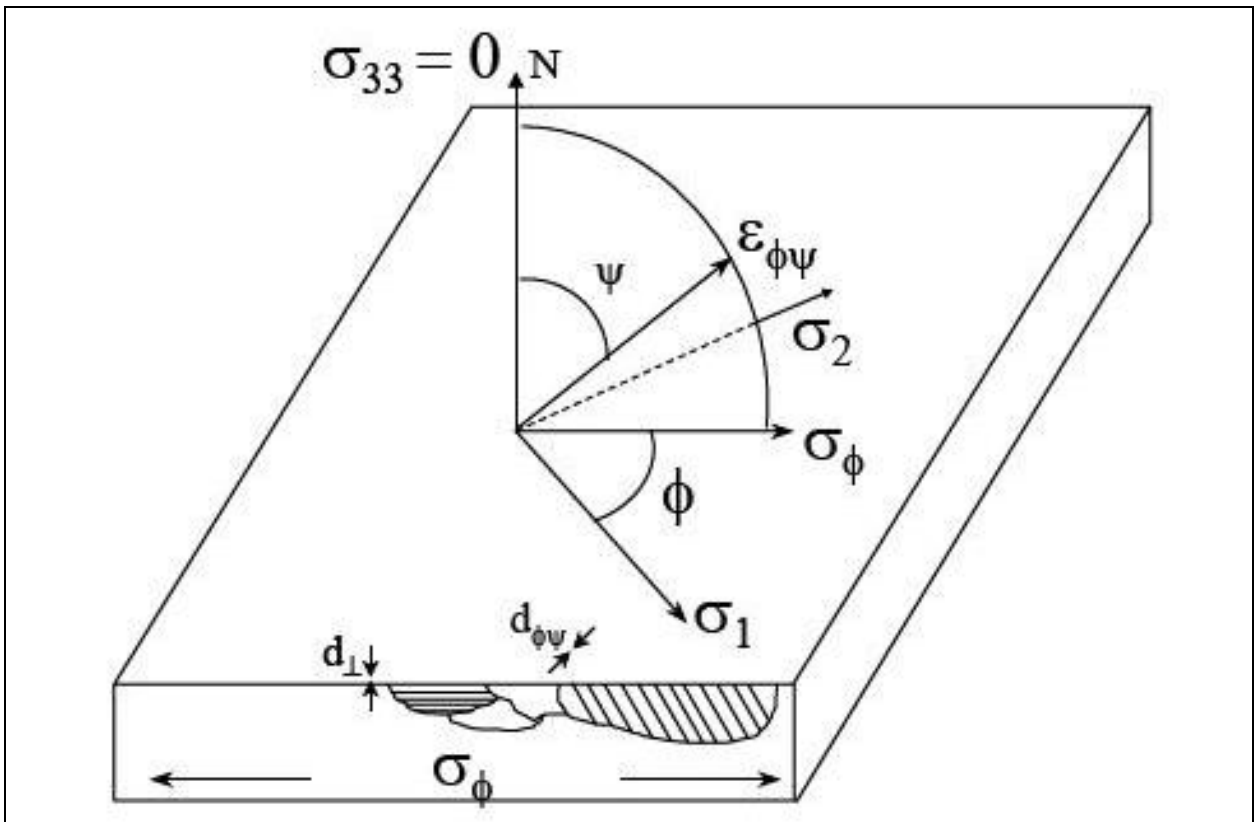


Figure 2.8 Diffraction planes parallel to the surface and at an angle  $\alpha$  (NPL, 2005)

The strain within the surface can be measured by comparing the unstressed lattice inter-planar spacing with the one that is strained. In order to perform such measurement it is required to measure precisely the unstrained sample of the material which can be achieved according to equation 4 in which formula for measurements taken normal to the surface is given. By altering the tilt of the specimen within the diffractometer, measurements of planes at an angle  $\psi$  can be made as in Figure 2.7 and thus the strain along that direction can be calculated using

$$\varepsilon_{\psi} = (d_{\phi\psi} - d_o) / (d_o) \quad 5$$

Figure 2.8 shows planes parallel to the surface of the material and planes at an angle  $\phi\psi$  to the surface. This points out how planes that are positioned at an angle to the surface are measured by tilting the specimen so that the planes are brought into a position where they will satisfy Bragg's Law.

### 2.3.8 Stress Determination

Having a concrete knowledge regarding the engineering stresses that are linked to the strains within the material is as essential as determining such stresses themselves. As given in Hooke's law

$$\sigma_y = E\varepsilon_y \quad 6$$

It is also very well known that a tensile force producing a strain in the X-direction will produce not only a linear strain in that direction but also strain grains in the transverse directions. Under the assumption that a state of plane stress exists such as  $\sigma_z = 0$ , and that the stresses are biaxial, then the ratio of the transverse to longitudinal strains is the so called Poisson's ratio,  $\nu$ ;

$$\varepsilon_x = \varepsilon_y = -\nu\varepsilon_z = -(\nu\sigma_y) / (E) \quad 7$$

Assuming that at the surface of the material, where the relevant X-ray measurements are considered to have been made,  $\sigma_z = 0$ , then we obtain

$$\varepsilon_z = -\nu(\varepsilon_x + \varepsilon_y) = (-\nu/E)(\sigma_x + \sigma_y) \quad 8$$



If we combine equations 4 and 8 we get

$$(d_n - d_o)/(d_o) = (-\nu/E)(\sigma_x + \sigma_y) \quad \mathbf{9}$$

Equation 9 is an indication of a general case where only the sum of the principal stresses can be obtained and value of  $d_o$  is yet to be precisely determined.

Elasticity theory to measure a single stress for an isotropic solid shows that the strain along an inclined line – such as  $m_3$  in Figure 2.7 - is given as follows;

$$\varepsilon_{\varphi\psi} = [((1 + \nu) / E) (\sigma_1 \cos^2 \varphi + \sigma_2 \sin^2 \varphi) \sin^2 \psi - ((\nu/E) (\sigma_1 \sigma_2))] \quad \mathbf{10}$$

Considering the strains in terms of inter – planar spacing, and using them to evaluate the stresses, it is possible to measure a single stress acting in some direction on the surface  $\sigma_\varphi$  which is mathematically expressed as follows;

$$\sigma_\varphi = (E/((1 + \nu) \sin^2 \psi))((d_\psi - d_n)/d_n) \quad \mathbf{11}$$

The above equation allows to calculate the stress in any chosen direction with respect to the inter – planar spacings which are determined by to measurements, made in a plane normal to the surface and containing the direction of the stress to be measured.

One of the most common methods used to determine the stress is the so called  $\sin^2 \psi$  method. Various XRD measurements are performed at different psi tilts as seen in Figure 2.8. Inter – planar spacing is measured and plotted as a curve similar to that shown in Figure 2.9.

By calculating the gradient of line together with basic knowledge of elastic properties, the stress can be defined. A stress free condition is assumed at  $d = d_n$  where  $d$  is the intercept on the y-axis when  $\sin^2 \psi$  is equal to 0, as indicated in Figure 2.9.

$$\sigma_\varphi = (E/(1 + \nu))m \quad \mathbf{12}$$

Where  $\sigma_\varphi$  is the stress and  $m$  is the gradient of the  $d$  vs.  $\sin^2 \psi$  curve.

The full derivation of the relevant equation is not given here since it is not the main point of interest at the moment.

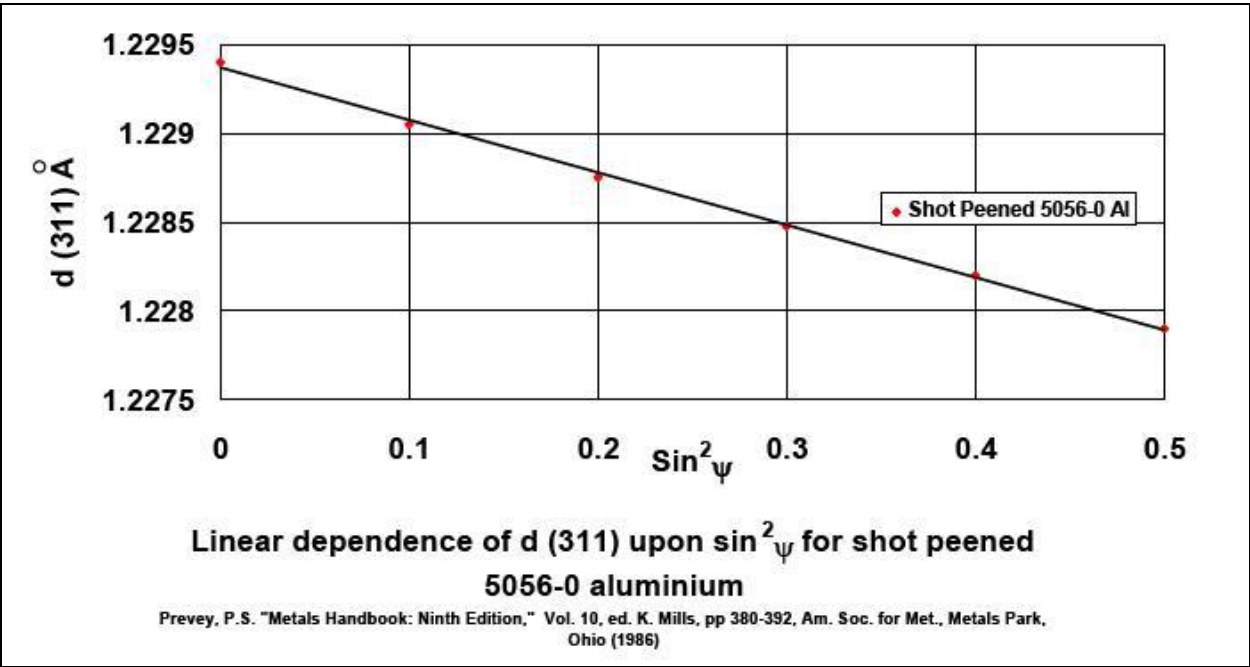


**Figure 2.9 Example of a  $d$  vs.  $\sin^2 \psi$  plot (NPL, 2007)**

There goes the basis and the basic principles of stress determination using X-ray diffraction. If we were to talk about more complex solutions regarding non ideal situations where, for instance, psi splitting caused by shear stresses occurs or there is presence of inhomogeneous stress state within the material as briefly pointed out in Figure 2.10.

One important issue is that, in equation 11, the modulus of the lattice plane used for the measurement is assumed to be the same as the bulk modulus, which quite often is not the case. Empirical calculation or precise measurement of the elastic constants of a particular plane are always favoured in order to get better results and such measurements can be done performing a bending test in the diffractometer. For further information regarding the issue, you are kindly asked to refer ASTM E-1426-94.

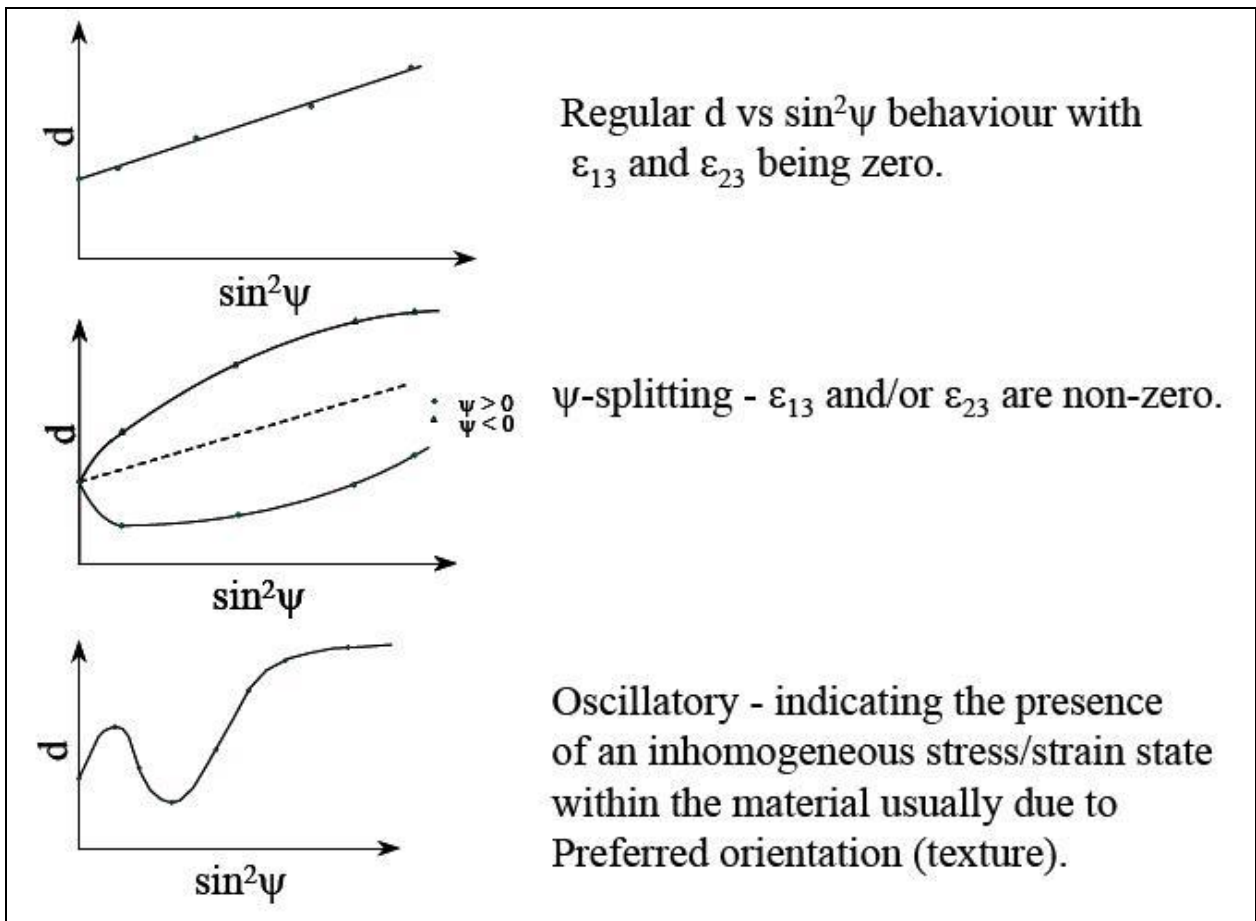


Figure 2.10 Further examples of  $d$  vs.  $\sin^2\psi$  plots (NPL, 2005)

### 2.3.9 Depth Penetration

One crucial question that comes to mind concerns the penetration depth of X-rays and the range along the depth through which the diffraction data truly apply. Since many metallic materials strongly absorb X-rays, the intensity of the incident beam is significantly reduced after a certain extent under the surface. Consequently, the diffraction phenomena occurs within a very thin surface layer meaning that residual stress measurements correspond only to that layer of the material.

Unfortunately, the penetration depth is unlikely to be determined precisely. It has to be taken into consideration that the intensity decreases exponentially with depth in material and the logic lying beneath would be that the loss in signal strength is proportional to the distance travelled along the depth of the material; hence, as the beams go deeper, layers or planes contribute less to diffraction.

Although, the exact penetration depth is quite out of judgement, the thickness of the effective layer ( $x$ ) can be calculated, according to equation 13.

$$x = [\ln((1/(1-G_x)))]/[\mu((1/(\sin(\varphi+\psi))) + (1/(\sin(\varphi-\psi))))] \quad 13$$

The penetration depths vs.  $\sin^2 \psi$  for materials commonly used for residual stress measurements are given in Figure 2.11.

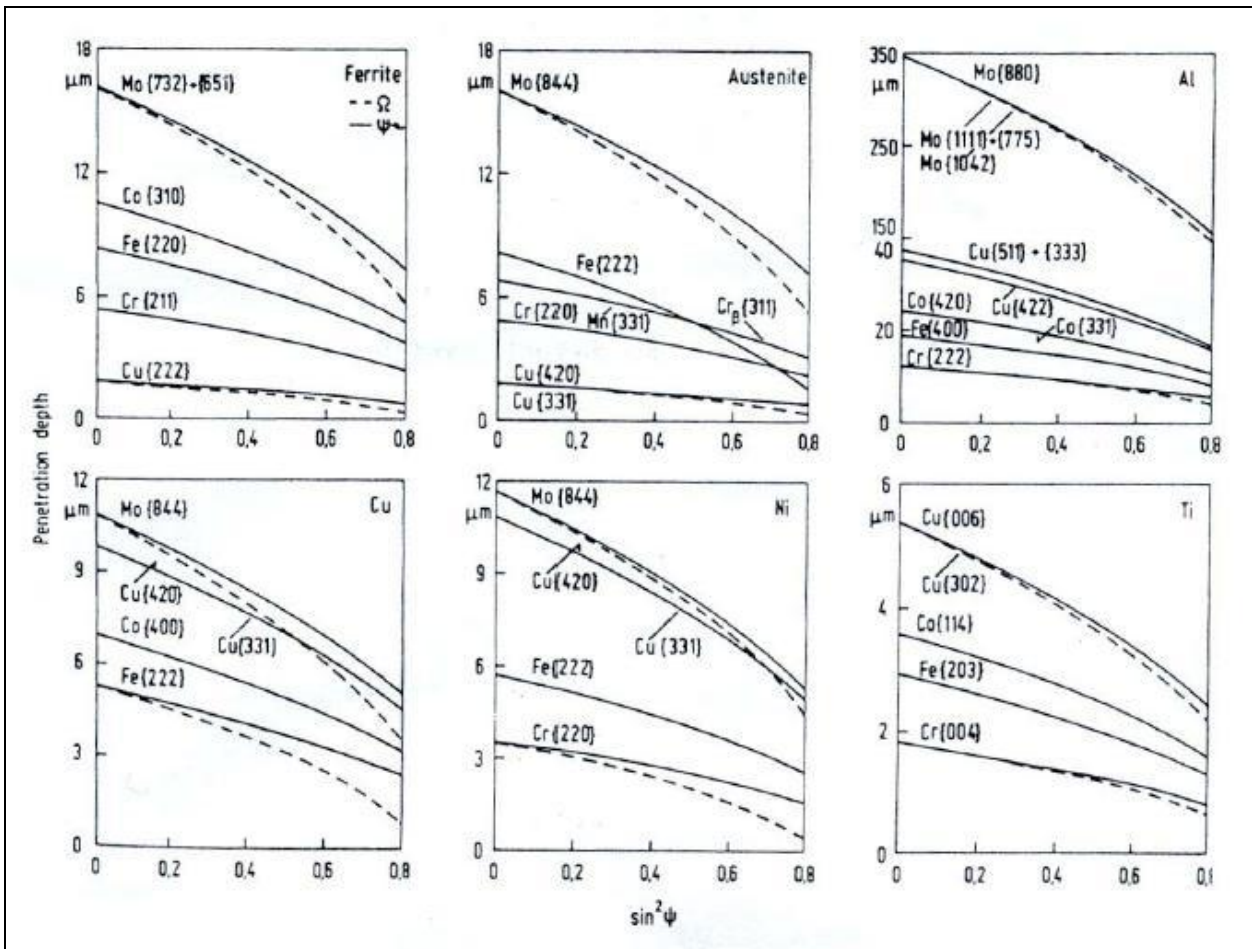


**Figure 2.11 Penetration depths vs.  $\sin^2 \psi$  of different metals and radiations (NPL, 2005)**

Hopefully, together with other methods that are yet to be discussed throughout the following sections, applications that dual phase steels undergo are to give a better insight and understanding on the behaviour of such steels under bending and on promising measurement techniques supported with concrete test parameters that could be relied on to the furthest extent by means of a healthy vehicle production process and vehicle's behaviour along its future life cycle.

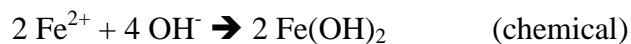
## 2.4 Electrochemical Corrosion

### 2.4.1 Basic Concepts

Corrosion refers to the process which involves deterioration or degradation of metal. The most common example to define corrosion would be the formation of rust on steel. Corrosion phenomena most of the time have an electrochemical nature which will soon be described more thoroughly. Corroding metals consist of at least two reactions on the surface, which are oxidation and reduction, and also referred as the anodic partial reaction (e.g., dissolution of iron) and the cathodic partial reaction (e.g., reduction of oxygen) respectively. The products of the electrochemical reactions may interfere with each other non-electrochemically to form the final product (e.g., rust). Such process follows a reaction path as follows;



The above reaction includes all three individual reactions mentioned previously; dissolution of iron, the reduction of oxygen and formation of rust:



### 2.4.2 Electrochemical Basis of Corrosion

Most metal corrosion occurs electrochemically at the interface between the metal and an electrolyte solution. Moisture on the surface of metals provides this kind of an electrolyte for such atmospheric corrosion.

The rate of corrosion is normally determined by equilibrium between anodic and cathodic reactions. When there exists a state of equilibrium between these two reactions, the flow of electrons is balanced and no net electron flow is observed. Electron flow in this case is associated

with the electrical current which is an important aspect in defining the principals and empirical relationships lying beneath the electrochemical corrosion phenomena. Anodic and cathodic reactions can take place on the same metal as well as two different materials that are electrically connected.

### 2.4.3 Calculation of Corrosion Rates

According to Faraday's law, there is a linear relationship between the corrosion rates (the metal dissolution rate),  $R_M$ , and the corrosion current  $i_{corr}$ :

$$R_M = (M/(nF\rho))i_{corr} \quad 14$$

Where M is the atomic weight of the metal,  $\rho$  is the density, n is the charge number which indicates the number of electrons exchanged in the dissolution reaction and F is the Faraday constant which is equal to 96.485 C/mol. The ratio M/n is also sometimes referred to as the equivalent weight.

### 2.4.4 Calculation of Corrosion Currents

In order to be able to calculate the corrosion rates, corrosion currents have to be determined. When relevant reaction mechanisms are known, the corrosion currents can be calculated using Tafel Slope analysis.

The relationship between current density and potential of anodic and cathodic electrode reactions under charge transfer control is schematized in Figure 2.12 and is given by the Butler – Volmer equation.

$$i = i_{corr} [e^{2.303(\eta/\beta_a)} + e^{-2.303(\eta/\beta_c)}] \quad 15$$

$$\eta = E - E_{corr} \quad 16$$

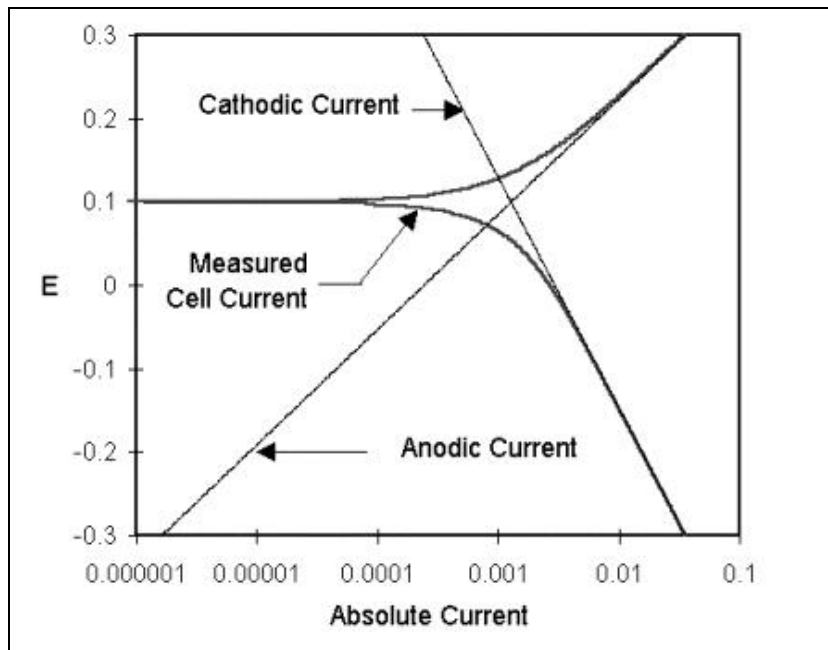


**Figure 2.12 Classic Tafel analysis (GAMRY, 2010)**

In the above given equation  $E$  is the applied potential whereas  $i$  is the measured current density. The overpotential  $\eta$  is defined as the difference between the applied potential and the corrosion potential  $E_{corr}$ . The corrosion potential  $E_{corr}$  is the open circuit potential of the corroding metal. The corrosion current  $i_{corr}$  and the Tafel constants  $\beta_a$  and  $\beta_c$  can be measured from the experimental data.

When large anodic overpotentials ( $\eta / \beta_a \gg 1$ ) are taken into consideration the Butler – Volmer equation simplifies to the Tafel equation for the anodic reaction:

$$\eta = \log i_{corr} + \beta_a \log i \quad 17$$

Analogously, for large cathodic overpotentials ( $\eta / \beta_c \ll -1$ ) the Tafel equation for the anodic reaction is given by:

$$\eta = \log i_{corr} - \beta_c \log |i| \quad 18$$

The Tafel equation foresees a straight line for the variation of the logarithm of current density with potential. Therefore, currents often are shown in semi logarithmic plots known as Tafel plots. This type of analysis is referred to as Tafel Slope Analysis.

## 2.5 Electrochemical Corrosion Measurement Techniques

### 2.5.1 A New Microcell for Material Surface Investigations at Large Current Densities

Capillary-based droplet cells may be considered as a rather new technology and were developments more or less ten years ago. The technique is now widely and reliably used for electrochemical surface analyses down to micron level. The theory beneath the process is as described above, consisting of the common 3 electrode setup with reference, counter and working electrode.

Besides the local resolution, the method has several advantages compared to the conventional techniques. To name a few;

- The sample doesn't need preparation and measurements can take place right away.
- Wetting is limited only with the area which is subject to investigation whereas the rest of the sample remains totally untouched
- Applied mechanical stress is small.
- Geometrical requirements of the sample are much less compared to other electrochemical surface investigation methods and in order to be able to perform some reliable tests, only a small portion of the total area has to be flat.
- The amount of electrolyte required to run the process is much less.

Together with many others, the analysis can be applied to polycrystalline materials like Dual Phase Steels which perfectly satisfies the needs of this study.

Other electrochemical surface analysis techniques such as Scanning Electrochemical Microscope (SECM) do not only require additional redox systems but also give a less defined working electrode area.

The capillary cells, despite being widely used, may possess some procedural problems if large current densities have to be present during the operation. In technical applications, large current densities are necessary to achieve large throughput rates and to suppress side reactions. In the capillary cell, large current densities results in high reaction rates and, thus, significant changes in



electrolyte composition. The problem is that reaction, in such a system briefly described above, reaction products may block the capillary tip and, therefore, the electronic contact to working electrode is lost. The phenomenon is schematized in Figure 2.13 where potentiostatic pulses were applied to a pure iron sample with potential steps from 5 to 10V. Current densities of 30 A/cm<sup>2</sup> are reached at the beginning until when the oxygen evolution, as a result of the chemical processes occurring, blocks the capillary, first partially and then completely.

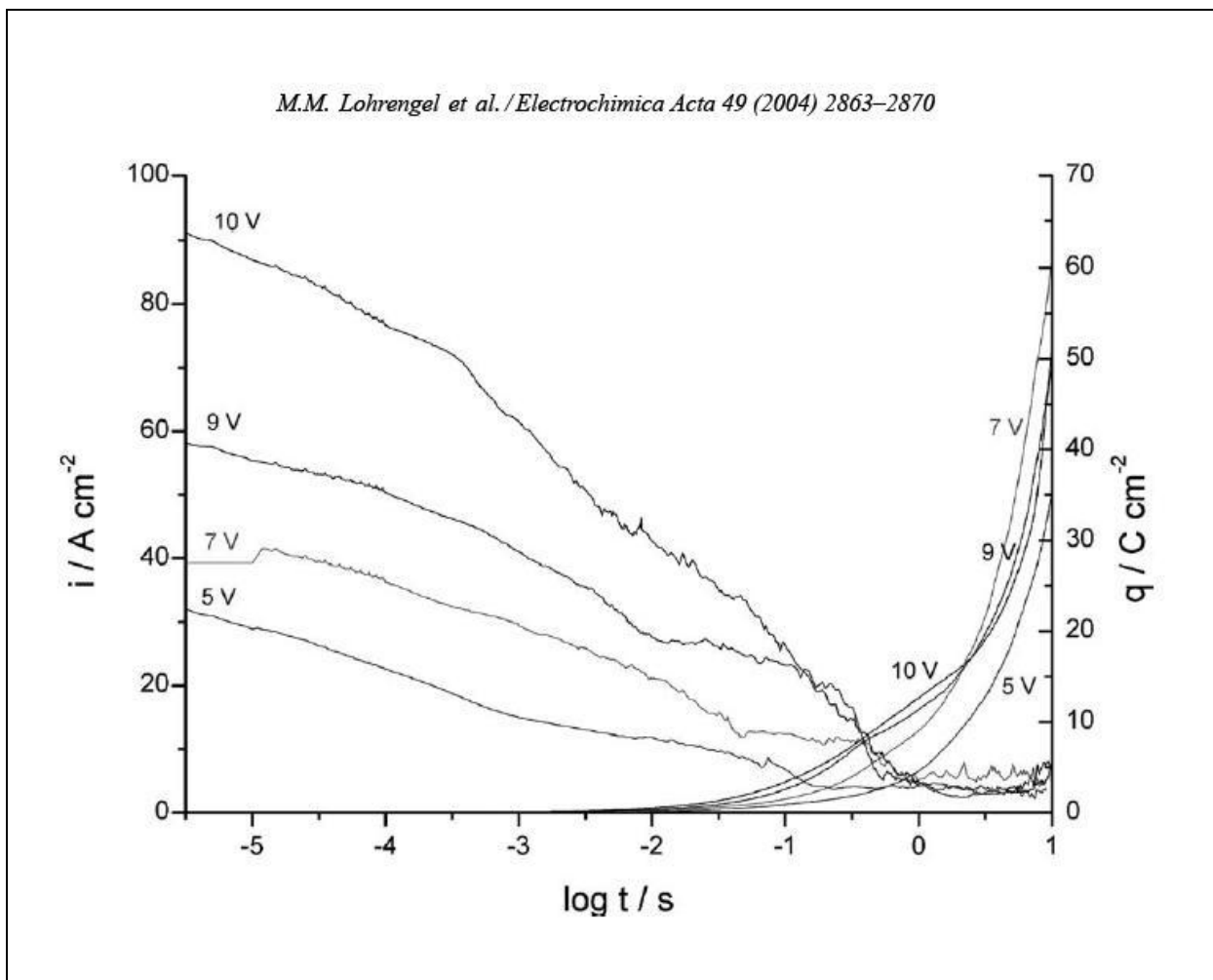


**Figure 2.13 Anodic dissolution transients and total charges of Fe in 250gl NaNO<sub>3</sub> at 25°C and at different potentials without electrolyte flow. The capillary is partially blocked by gas bubbles after some ms and charges (LOHRENGEL, 2004)<sup>4</sup>**

<sup>4</sup> LOHRENGEL M.M., ROSENKRANKZ C., KLUPPEL I., MOEHRING A., BETTERMANN H., VAN DEN BOSSCHE B., DECONINCK J.

The problem has been partially overcome by the development of a new capillary microcell. In a recent study done by a research team led by various German and Belgian academicians<sup>5</sup>, a new capillary design has been tested. The so called theta-capillaries, i.e. capillaries with two channels, separated by a partition wall in between are used and Figure 2.14 schematizes such capillary type. A micro photo of the capillary is also given in Figure 2.15.

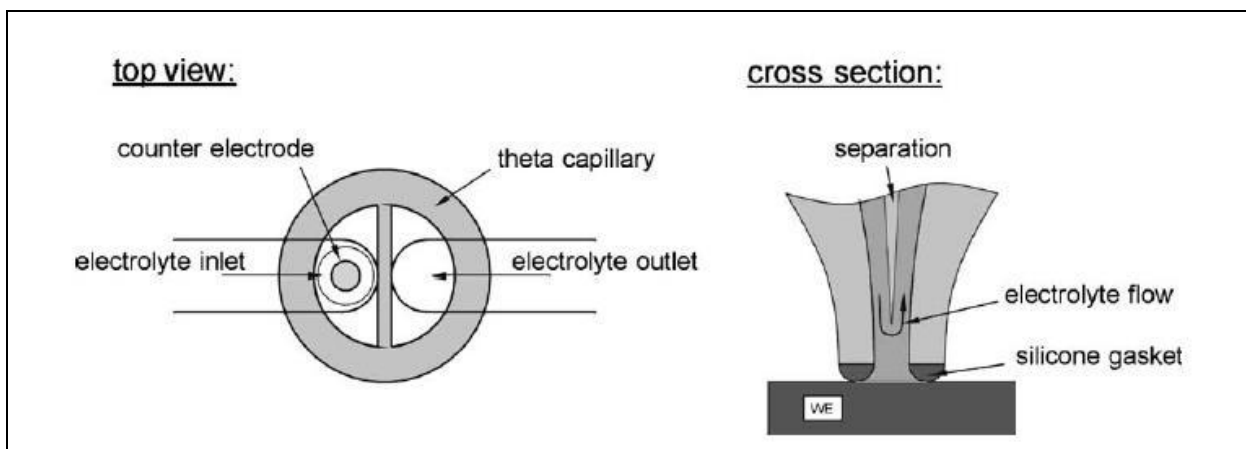


**Figure 2.14 Schematic views of the theta capillary cell: cross-section with counter electrode (left) and side view with gasket and sample (right) (LOHRENGEL, 2004)**

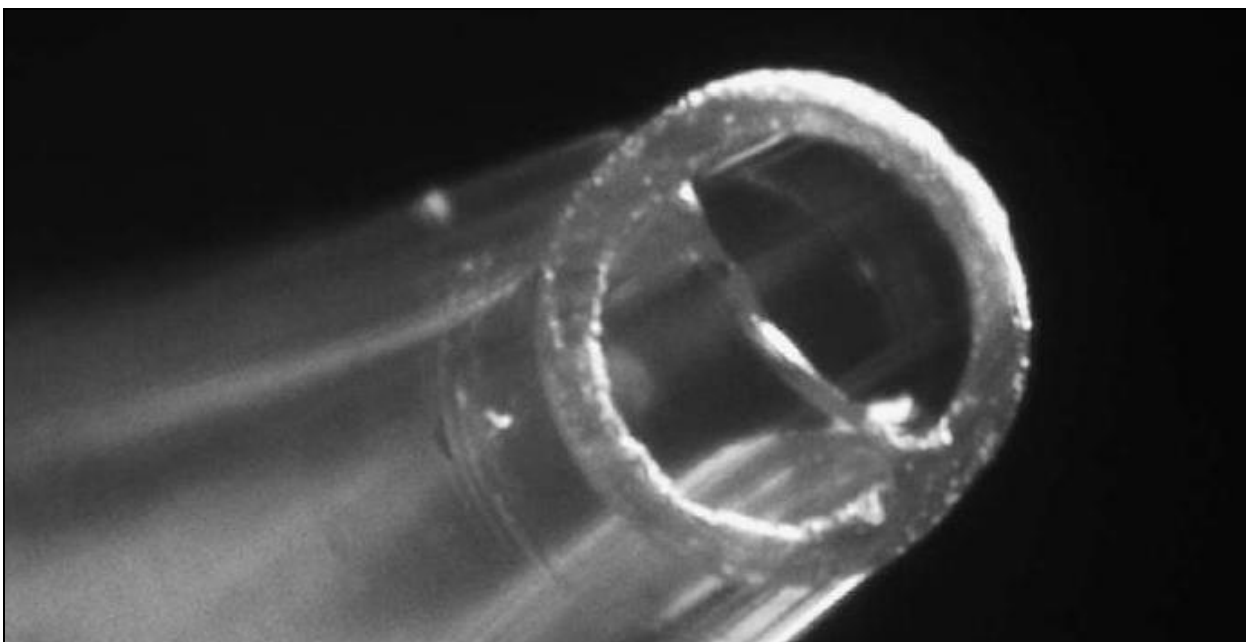


**Figure 2.15 Micro photo of ground capillary tip, inner diameter around (LOHRENGEL, 2004)**

<sup>5</sup> LOHRENGEL M.M., ROSENKRANKZ C., KLUPPEL I., MOEHRING A., BETTERMANN H., VAN DEN BOSSCHE B., DECONINCK J.

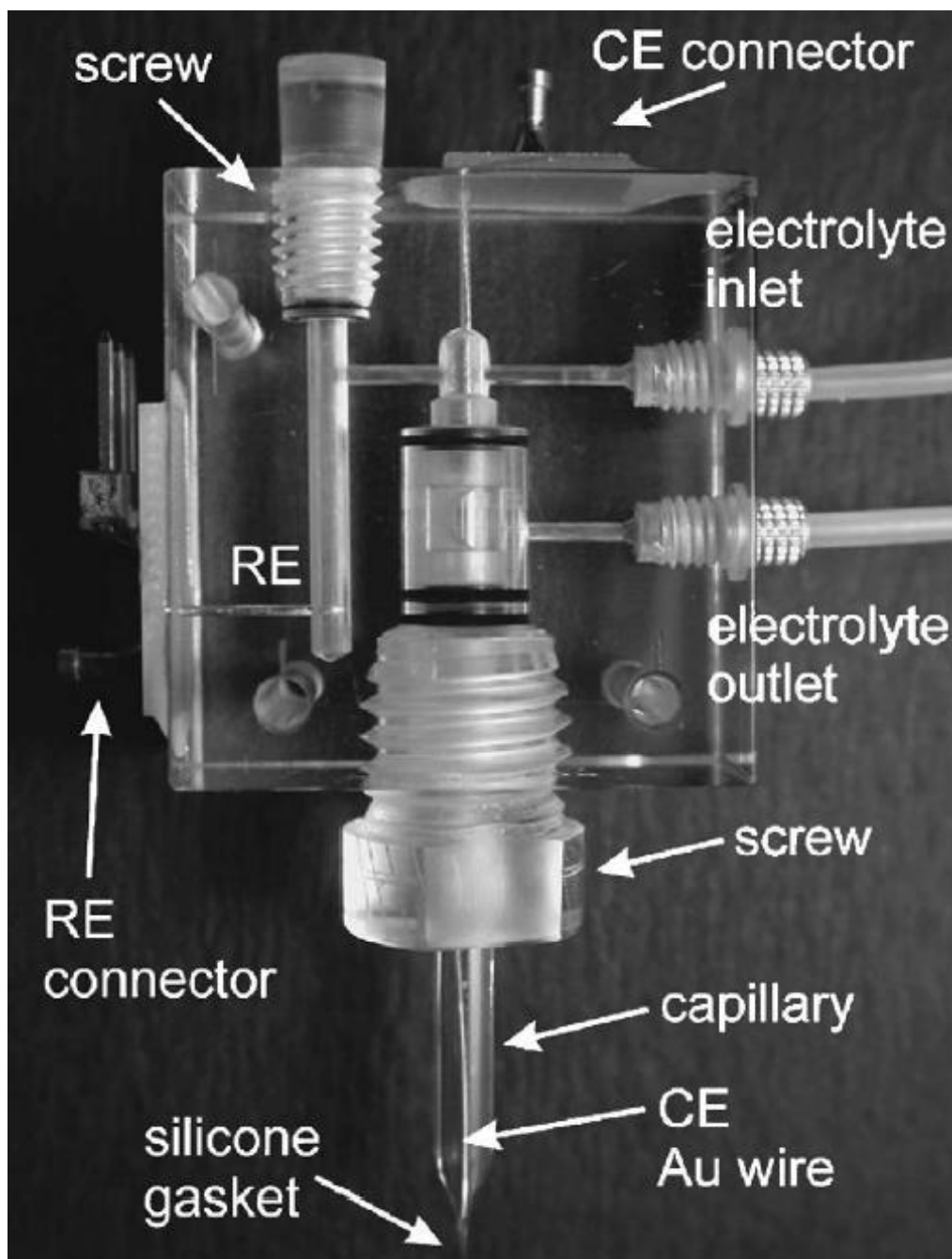


**Figure 2.16** Capillary carrier with capillary, counter electrode, electric connectors and electrolyte inlet and outlet (LOHRENGEL, 2004)

The research group further describes the rest of structure of the capillary as follows: *“The partition wall is removed close to the tip of the capillary by etching and, thus, an electrolyte flow becomes possible. One of the channels is used as an electrolyte inlet, while the second one is the outlet. A silicone gasket at the tip of the capillary defines the working electrode area. A special Plexiglass<sup>®</sup> was developed to realize electrolyte flow and to enable a fast exchange of the*

capillaries as the silicone ring's life time is limited. The carrier contains a micro reference electrode (mercury acetate, mercury sulphate or mercury oxide), counter electrode (thin gold wire inside the capillary), electric connectors to the potentiostat, and the fittings for the electrolyte tubes. The capillary is held by two O-rings and a female screw. The sample is fitted to an XYZ positioning system below the capillary. A video microscope is used to control the capillary position and to identify structures on the investigated surface.”

The experimental setup which takes part in this study is very similar to the one described above and, thus, Figure 2.16 would resemble both setups.

Frankly, what is to be expected to achieve as a result of such measurements regarding the electrochemical nature of the material, would be a current density vs. potential graph of the kind indicated in Figure 2.17. This way, it would be possible to analyse the electrochemical corrosion behaviour of dual phase steels that are subject to different bending processes by means of different testing parameters and establishing some sort of a comparison between the results and their direct relationships with the changing test parameters.

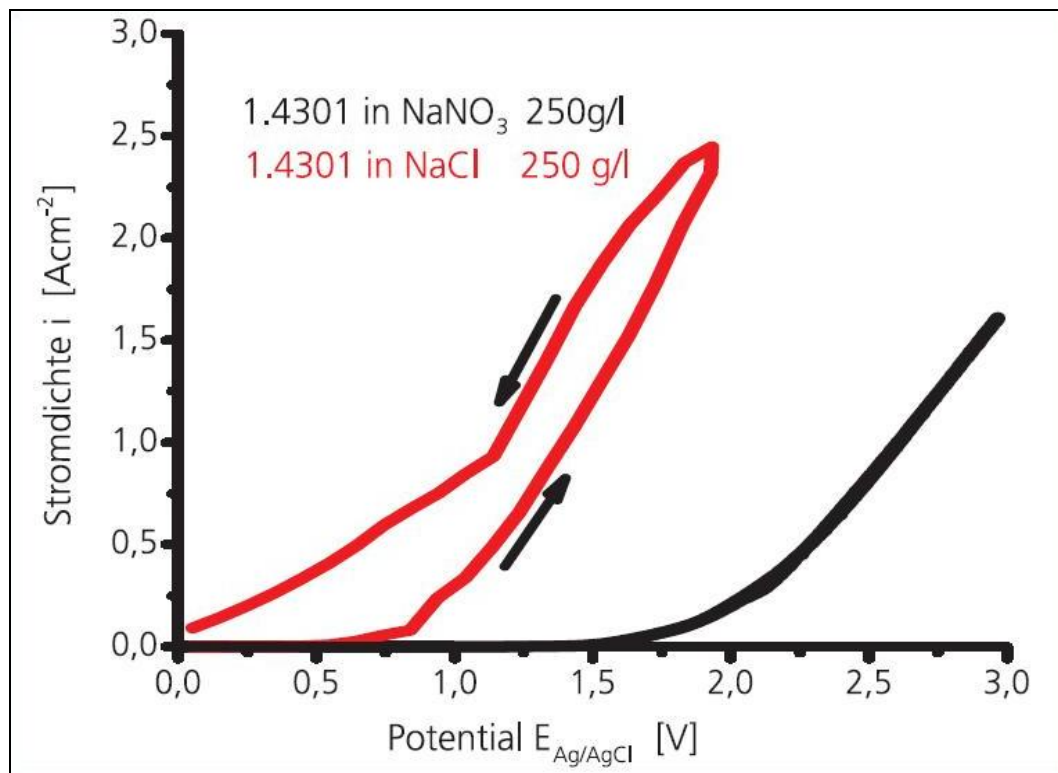


**Figure 2.17 Current density / potential measurements to analyse the behaviour at strong anodic dissolution in different electrolytes ( $dE/dt=mV/s$ ) (FRAUNHOFER, 2011)**

## Chapter 3 Experiments

### 3.1 Surface Crack Investigation

#### 3.1.1 V Bend Test

The dual phase steel which is the subject of this study was industrially produced by one of the leading steel companies in the world and from now on it will be referred as to CR 980 DP. “CR” indicates that the steel sheet is cold rolled<sup>6</sup> whereas “980” and “DP” refer to the tensile strength of the steel and its dual phased nature, respectively. The composition of the material is given below in table 3.1 and the thickness is 1.4 mm and constant for all the applications performed throughout the investigation. One of the main reasons for setting such limits is that the quantity wise complex and time consuming procedures wouldn’t allow a distinction of certain variables and parameters by means of preserving the capability of pursuing a promising investigation and reliable findings.

CR 980 DP		
<u>C</u>	<u>Si</u>	<u>Mn</u>
~0.11 %	~0.7 %	~2.9 %

**Table 3.1 Chemical composition of CR 980 dual phase steel (% weight)**

For the V Bending experiments, the maximum applied load remains the same and is 80 kN. When it reaches to 80 kN, the load is automatically released and the system goes back to its initial position. Tests are repeated under numerous parameters concerning the phenomena such as bend speed, bend radius, etc. and the samples were examined both by eye and under microscope in order to investigate crack behaviour along the bent portion of CR 980 DP. Figure 3.1 shows the instrument used to run relevant tests regarding V Bend.

---

<sup>6</sup> Technical information regarding the process is not the main concern of this investigation and, therefore, not shared here. Readers who would be interested in knowing more on cold rolling are recommended to consult text books such as “COLD ROLLING OF STEEL” by William L. Roberts (1978).

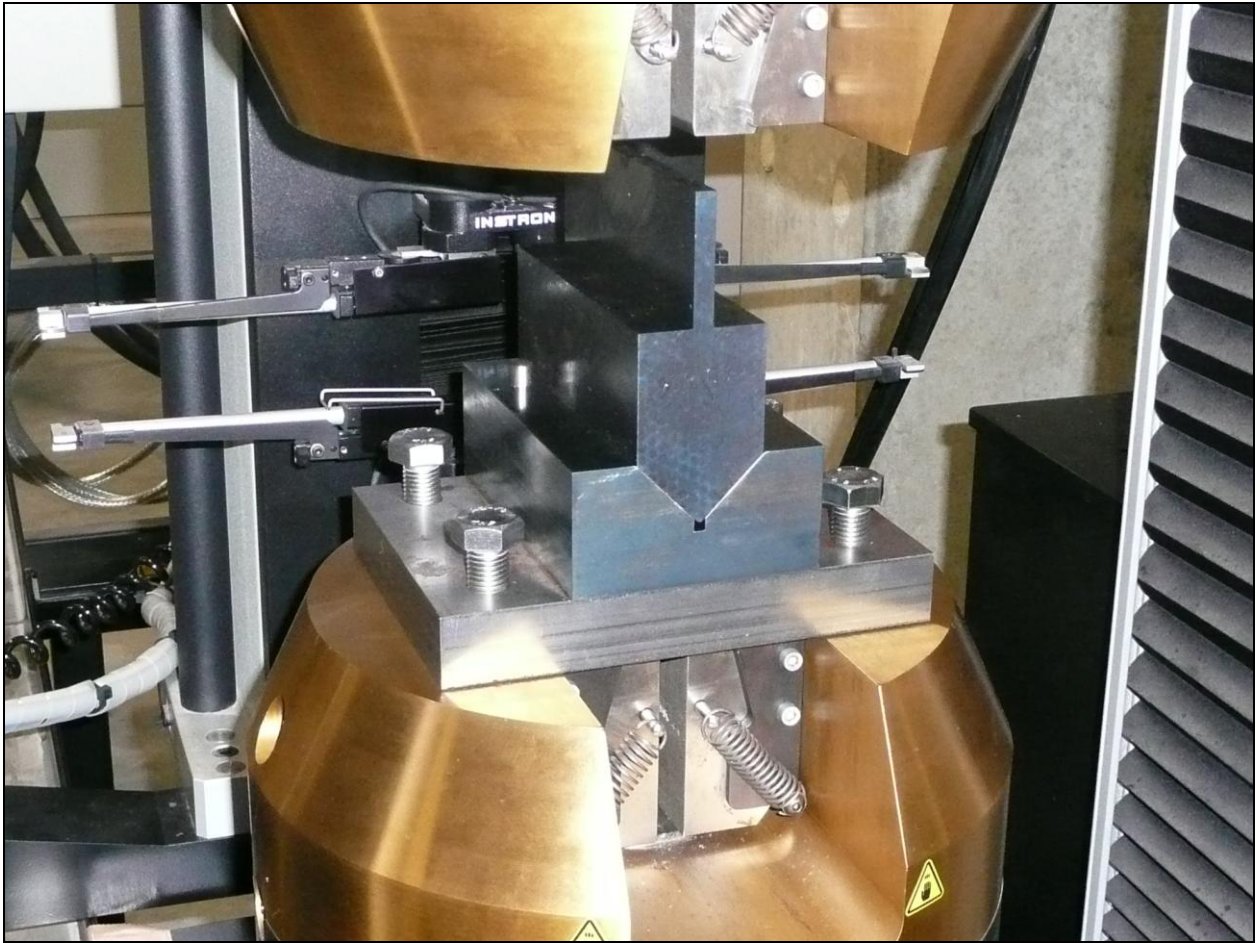


**Figure 3.1 V Bend Tester (INSTRON)**

### **3.1.2 Sample Preparation and Criteria Judgement**

The samples are prepared using a shearing machine. Cutting directions shall lie perpendicular to the plane which is parallel to the side of the test piece that has the largest surface area meaning that the burr on the edge portion of the test piece is positioned along the same plane mentioned above as shown in Figure 3.2. This way the difference in local stresses associated with the process is kept relatively balanced in order to obtain a reliable crack evaluation afterwards.

In this investigation, by means of burr location, 3 different positioning is applied: The standard method where the burr is not on the initially bent site of the test piece, the condition in which the burr is upside down so that torn down edge portion is not closer to the primary bent section where crack evaluation is performed and the condition in which the edges are grinded by which it is aimed to get rid of the heterogeneous stress distribution which is suspected to have an indirect effect on the crack behaviour along the bend portion, starting from the edge and till the middle

section. The relevance regarding different behaviours under various conditions is further investigated and results will be shared throughout the following sections.

A full list of parameters that concerns macro crack evaluations is given in Figure 3.3 whereas Figure 3.4 shows the judgement criteria of V Bend Test.

Regarding Figure 3.4, it has to be mentioned that the sample has to have an evaluation grade of at least 9 in order to be able to be considered OK. Another reason why crack behaviours are assigned numbers is to observe the trend within the same set of parameters and compare them to that of various sets. 3 trials are performed for every single parameter to ensure the consistency of the application. Having said that, please keep in mind that in some very rare cases, this number may change due to an attempt to obtain better results and understanding of the concept, if that is believed to be the case.

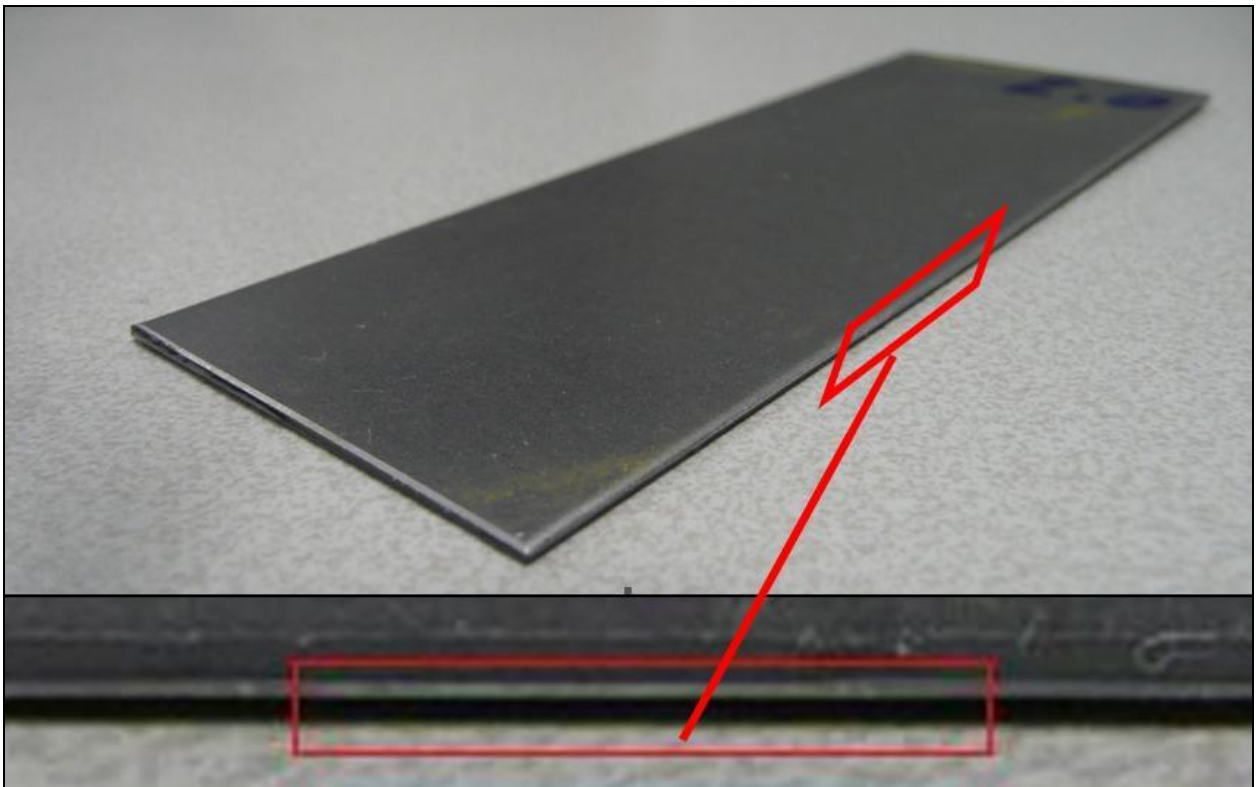


**Figure 3.2 Dual phase steel sheet test piece with the shiny region that indicates the shear zone outlined by the red box**

The tests performed under various parameters taking the criteria given into consideration, are introduced and described in detail from this point on.

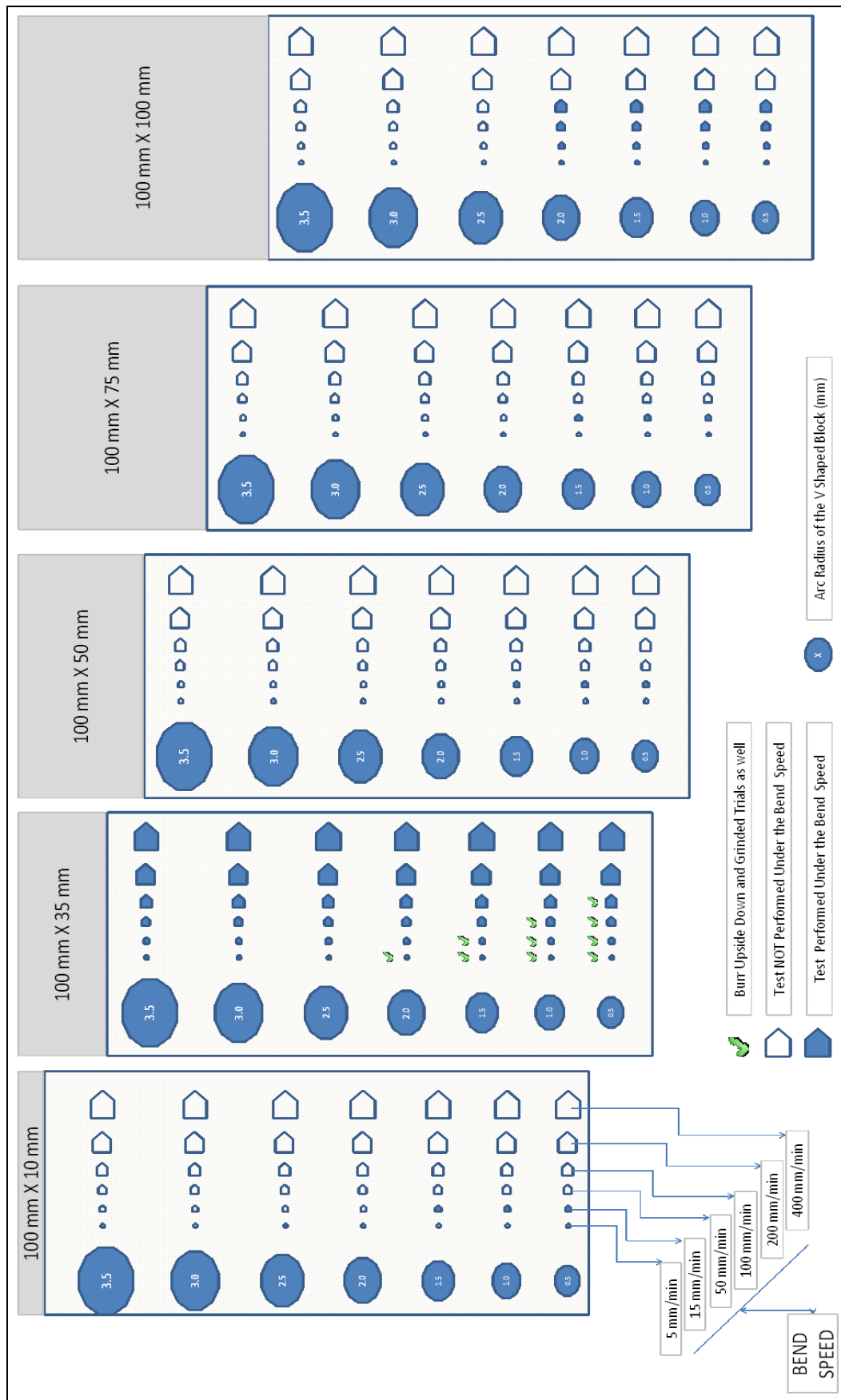








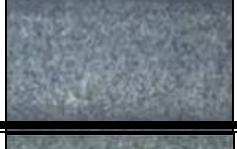



Figure 3.3 Full list of parameters that are subject to testing (V Bend)



Sample is completely separated by one single big crack	1		NG
Continuous deep cracks of large width are observed	2		NG
Continuous deep cracks of small width are observed	3		NG
Non continuing cracks are widely observed	4		NG
Cracks are clearly observed by naked eye on some portions of the bent surface	5		NG
Cracks are observed by naked eye on some portions of the bent surface	6		NG
Cracks are observed by naked eye after careful observation on some portions of the bent surface	7		NG
Cracks are observed only by magnification on some portions of the bent surface	8		NG
Only wrinkles along the bent surface are observed	9		OK
Neither crack nor wrinkle occurrence	10		OK

**Figure 3.4 Judgement criteria of V bend test**

The results are shared below and the discussions regarding the data obtained are made at the end of this chapter.

### 3.1.3 Sample Dimensions 100 mm X 35 mm

Since the dimensions given in the title cover the major requirements for a standard base test we have initially set, largest number of tests is performed for relevant dimensions. All of the V shaped blocks and bend speeds in question are applied to numerous samples. Initial findings are taken as the starting point of the rest of the investigation and the road map that leads to a concrete conclusion is based on such primary evaluations. Table 3.2 summarizes the results of all the tests performed regarding the parameters mentioned in the title.

Sample Dimensions: 100 mm X 35 mm																		
R	5 mm/min			15 mm/min			50 mm/min			100 mm/min			200 mm/min			400 mm/min		
3,5	9	9	9	9	9	9	9	9	9	9	9	9	9	9	9	9	9	9
3,0	9	9	9	9	9	9	9	9	9	9	9	9	9	9	9	9	9	9
2,5	8	9	9	9	9	9	9	9	9	9	9	9	9	9	9	9	9	9
2,0	8	8	8	9	9	9	9(8)	9	9	9	9	9	9	9	9	9	9	9
1,5	8	7	7	7	9	9	8	8	9	9	9	9	9	9	9	9	9	9
1,0	4	4	6	6	8	8	8	8	9	7	9	9	9	9	9	9	9	9
0,5	3	5	6	7	8	8	4(6)	8	9(8)	5	8	9	6	8	9	9	9	9

R	AVG	5 mm/min	15 mm/min	50 mm/min	100 mm/min	200 mm/min	400 mm/min
3,5	Average	9,0	9,0	9,0	9,0	9,0	9,0
3,0	Average	9,0	9,0	9,0	9,0	9,0	9,0
2,5	Average	8,7	9,0	9,0	9,0	9,0	9,0
2,0	Average	8,0	9,0	9,0	9,0	9,0	9,0
1,5	Average	7,3	8,3	8,3	9,0	9,0	9,0
1,0	Average	4,7	7,3	8,3	8,3	9,0	9,0
0,5	Average	4,7	7,7	7,7	7,3	7,7	9,0

**Table 3.2 Crack evaluation results (Standard)**

In order to obtain an OK result, the material has to satisfy the requirements in all 3 tests and sufficient results are represented with white boxes whereas the red boxes indicate that the material, under given bend speed and bending radius, fails the tests. As clearly seen above there is an obvious behaviour directly related to speed and radius. Demonstrating the obtained data in a graph makes it easier to understand the trend concerning the relevant parameters. Such a graph is given in Figure 3.5.

When Table 3.2 and Figure 3.5 are further observed, it is seen that as the bending radius and speed decreases the crack occurrence increases as well as the severity of the cracks formed. The possible reasons for this phenomenon will be investigated and discussed in the results section together with other findings.

As schematized in Figure 3.6, Figures 3.7 and 3.8 show pictures of non-bent standard test pieces taken under microscope. The pictures were taken from the top and at a right angle to the normal of bent plane. For a through comparison between the dull samples and the ones that underwent V bend test, the microscope images under various magnifications of the bend zones after relevant tests are performed are also given.

Figure 3.9, Figure 3.10, Figure 3.11, Figure 3.12, Figure 3.13 and Figure 3.14 show the microscopic images of the bent zone in order to be able to gather some macro findings. The observations are made under various magnifications using confocal laser scanning microscope. “N” on the lower left hand side indicates that the pictures belong to the bent plane whereas “90°” indicates that the pictures were taken along a plane which is normal to the bent one (Figure 3.6). This way, it is aimed to make an observation both directly on the bent surface and on the effect of bending process along the depth of the test piece. The procedure is repeated for tests performed under other different circumstances, more precisely under different bending speeds.

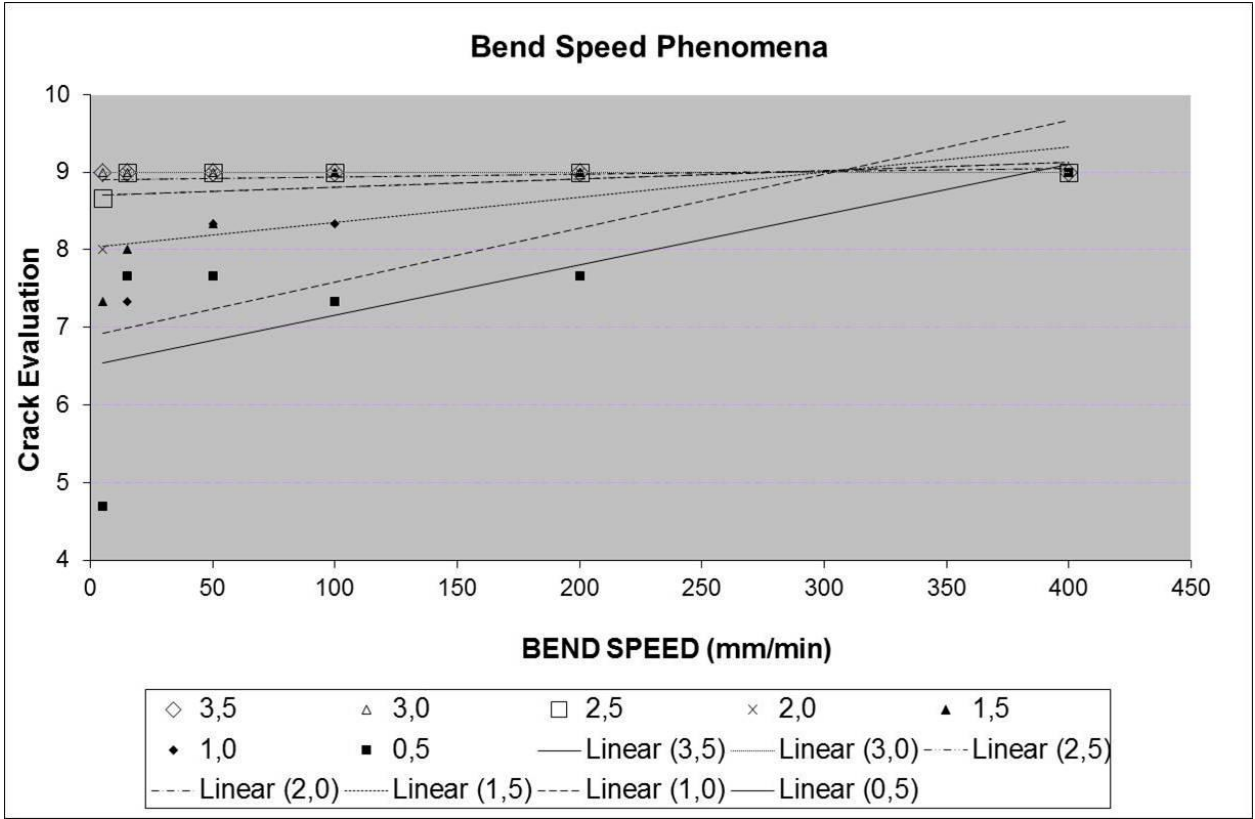
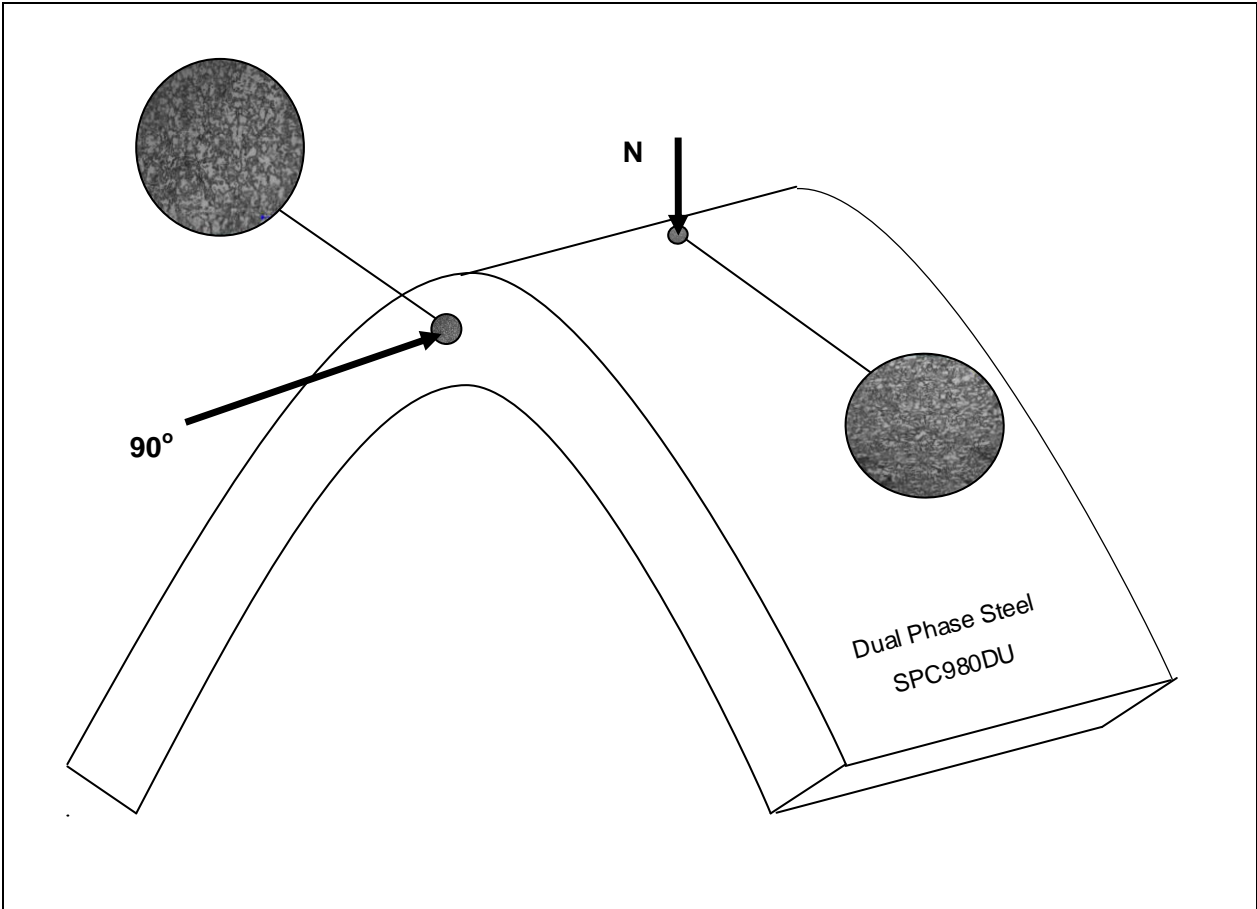


Figure 3.5 Crack evaluations under various bend speeds (Standard)

Basically, what is desired to be achieved by observing such pictures is to have a brief idea on the possible changes in the movement paths and their diverse behaviours under various speeds. The findings at the moment are left as they are until when they are to be discussed in detail in the following chapters where the phenomena occurring are combined with other aspects taken into consideration throughout this investigation.

As mentioned before, relevance of the images to the general outcome of the investigations is further to be investigated and discussed later on. Combining such data with other micro findings would be leading and it is of great importance to make sure to have enough technical understanding before to go ahead and end of with conclusions which may not be very accurate at this point.



**Figure 3.6 Microscope image planes**

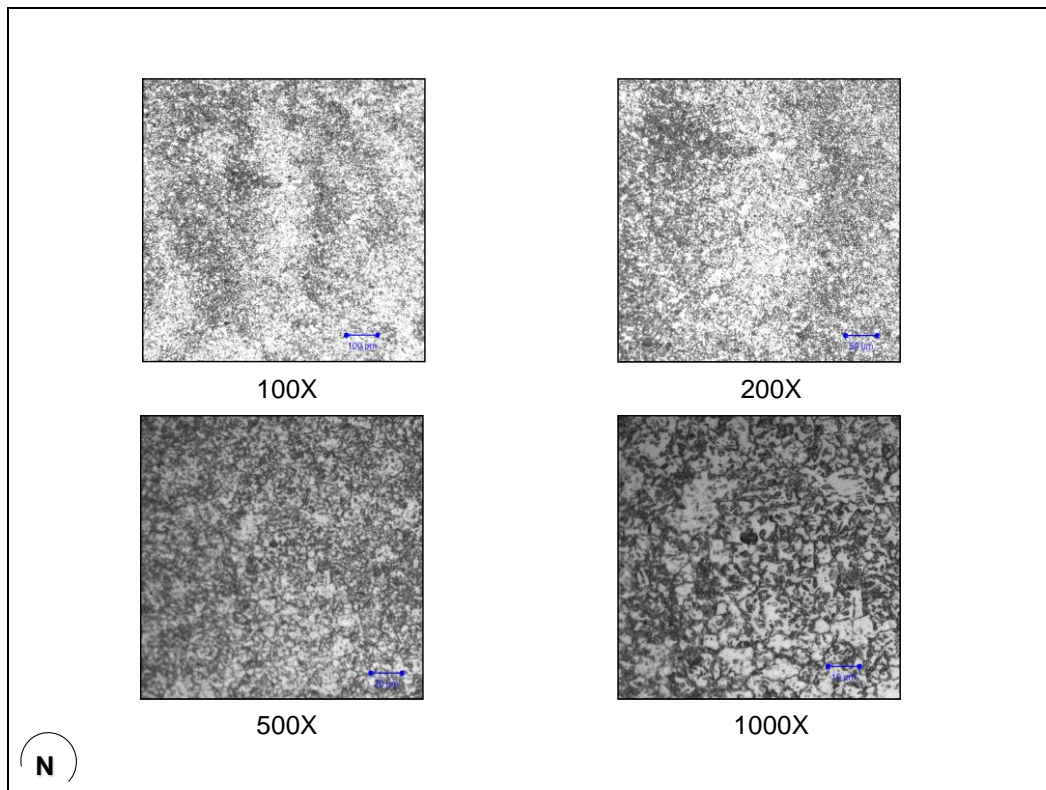


**Figure 3.7 Microscope image of a non-bent test piece (Top view)**

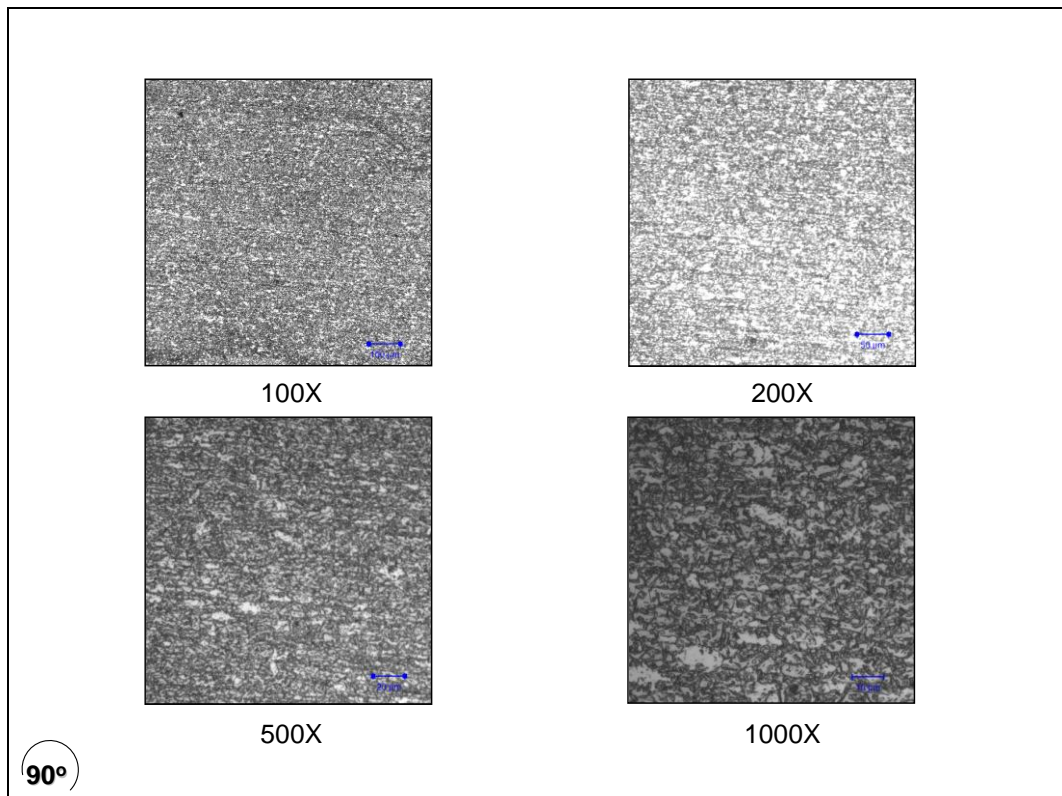


**Figure 3.8 Microscope image of a non-bent test piece (90°)**

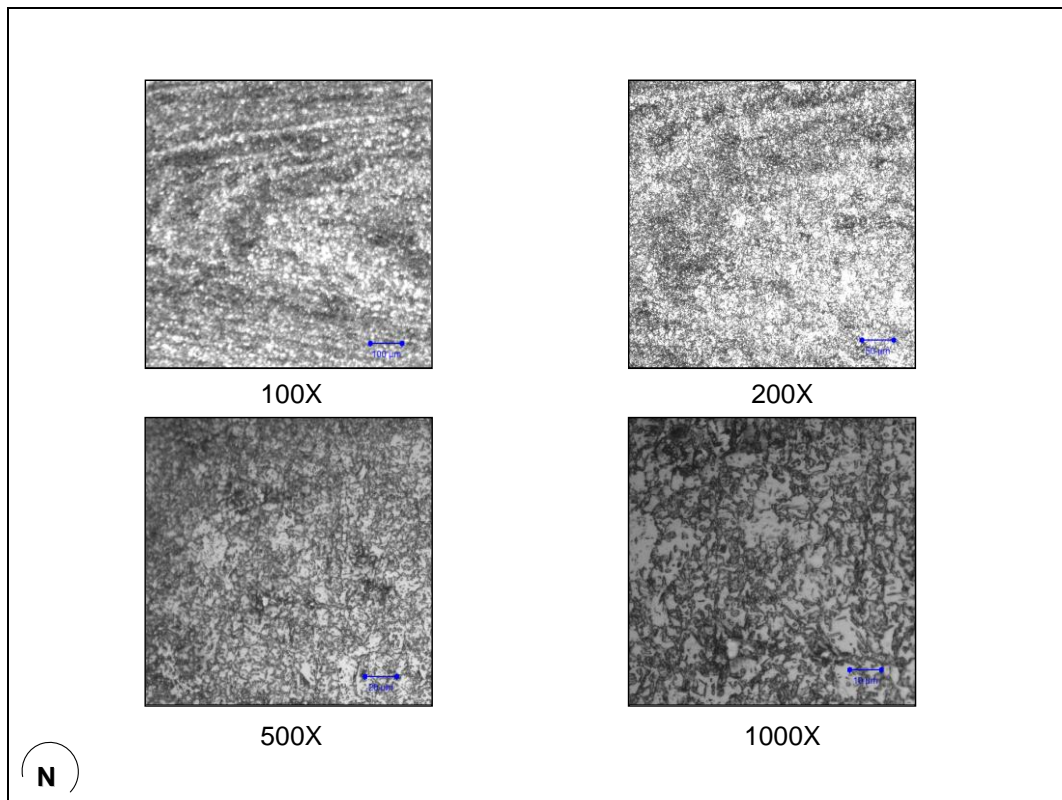


**Figure 3.9** Microscope image of a test piece bent with a speed of 1 mm/min (Top view)

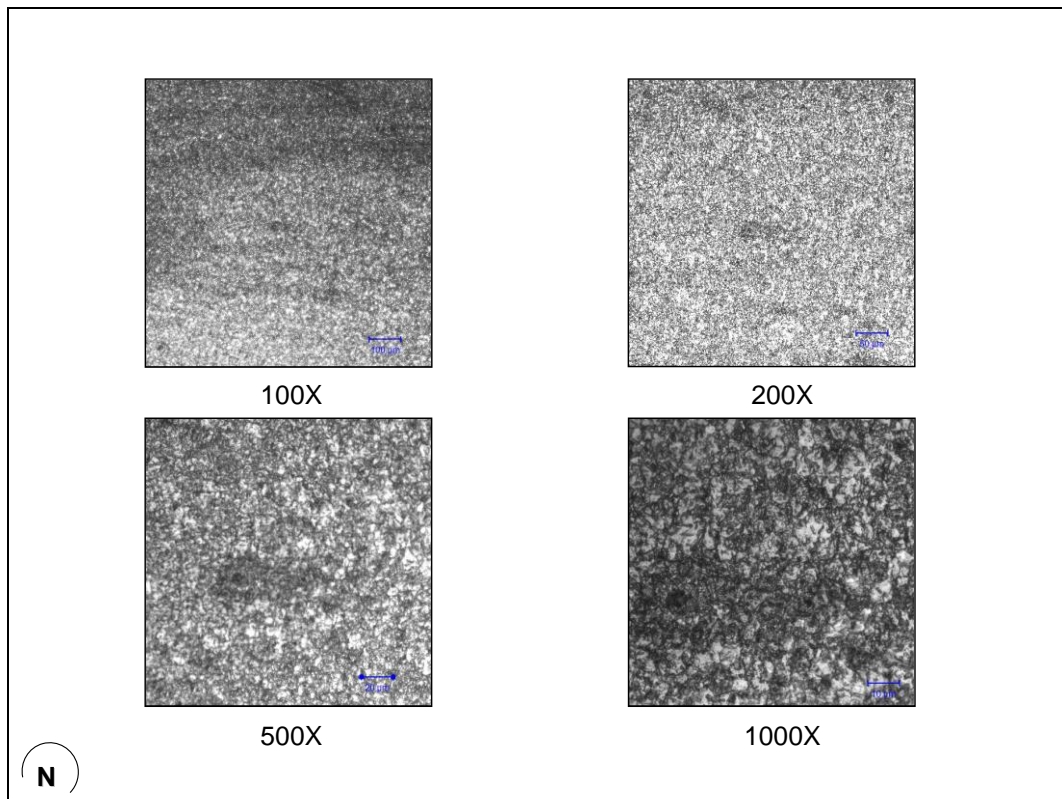


**Figure 3.10** Microscope image of a test piece bent with a speed of 15 mm/min (Top view)

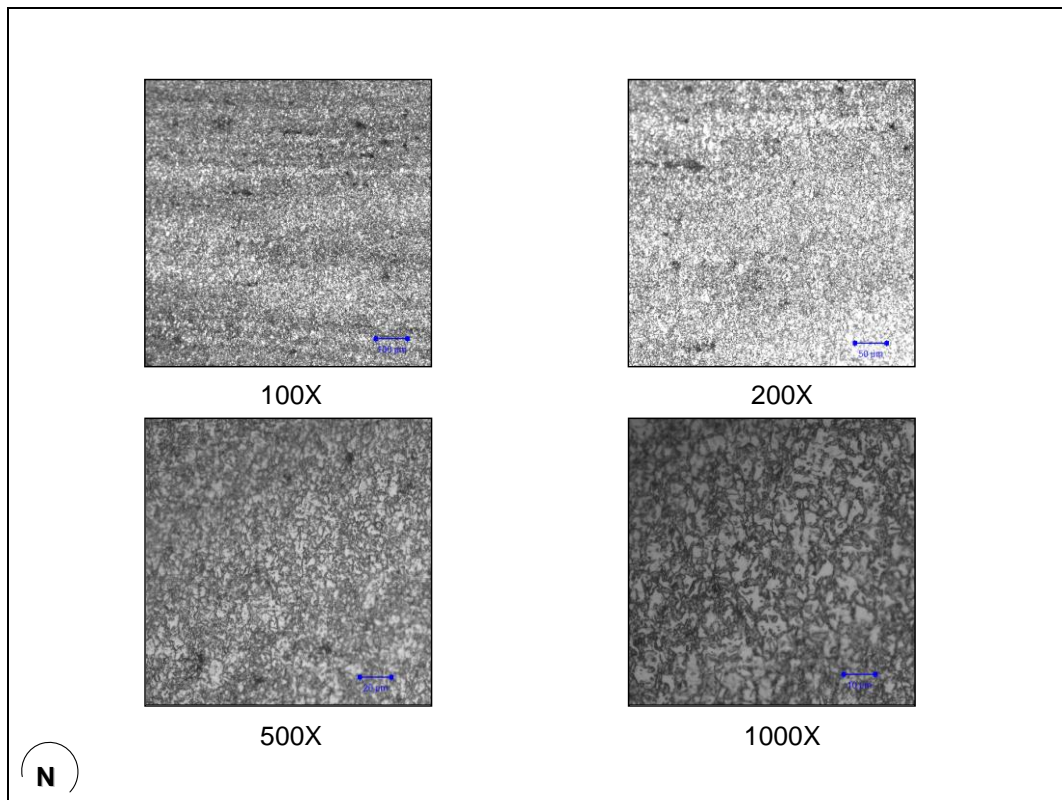


**Figure 3.11** Microscope image of a test piece bent with a speed of 400 mm/min (Top view)

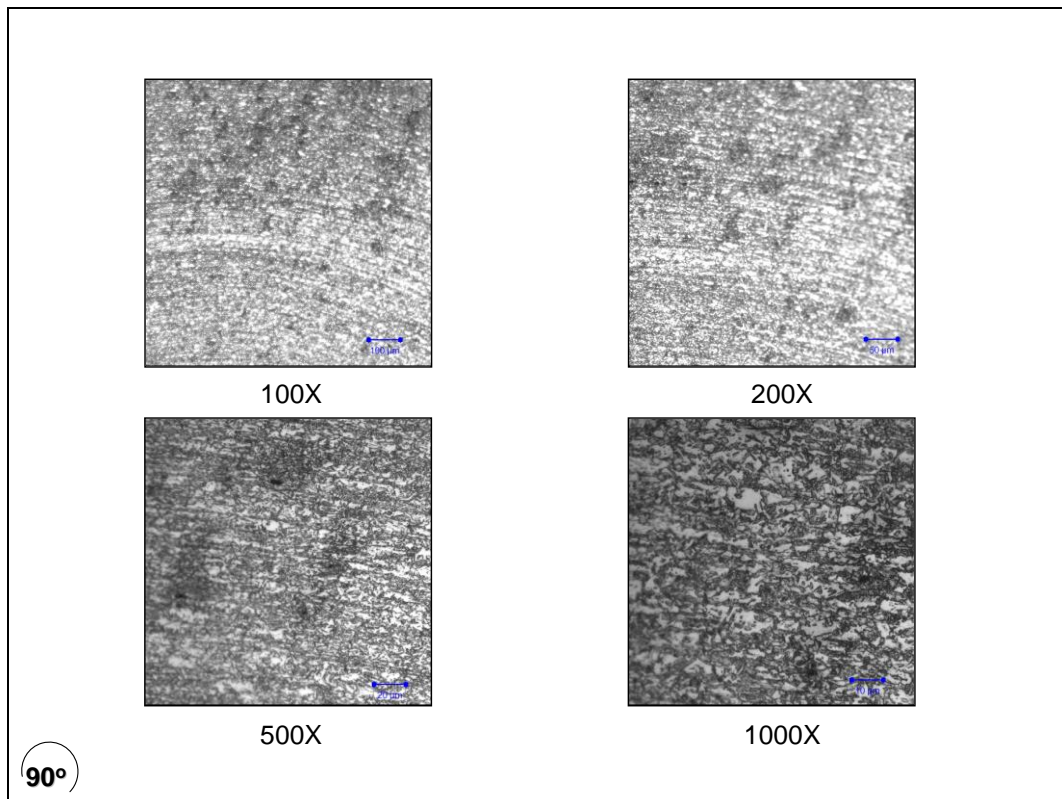


**Figure 3.12** Microscope image of a test piece bent with a speed of 1 mm/min (90°)

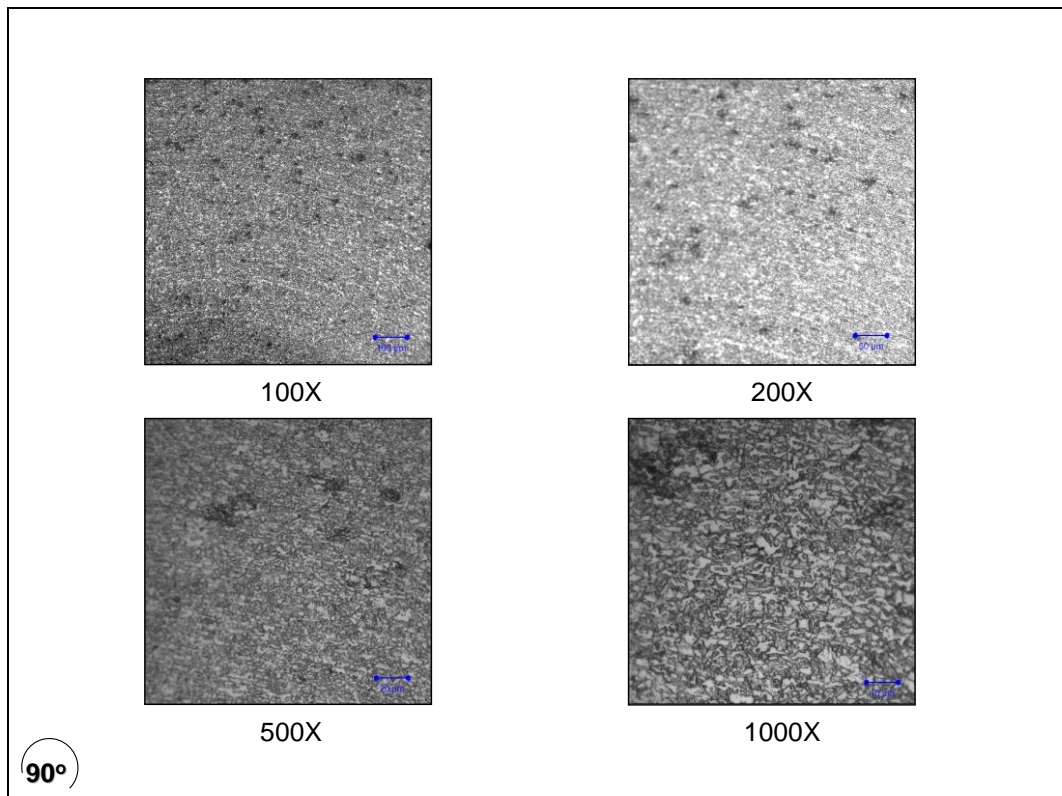


**Figure 3.13** Microscope image of a test piece bent with a speed of 15 mm/min (90°)

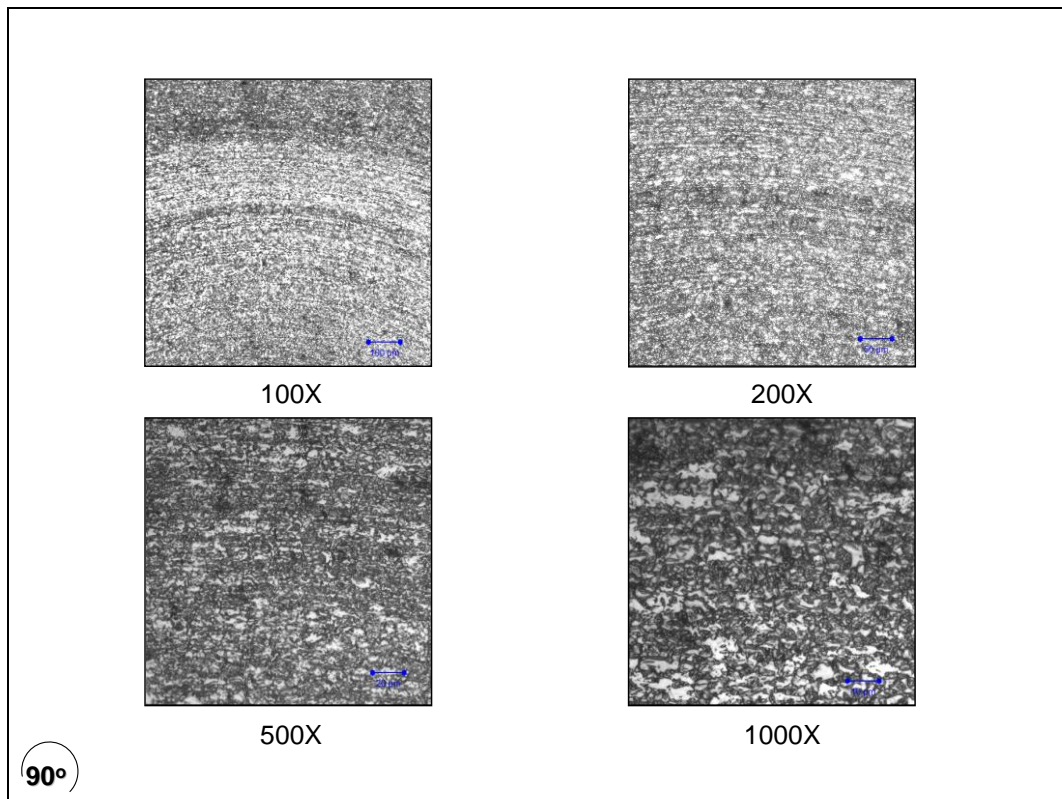


**Figure 3.14** Microscope image of a test piece bent with a speed of 400 mm/min (90°)



### 3.1.4 Sample Dimensions 100 mm X 35 mm; Burr Upside Down

In order to be able to understand if the position of burr has a direct or indirect effect on crack behaviour close to the edge portion and along the bent surface, relevant tests are performed turning the sample upside down prior to the bending operation. It was stressed beforehand that, due to the method applied to prepare the sample (shearing machine), the stresses that the test piece possess within are not expected to be homogeneously distributed throughout the material. The tests are applied only under bend radii and bend speeds where the test pieces had failed under previous standard conditions. The results concerning all trials are given in Table 3.3 and Figure 3.15 schematizes the results.

Sample Dimensions: 100 mm X 35 mm (BURR UPSIDE DOWN)													
R		5 mm/min			15 mm/min			50 mm/min			100 mm/min		
2,0		9	9	9									
1,5		8	9	8	9	9	9						
1,0		9	4	8	9	9	8	9	9	8			
0,5		9	4	4	9	4	4	9	9	4	8	9	8
R	AVG	5 mm/min			15 mm/min			50 mm/min			100 mm/min		
2,0	Average	9,0											
1,5	Average	8,3			9,0								
1,0	Average	7,0			8,7			8,7					
0,5	Average	5,7			5,7			7,3			8,3		

**Table 3.3 Crack evaluation results (Burr upside down)**

It is observed that, the results are rather satisfying compared to the tests run under standard conditions. Table 3.3 shows that, although the test results were not OK except the one performed under  $R = 2.0$  and  $R = 1.5$ , when the burr is positioned upside down, the average results are more satisfying. Another important point that should be taken into consideration is that there is a rather more obvious change in the range of results obtained especially around the lower left hand side of the table, which resembles small bend radius and slow speed. In other words, the material tends to crack almost severely or preserves its well-being even under “defined as severe” conditions according to previous leading tests. A smooth transition between an OK and NG results is less likely to occur. It could reveal some important aspects regarding the residual stress distributions around the edge portion and they are to be examined more thoroughly later on, together with the rest of the data we seek to make healthier judgements.

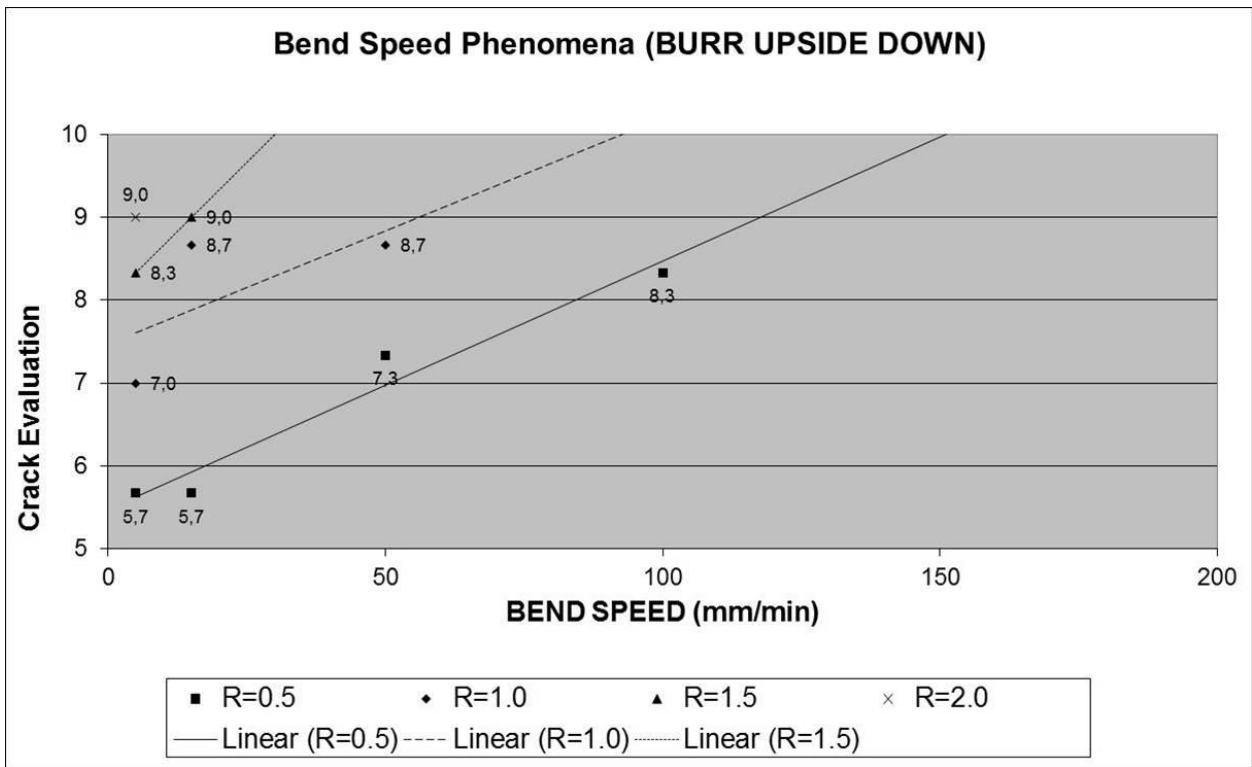


**Figure 3.15 Crack evaluations under various bend speeds (Burr upside down)**

Another issue that has to be underlined at this very point would regard the change in the quantity and the quality of crack observed around the edge portion which, according to our observations, doesn't have a direct effect on the crack evaluation along the bent portion unless they reach out up to a certain point along the middle section. Still, there may be some indirect relation between such cracks and their general behaviour along the bending axis. The possible reasons and effects on the full picture are to be discussed.

### 3.1.5 Sample Dimensions 100 mm X 35 mm; Grinded

Investigations are taken to a further step by performing various tests for which test pieces were grinded on the edges to remove stress inhomogeneity due to different cutting operation performed by the shearing machine. Parameter wise, the procedure as in the testing of upside down samples is followed. The crack evaluation results are given in Table 3.4 and Figure 3.16

As clearly observed, the results obtained for grinded samples are even better in terms of crack resistance. Unlike the "burr upside down" condition more than one OK result is obtained within the range where the results were NG under standard parameters. The trend which is thought to exist continues to prove itself correct since, as the speed and radius decrease, cracks tend to occur

more frequently along the bent surface. Cracks don't seem to have a strict range as in the previous "burr upside down" condition meaning that severity of cracks are less and rather without any sign of an obvious jump between the OK condition and the NG condition.

Sample Dimensions: 100 mm X 35 mm (GRINDED)													
R		5 mm/min			15 mm/min			50 mm/min			100 mm/min		
2.0		9	9	9									
1.5		9	9	9	9	9	9						
1.0		9	9	8	9	9	9	9	9	9			
0.5		8	8	5	9	9	7	9	9	5	9	9	

R	AVG	5 mm/min	15 mm/min	50 mm/min	100 mm/min
2.0	Average	9,0			
1.5	Average	9,0	9,0		
1.0	Average	8,7	9,0	9,0	
0.5	Average	7,0	8,3	7,7	8,7

Table 3.4 Crack evaluation results (Grinded)

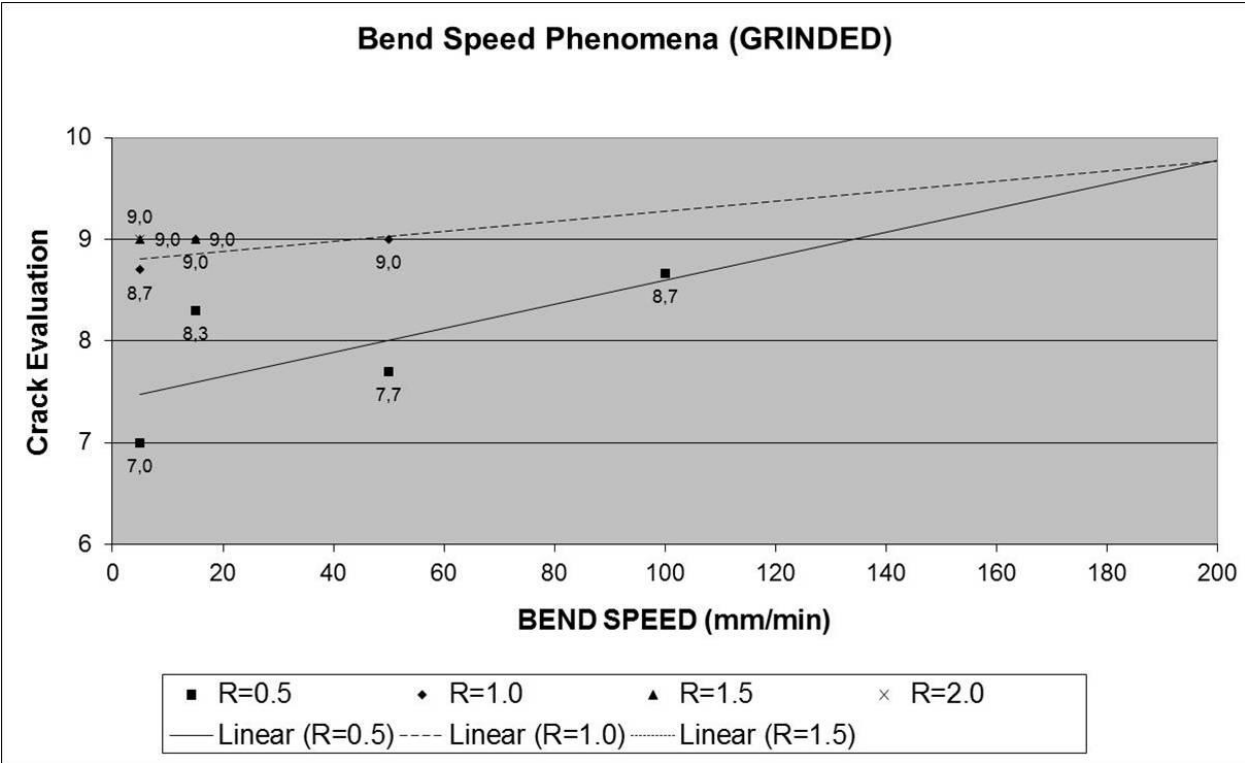


Figure 3.16 Crack evaluations under various bend speeds (Grinded)

In general, resistance to crack occurrence is clearly higher compared to those of standard and "upside down" conditions. Therefore, it may easily be suggested that removing the stress on the

edge portion has a positive effect on the crack resistance that the material acquires. This insight, as well, will further be discussed shortly.

### 3.1.6 Sample Dimensions 100 mm X 100 mm

The assumption that sample dimensions may have an effect on macro crack behaviour observed brings with itself the necessity of performing tests to further investigate such circumstances. Standard parameters remain as they are and various tests are performed under conditions which failed to demonstrate a sufficient resistance against cracking when main parameters concerning speed, radius and dimensions are taken into consideration. The results are shared in Table 3.5 and Figure 3.17.

Sample Dimensions: 100 mm X 100 mm													
R		5 mm/min			15 mm/min			50 mm/min			100 mm/min		
2.0		9	9	9									
1.5		9	9	9	9	9	9						
1.0		9	9	9	9	9	9	9	9	9			
0.5		7	9	6	8	8	8	9	9	7	9	9	
R	AVG	5 mm/min			15 mm/min			50 mm/min			100 mm/min		
2.0	Average	9,0											
1.5	Average	9,0			9,0								
1.0	Average	9,0			9,0			9,0					
0.5	Average	7,3			8,0			8,3			9,0		

**Table 3.5 Crack evaluation results (Sample Dimensions 100 X 100)**

### 3.1.7 Dimension Variations

In order to be able to accurately investigate the relation between the dimensions and the crack behaviour, tests are repeated under various dimensions. Bending speed is taken as 15 mm/min, which is the standard bending speed. First the 3 trial standard applied and a proportional correlation is not observed as in the previous sections. To be sure of the trend 6 trial tests are performed under same parameters and the results are given in Table 3.6, Figure 3.18, Table 3.7 and Figure 3.19 respectively.

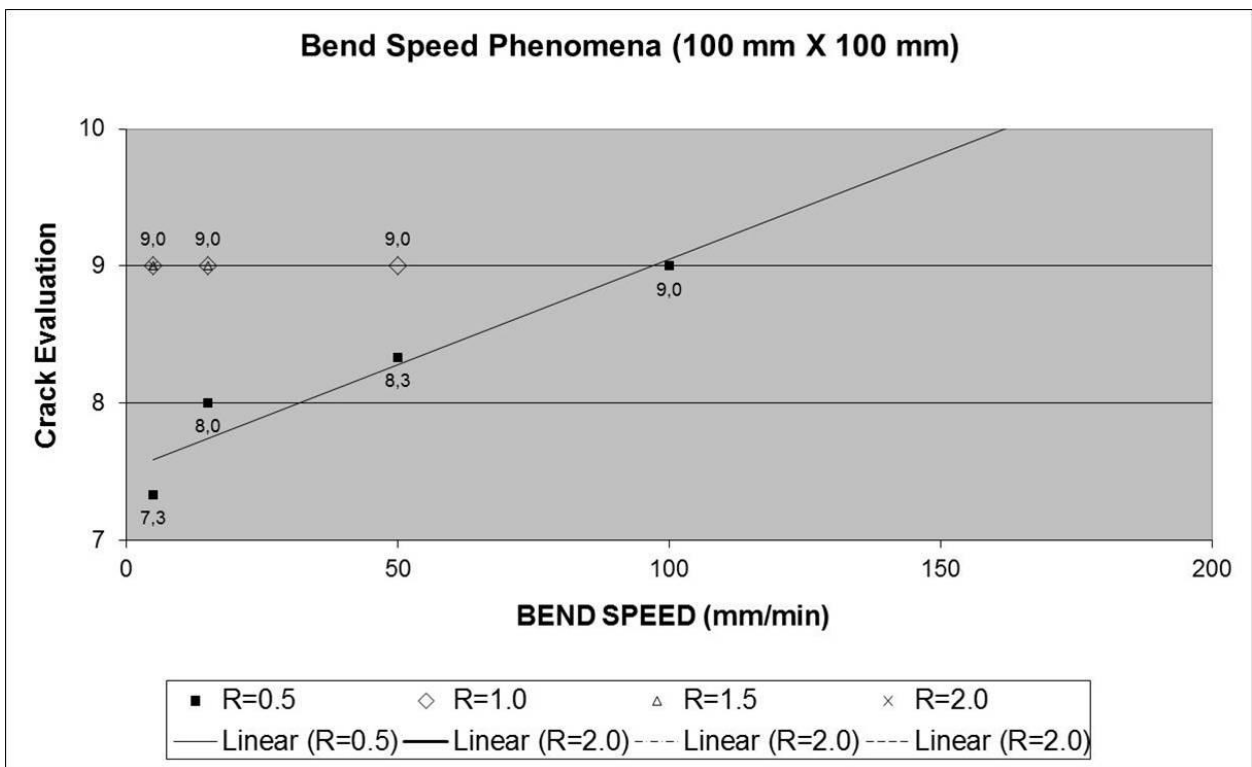


**Figure 3.17 Crack evaluations under various bend speeds (Sample Dimensions 100 X 100)**

It is observed that, instead of a proportional relation between the crack behaviour and sample width, there is a trend that tends to change its character along the line. Under narrow widths, crack resistance for the given parameters tends to increase with respect to a certain width. The lowest crack resistance for each bend radius taken into consideration is recorded around 50-60 mm of width after which the resistance seems to be increasing again. Since it was an unexpected behaviour, trial numbers were increased to make sure that some systematic or human errors tricks the observant into making misleading judgements. Despite slightly shifting its lowest point for the lowest bend radius, the same behaviour is repeated. Henceforth, the assumption and the statement given above can be considered as fairly accurate.

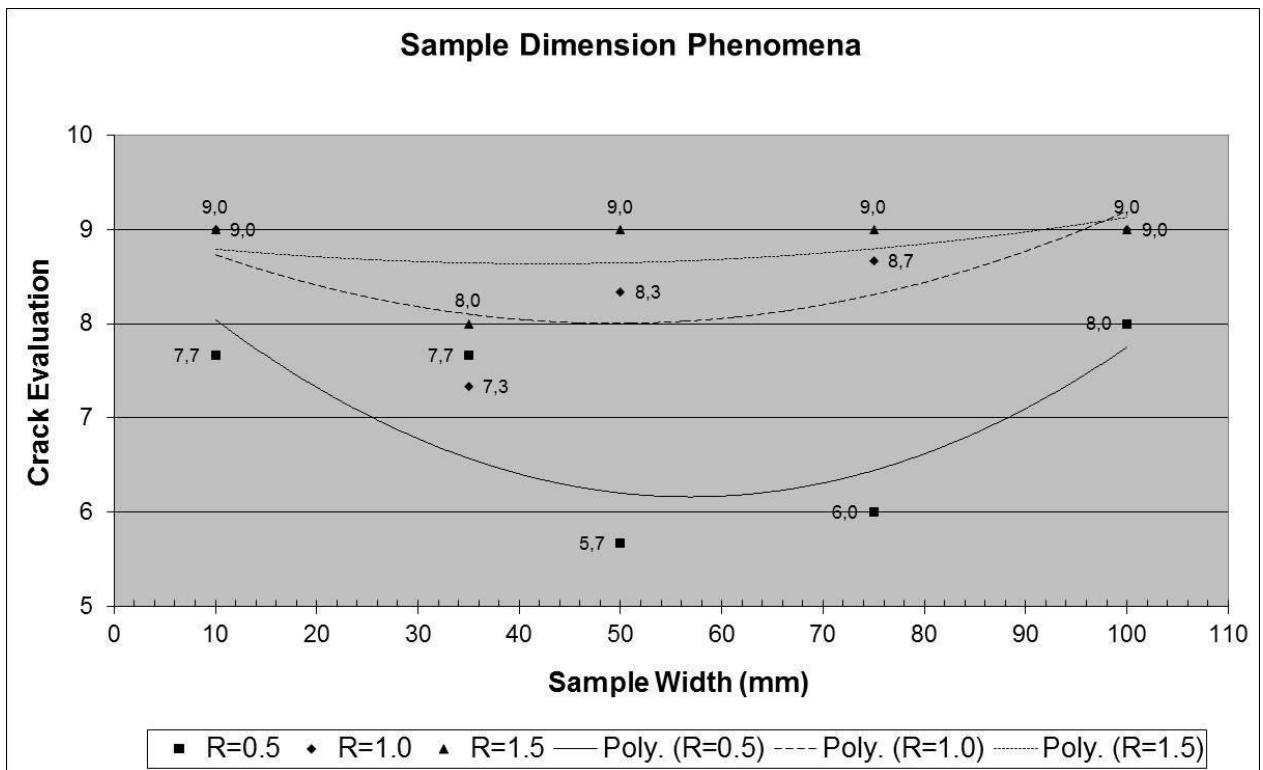
Evaluating the data obtained, it is more to possible to also claim that crack resistance increases with increasing bend radius.

Bend Speed: 15 mm/min (3 Trials)																
R		100 mm X 10 mm			100 mm X 35 mm			100 mm X 50 mm			100 mm X 75 mm			100 mm X 100 mm		
1,5		9	9	9	7	9	9	9(8)	9	9	9	9	9	9	9	9
1,0		9	9	9	6	8	8	8	8	9	9	9	8	9	9	9
0,5		5	9	9	7	8	8	4	9	4	3	9	6	8	8	8
R	AVG	100 mm X 10 mm			100 mm X 35 mm			100 mm X 50 mm			100 mm X 75 mm			100 mm X 100 mm		
1,5	Average	9,0			8,3			9,0			9,0			9,0		
1,0	Average	9,0			7,3			8,3			8,7			9,0		
0,5	Average	7,7			7,7			5,7			6,0			8,0		

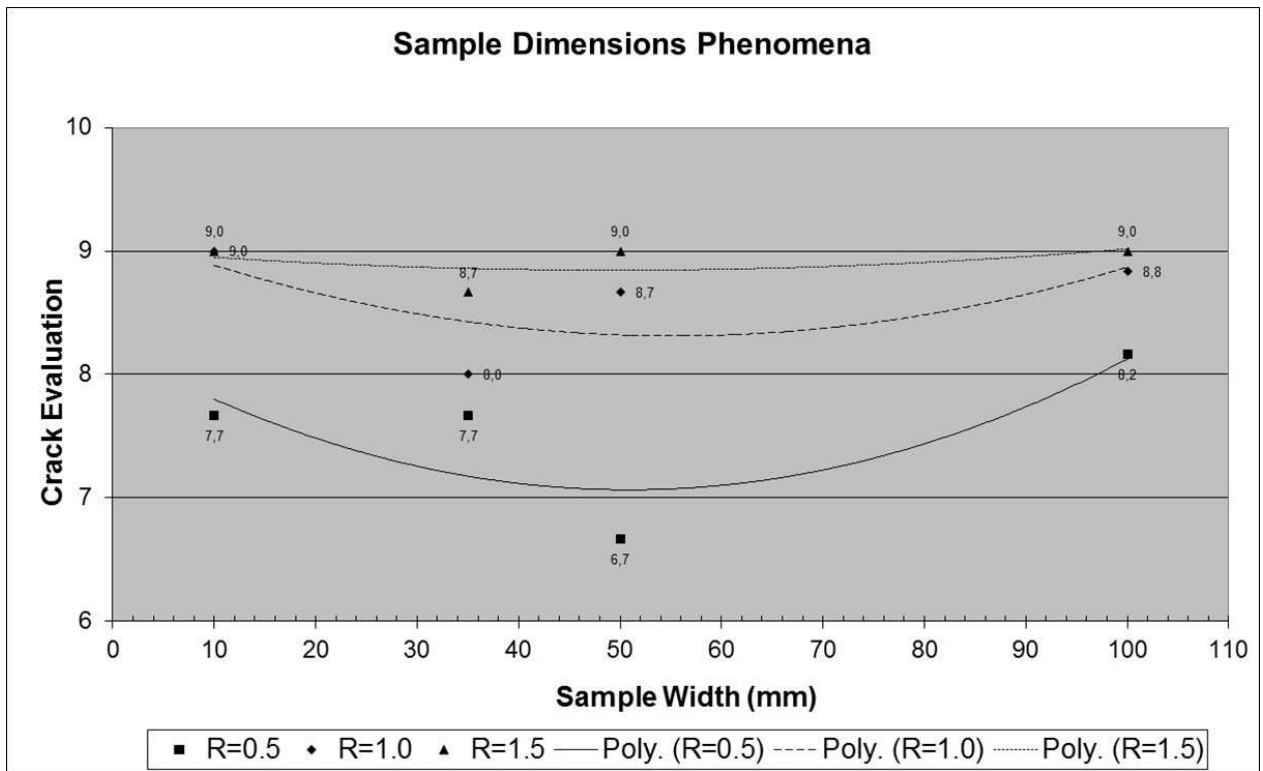
  

Bend Speed: 15 mm/min (6 Trials)																
R		100 mm X 10 mm			100 mm X 35 mm			100 mm X 50 mm			100 mm X 75 mm			100 mm X 100 mm		
1,5		9	9	9	9	9	9	9	9	9	9	9	9	9	9	9
1,0		9	9	9	6	8	8	8	8	9	9	9	8	9	9	8
0,5		5	9	9	6	8	7	5	4	9	3	9	6	4	5	8
R	AVG	100 mm X 10 mm			100 mm X 35 mm			100 mm X 50 mm			100 mm X 75 mm			100 mm X 100 mm		
1,5	Average	9,0			8,7			9,0			9,0			9,0		
1,0	Average	9,0			8,0			8,7			8,7			8,8		
0,5	Average	7,7			7,7			6,7			5,8			8,2		

**Table 3.6 Crack evaluation results (Various sample dimensions, 3 trials)**



**Figure 3.18 Crack evaluations under various sample dimensions (3 trials)**



**Figure 3.19 Crack evaluations under various sample dimensions (6 trials)**

### 3.1.8 Load vs. Extension Curves

While the V bend test was being performed, the relation between the load applied and extension was recorded simultaneously. The aim is to see if there may be found a correlation between the relevant parameters, under various conditions. To obtain the curves, samples having standard dimensions (100 mm X 35 mm) are taken and test are repeated under different bend speeds. Bend radius is taken as 2.0 at all times.

Evaluating the data obtained, it is observed that, despite the fact that there are some obvious slight changes under extended scales, they are still far from being concrete in the sense that the distinguishment is not enough to be able to make a certain judgement regarding such behaviours and their effects on macro cracks along the bent portion of the steel. Although some clear relations between crack evaluation and bending speed was previously observed, there doesn't seem to be direct effect of bending speed on the load path of CR 980 DP.

## 3.2 Hardness Measurements

Next step is to perform some hardness test to be able to judge if the material demonstrates different reactions under various parameters by means of its hardness. Figure 3.20 schematizes the procedure followed to run such tests. Bend radius is chosen as 2.0 for all samples whereas the bending speed varies. Tests were performed under each bend speed that is subject to our investigation. A standard Vickers Hardness Tester is used for the hardness tests. In order to distinguish slight differences between the values within and between the samples, load is kept as down as to 3 kg and the dwelling time is 5 seconds. The results obtained are given below in Table 3.7.

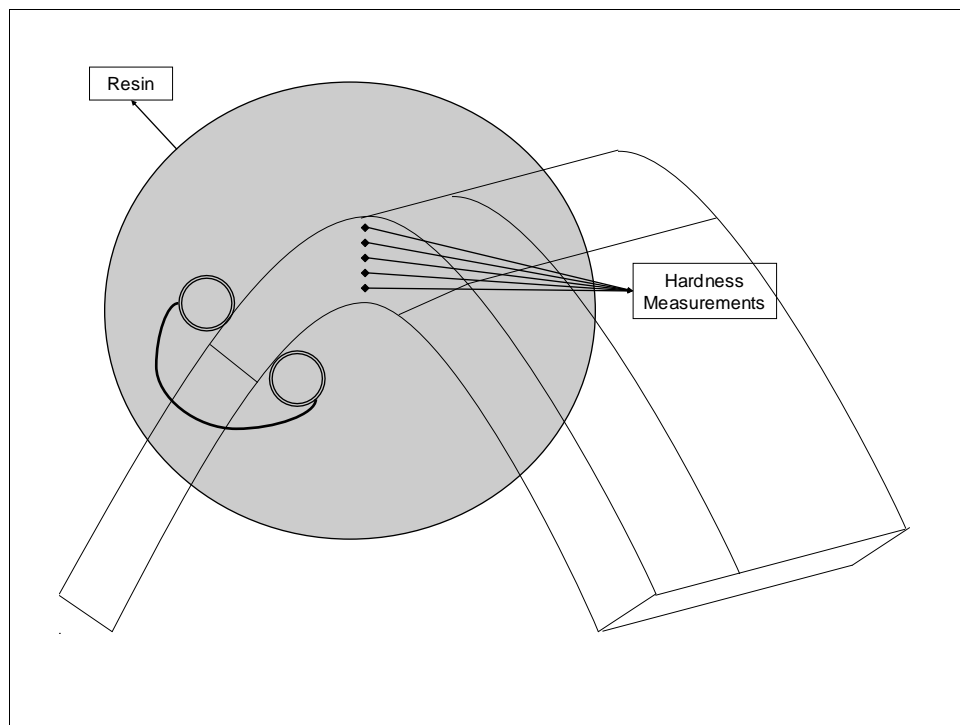


**Figure 3.20 Schematic representation of hardness test set up (Materialwise)**

Figure 3.21 schematizes the hardness distributions along the depth. An obvious trend observed is that the hardness values are measured to be higher as the indentation gets closer to the top and bottom surfaces, whereas, the hardness values are recorded slightly but clearly less in the middle zone.



VICKERS HARDNESS (LOAD = 3kg; DWELL TIME = 5 seconds; R = 2 mm)									
Depth (mm)	0.30			0.65			0.95		
Bend Speed (mm/min)	Test #1	Test #2	Test #3	Test #1	Test #2	Test #3	Test #1	Test #2	Test #3
5	394,5	395,8	398,2	329,4	327,4	329,4	378,7	376,6	380,0
15	397,5	398,5	398,9	342,0	342,8	347,1	372,3	376,2	377,8
50	386,7	380,0	385,4	347,7	350,4	354,4	373,5	375,6	376,2
100	388,3	394,8	389,9	339,6	344,4	338,5	372,3	366,2	371,9
200	376,6	380,3	379,4	331,2	335,1	334,3	388,0	386,7	381,2
400	392,2	390,2	393,5	353,5	357,5	356,1	384,7	381,6	380,6
15 (R = 0.5)	371,8	371,0	369,8	344,7	349,3	351,5	361,5	368,0	361,8

Depth (mm)	0.30	0.65	0.95
Bend Speed (mm/min)	Average	Average	Average
5	396,2	328,7	378,4
15	398,3	344,0	375,4
50	384,0	350,8	375,1
100	391,0	340,8	370,1
200	378,8	333,5	385,3
400	392,0	355,7	382,3
15 (R = 0.5)	370,9	348,5	363,8

Table 3.7 Vickers hardness measurements

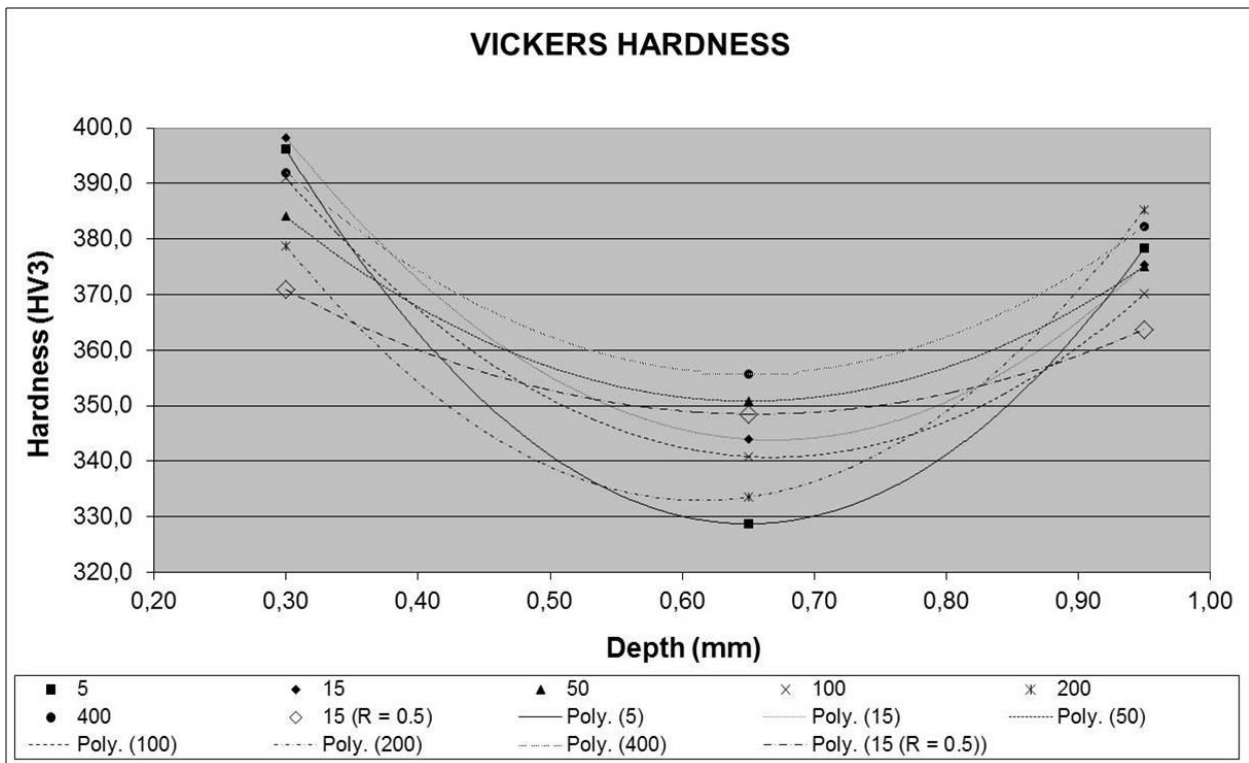
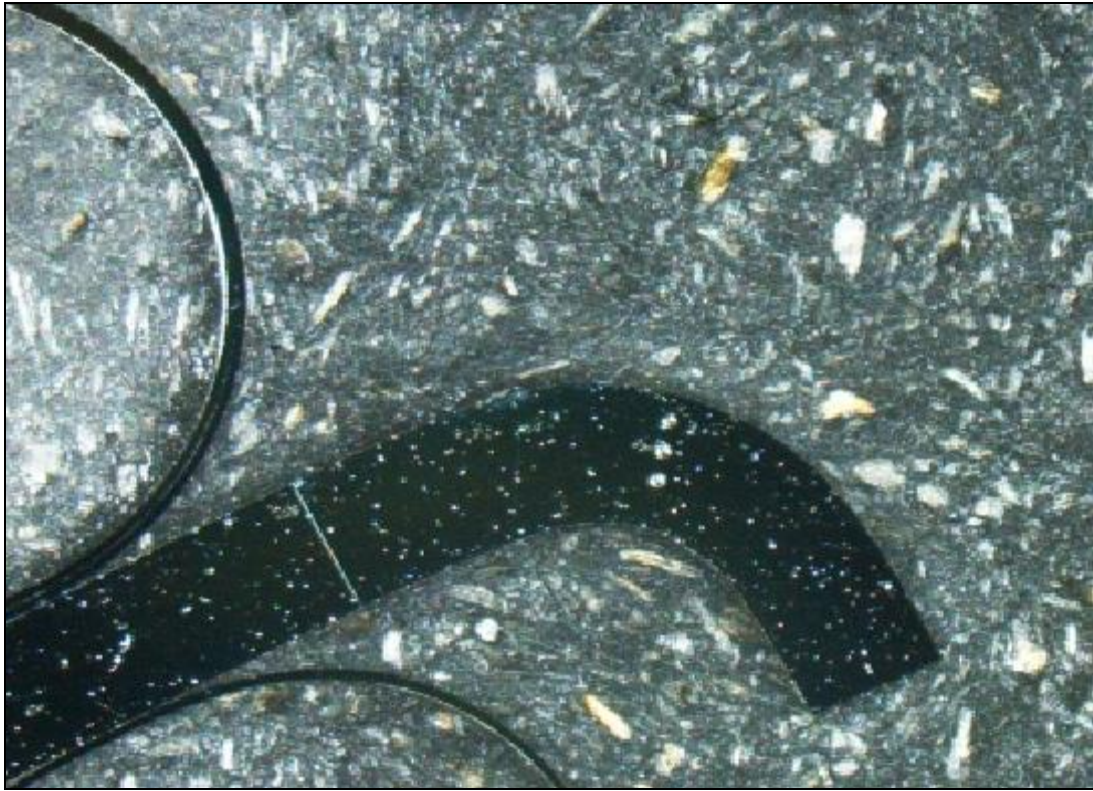


Figure 3.21 Hardness distributions along the depth



**Figure 3.22 Microscope image of hardness test set up (Materialwise)**

Again looking at Figure 3.21 the general trend applies to all samples bent under different bending speeds but claiming that there is a unique behaviour for each bending speed would be quite unfair. As mentioned before, the magnitudes of the indentations are kept low on purpose in order to be able to increase the possibility of a leading distinguishment. Still, tests that were performed weren't sensitive enough to make a promising judgement in that sense. Further investigation on hardness will be taken into consideration in the next section where the main focus is micro behaviours concerning the dual phase steel.

Figure 3.22 and Figure 3.23 show images of indentations and their positioning under high magnifications. A more through approach regarding the hardness phenomena will be held in the conclusion part, together with other findings.

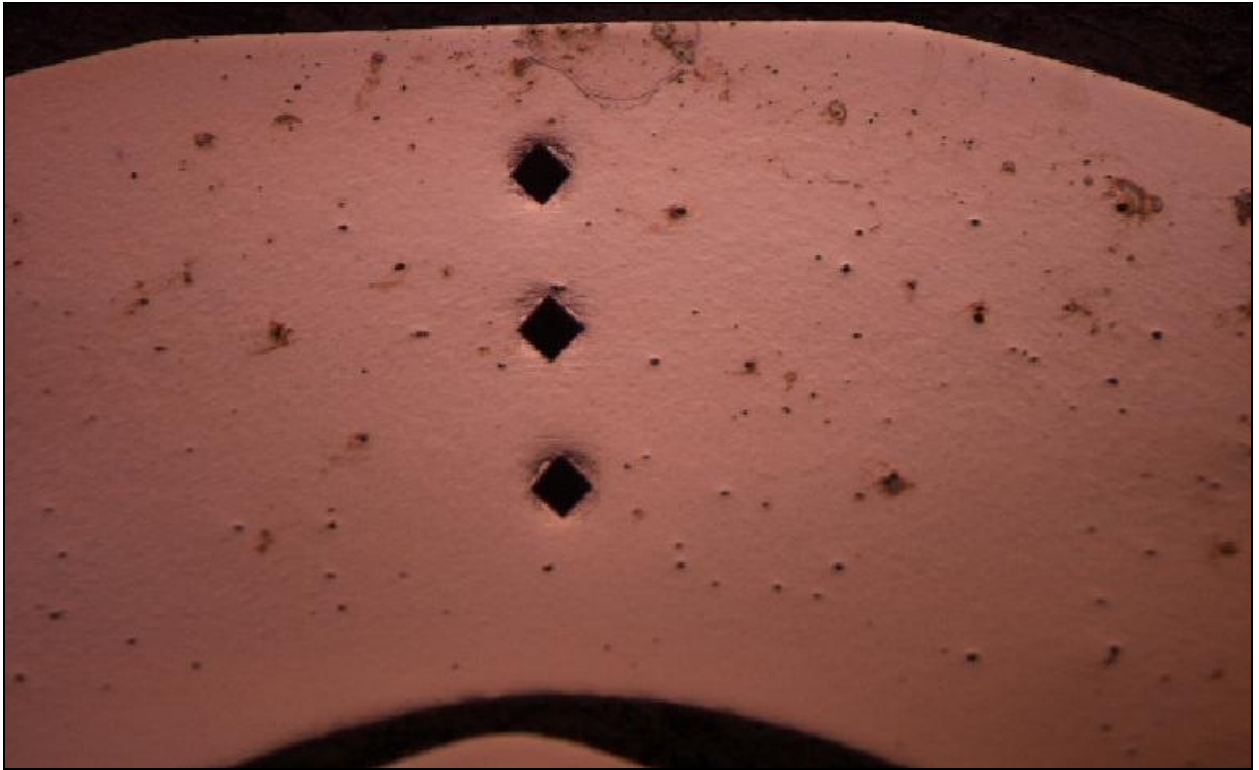


**Figure 3.23 Microscope image of indentations and their positioning with respect to each other and the test piece (Thickness = 1.4 mm)**

### 3.3 XRD Residual Stress Measurements

The definition and basic principles of the process was briefly explained previously in the relevant section. To combine the findings of the first part regarding the V bend test, micro stresses were to be investigated in order to develop a further understanding of the behaviours demonstrated under various bending parameters and sample dimensions. Localised stresses and their distribution trend would, therefore, be investigated in more detail. Due to technical and time restrictions, residual stress measurements were unable to be performed in this investigation by all means.

Therefore, in this section, the methods which should have been followed and the details of the measurements that had been set to achieve are shared together with the results of the tests performed so far. Initial findings are taken into consideration to make the reader understand the nature of residual stress investigations and what kind of results we are and we should be expecting to get later on in order to demonstrate a better understanding of the concept and its relation with the optimization phenomena that has been investigated throughout this study.

Table 3.8, Table 3.9 and Figure 3.24, Figure 3.25 and Figure 3.26 show the results of preliminary internal stress measurements performed for the bent surface and the dull one. When data is analysed, taking the stress components and their directions into consideration, it is understood that the compression stress due to the sprinback effect of the material turns out to be relatively high. Tension stress is found to be 610 MPa for the bent surface and 308 MPa for the dull CR 980 DP. The internal stresses recorded within the dull material are mainly introduced during the steel sheet production. Figure 3.29 indicates 2 single points of measurement in order to make a comparison between the internal stresses on the bent surface and on the dull material. The stress tensors of bent and dull surfaces are given also in Figure 3.28, together with directions of stresses and detailed explanation on initial findings. Having an insight on the residual stress phenomena (please refer to 2.3), the difference between the stress values of bent and non-bent sections opens a path of further investigations since the sensitivity of the measurements seem to be quite able to point out different characteristics demonstrated under various parameters as discussed before. It is obvious that bending process introduces a relatively high amount of additional internal stresses to the material. The extent of such stress is likely to depend on the bending conditions. Matters concerning the processing of further data on the issues previously underlined will be discussed shortly and an appropriate set of steps for future contribution will be proposed.

Normal and shear calculations - elliptical fit						
	Phi = 0		Phi = 45		Phi = 90	
<i>Threshold</i>	<i>Normal (Mpa)</i>	<i>Shear (Mpa)</i>	<i>Normal (Mpa)</i>	<i>Shear (Mpa)</i>	<i>Normal (Mpa)</i>	<i>Shear (Mpa)</i>
Slid.Grav. 10%	-377	56	-426	61	510	41
Slid.Grav. 20%	-486	61	-305	52	333	23
Slid.Grav. 30%	-691	62	-150	48	227	18
Slid.Grav. 40%	-686	63	-52	42	197	18
Slid.Grav. 50%	-730	65	-54	40	133	19
Slid.Grav. 60%	-778	66	-46	41	-10	22
Slid.Grav. 70%	-758	66	-69	44	-28	29
Slid.Grav. 80%	-728	62	-184	44	39	27
Gravity 30%	-591	62	-150	48	227	18
Fit	-569	60	-216	49	245	23
Average Gravity	-598	61	-187	46	224	21

Table 3.8 Normal and shear calculations – elliptical fit (bent surface)

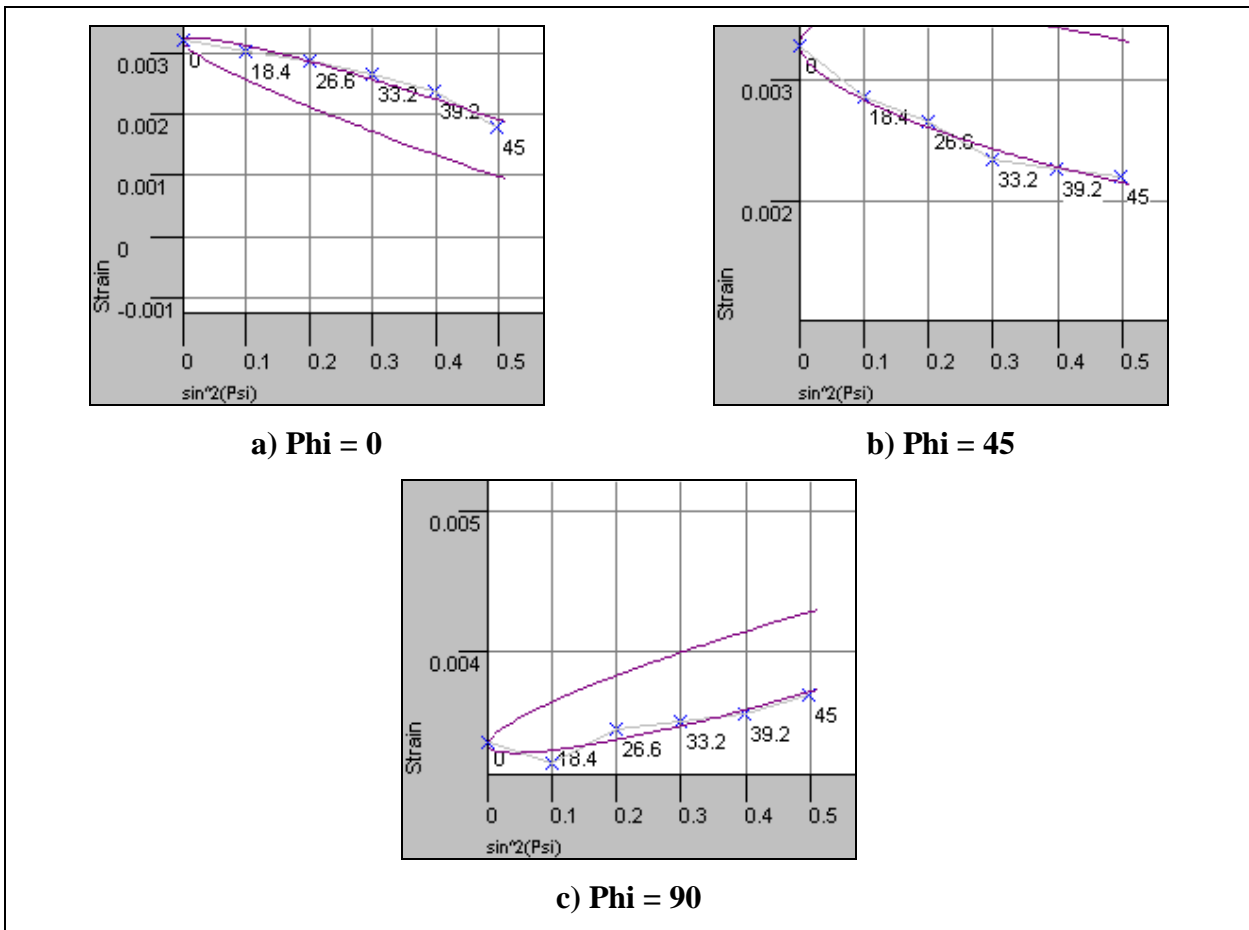


Figure 3.24 d vs.  $\sin^2\psi$  plots of CR 980 DP (bent) for a) phi = 0 b) phi = 45 c) phi = 90

Normal and shear calculations - elliptical fit						
Threshold	Phi = 0		Phi = 45		Phi = 90	
	Normal (Mpa)	Shear (Mpa)	Normal (Mpa)	Shear (Mpa)	Normal (Mpa)	Shear (Mpa)
Slid.Grav. 10%	-415	8	-371	-17	-171	-28
Slid.Grav. 20%	-376	-2	-313	-39	-158	-13
Slid.Grav. 30%	-306	-26	-325	-15	-125	-11
Slid.Grav. 40%	-239	-40	-318	-14	-112	-7
Slid.Grav. 50%	-243	-35	-315	-14	-143	7
Slid.Grav. 60%	-287	-21	-302	-18	-147	9
Slid.Grav. 70%	-341	-8	-321	-8	-104	-16
Slid.Grav. 80%	-389	13	-288	-8	-59	-25
Gravity 30%	-306	-26	-325	-15	-125	-11
Fit	-358	-6	-307	-23	-175	3
Average Gravity	-317	-19	-321	-21	-135	-10

Table 3.9 Normal and shear calculations – elliptical fit (dull material)

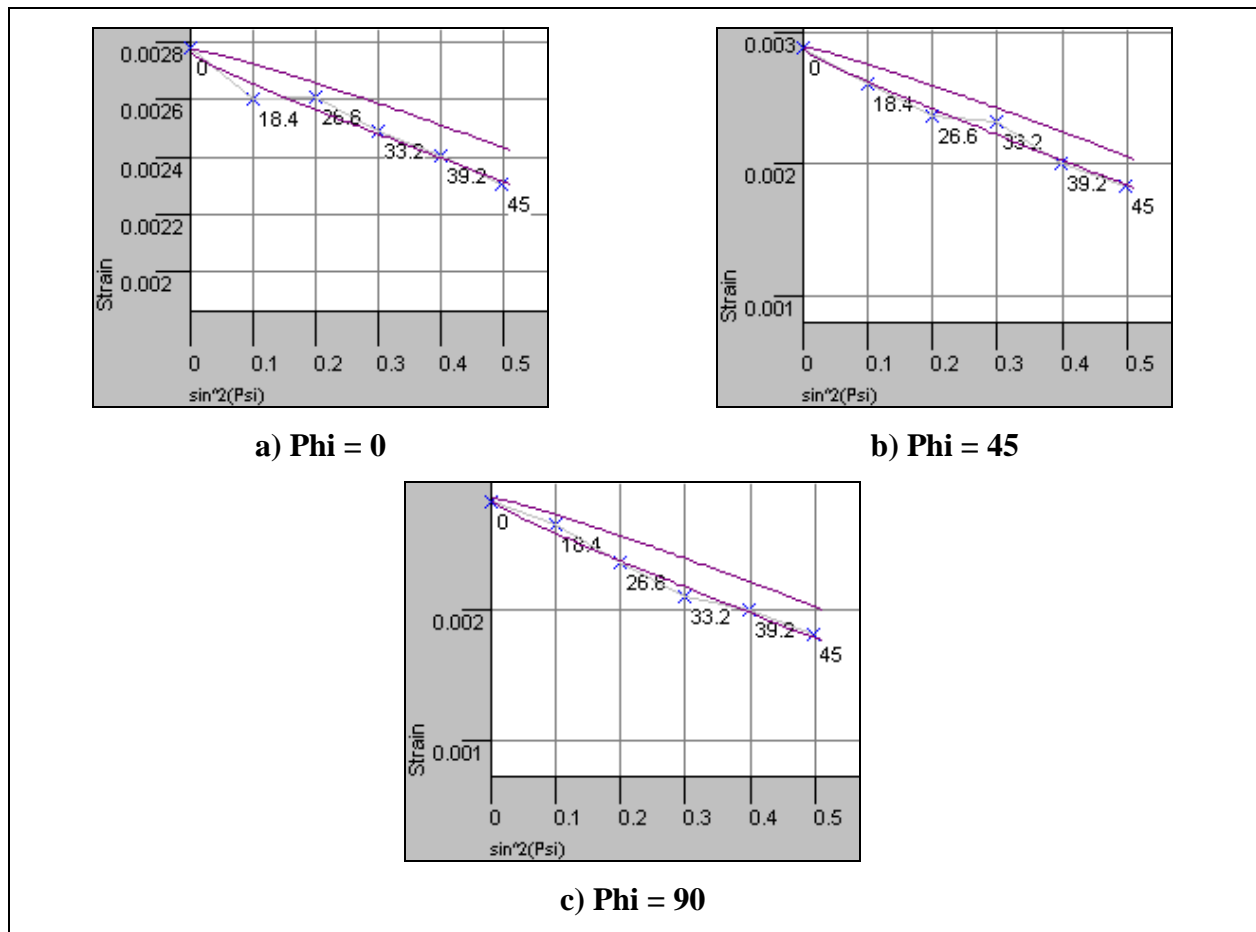


Figure 3.25 d vs.  $\sin^2\psi$  plots of CR 980 DP (dull) for a)  $\phi = 0$  b)  $\phi = 45$  c)  $\phi = 90$

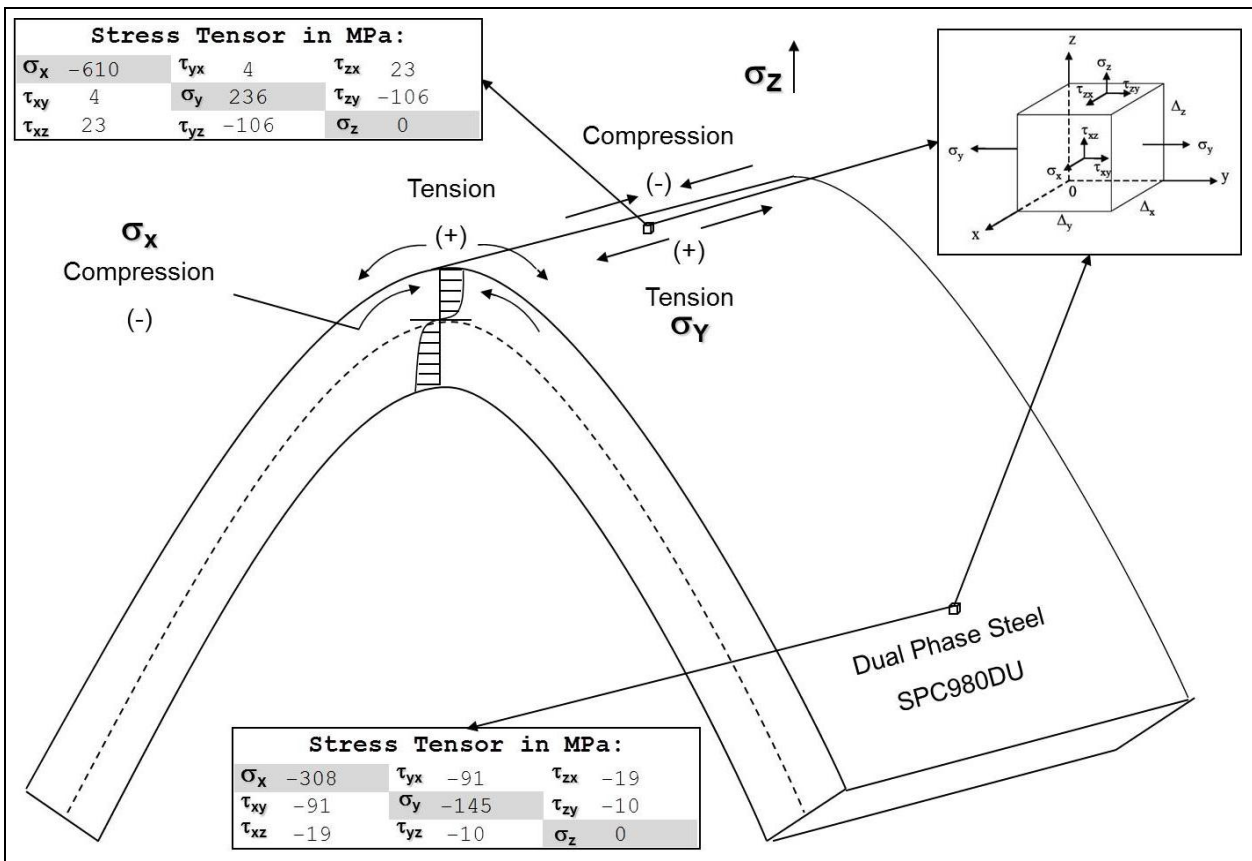


Figure 3.26 Stress tensor directions and values for the bent surface and the dull material

### 3.4 Electrochemical Corrosion Measurements

Electrochemical Corrosion Measurements using the cell apparatus previously explained in detail is quite essential by means of revealing information regarding the corrosion behaviour of the samples that subject to various testing under different parameters. As for the relevance of the method to this investigation, the necessity to underline the fact that micro cracks on the surface may or may not be related to deeper micro cracks that most of the time have a direct effect on crack initiation and propagation that occur on the surface.

Corrosion resistance of a metal piece, taking into consideration that the test is sensitive in a way that would distinguish well enough the characteristic properties and how they may be affected by different bending conditions, is an important part to conclude our investigation.

A simple sketch on the process is shown in Figure 3.27. The procedure was explained beforehand, together with the electrochemical theory that lies beneath.

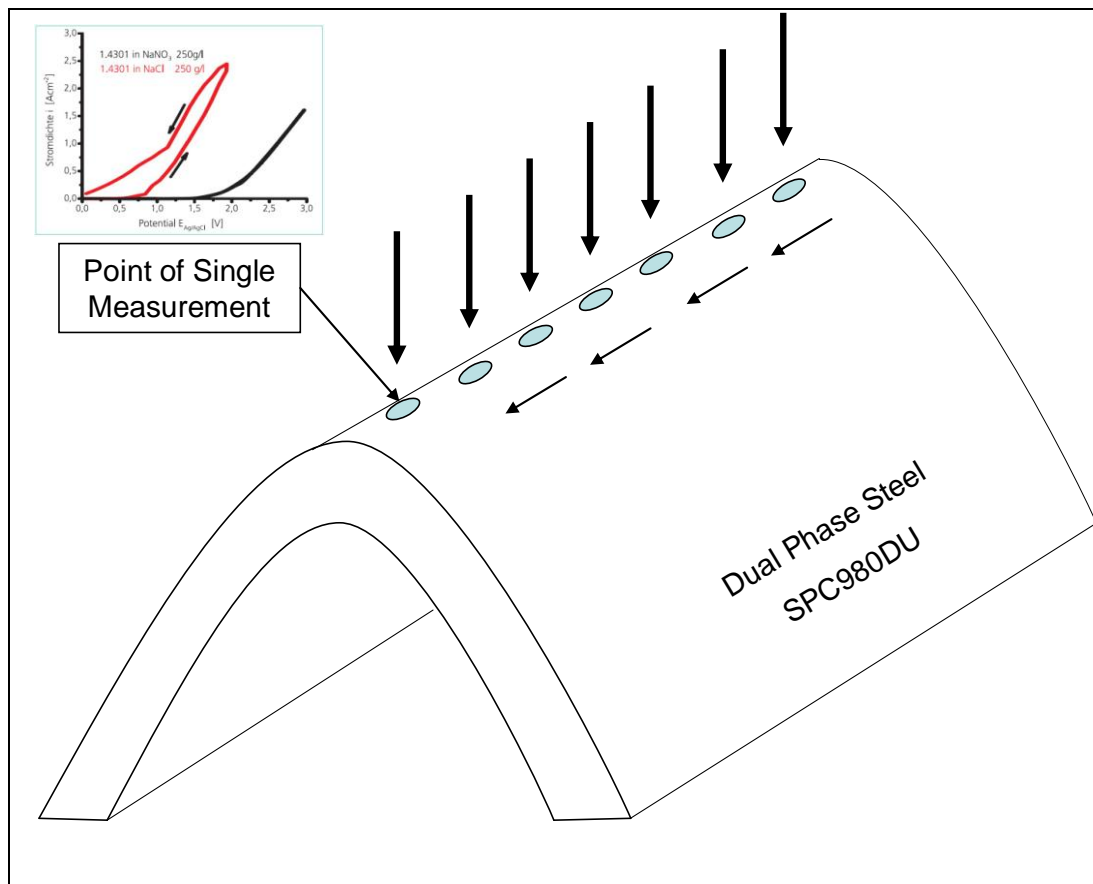


**Figure 3.27** Materialwise experimental set up for electrochemical corrosion measurements



## Chapter 4 Results

Summarizing the results obtained in the previous section, the most important trend that has to be underlined is the crack behaviour of CR 980 DP depending on the bend speed and bend radius.

Investigations clearly reveal out that, as bending speed increases, crack resistance also increases. This assumption is valid for all bend radii and same trend continues for all 3 sample categories in terms of material preparation (standard, burr upside down and grinded). If we are to enumerate crack behaviours of such categories under same parameters, we would come up a result as follows;

$$CR_{standard} < CR_{burrupside\ down} < CR_{grinded} \quad \mathbf{19}$$

In equation **19** *CR* indicates the crack resistance of CR 980 DP. Looking at the behaviours demonstrated by the samples under different bend radii, a similar trend of the above sort is observed for all 3 sample categories. As bend radius decreases, SPC 980 gets more vulnerable to crack initiation and propagation. The crack resistance enumeration between sample categories is the same as eq. **19**.

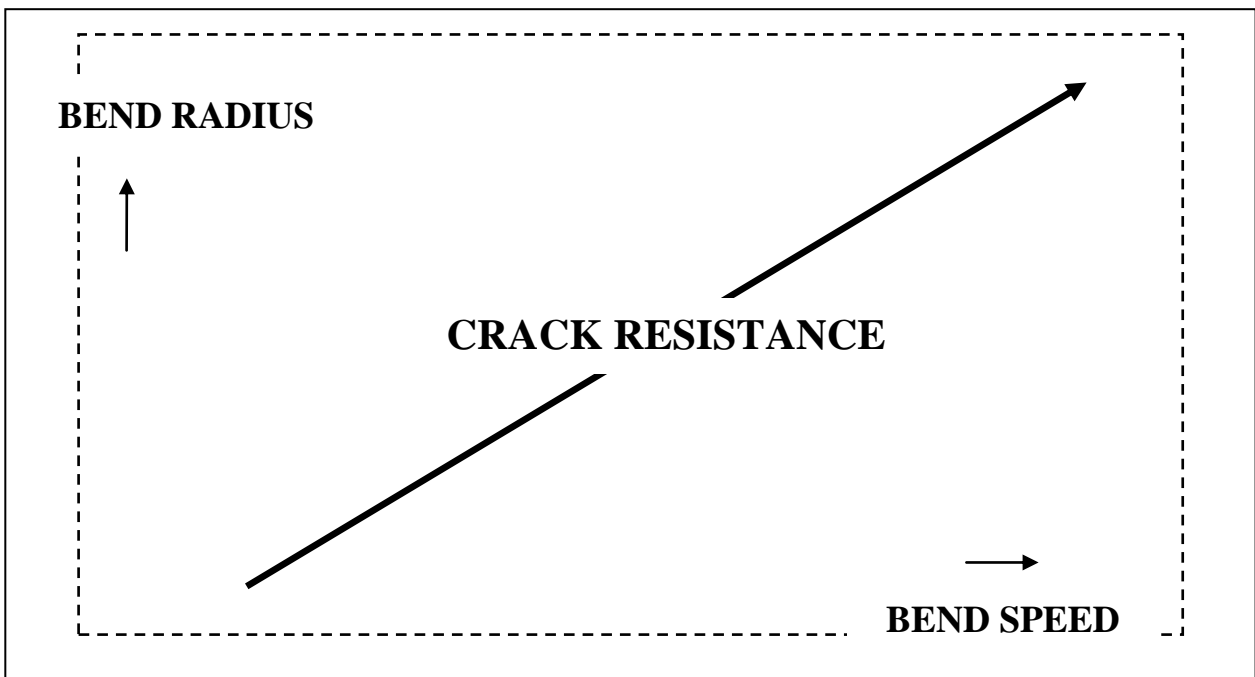


**Figure 4.1 Crack resistance trend**

Figure 4.1 shows the general trend of crack evaluation under different bend speeds and radii.

The cracking phenomena on the edge portion of the bent surface is observed not to have a direct effect on the crack evaluation trend along the bent surface, whereas, such a statement can only be made for sure after evaluating the microscopic nature of CR 980 DP, more accurately, performing residual stress measurements which are not thoroughly held for reasons explained within the relevant section. Further explanation regarding this issue will be handled in the future work and suggestions.

On a macroscopic level, the edge portion crack occurrence is shown in Figure 4.2.

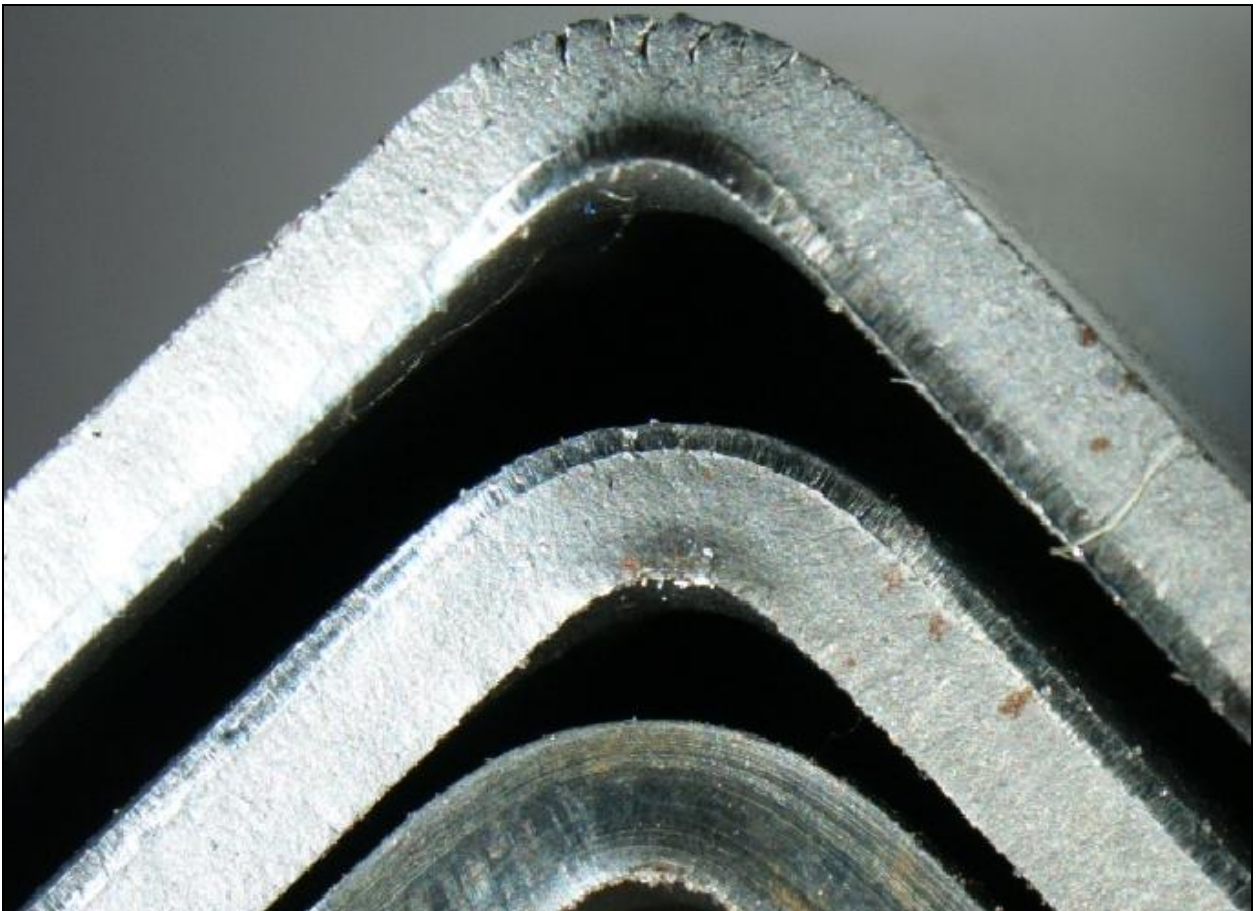


**Figure 4.2 Crack evaluation comparisons on the edge portion of bent samples. Bend speed 15 mm/min; Bend radius 1.5 mm (From top to bottom: Burr upside down, Standard sample, Grinded sample)**

Looking at Figure 4.2, it is clearly seen that, upside down sample has wider and deeper crack occurrence on the edge portion whereas the standard sample has minor cracks. Grinded samples do not demonstrate any sign of macro cracks, even under magnification. Visually, such cracks don't seem to be affecting the crack behaviour along the bent surface. Whether they take a part in determining the crack resistance of CR 980 DP, is yet to be determined once the residual stress data is obtained. Still, looking at the data acquired previously, since non-standard samples demonstrate better results by means of crack resistance, it may be suggested that they don't have an obvious negative effect on the outcomes.

Microscope images of samples bent under different speeds don't reveal much information in the sense that the internal changes occurring within the material itself should be looked for by analysis of micro phenomena like residual stresses rather than concentrating on the geometrical deformations of phases. In some cases, grouping of one or both of the phases would be an issue that indicates certain changes occurring in the microstructure. If, for instance, variations under different temperatures were to be analysed, such findings would more likely be obvious. In our case, since we have dealt with constant atmospheric conditions, phases don't seem to be verifying from bend speed to bend speed and, therefore, coming up with a concrete conclusion is not most probable.

Hardness values concerning samples bent under various speeds are consistent and clearly agree with the expected behaviour along the tension / compression zones but they are yet insufficient to suggest a clear distinction between varying parameters and material's dependency on them. Together with the load curves that has been analysed, information gathered regarding the crack behaviour under different bending speeds doesn't come handy. Still, there is one question existing about the consistency of the results. Due to the necessity to prepare the sample to run the relevant test, the real hardness values may be slightly affected by the change in residual stresses and the work hardening phenomena occurring during the cutting and following processes. This is an issue that has to be taken into consideration meaning that the values may not reflect the actual true hardness of the sample. However, since all the samples that are subject to hardness testing undergo the same steps by means of sample preparation, a comparison of the sort that has been recently discussed is still very valid and the relative relationships between the samples remain still.

Residual stress measurements show that the compression component turns out to be relatively high for the sample bent under the base parameters set at the beginning of this study (100 mm X 35 mm, R = 2.0, Bend speed = 15 mm/min).

In multiphase materials such as CR 980 DP, it is necessary to record the stresses in both phases of the material or at least make sure that the results provide a complete representation of the stress state within the material. In our case, it is quite unlikely to ensure such conditions due to geometrical complications. Therefore, results obtained are judged considering the fact that they represent an average of ferritic and martensitic phases. Since we aren't directly interested in the exact state of the sample but more like an opportunity to compare the behaviours under various conditions, we are still able to come up with consistent conclusions assuming to have overcome technical restrictions mentioned here and there.

Comparing the compression stress ( $-\sigma_x$ ) of the bent surface and the dull material, it is understood that bending process under relevant conditions introduces an additional internal stress of around 300 MPa to the material. When necking<sup>7</sup> starts to occur internal stresses that had been previously introduced is one of the factors that determines if the surface is vulnerable to crack initiation and propagation. Removing or at least minimising the negative effect of the source of additional internal stresses would decrease the possibility of having a breakdown as a result of hindered crack resistance. Macro crack evaluation had shown that bend radius and bend speed is proportional with the crack resistance of the material. Therefore, it may be suggested that increasing the speed and radius results in less additional stress within the possession of CR 980 DP. Repeating the residual stress measurements in this sense would prove this theory to be true, assuming that this educated guess is accurate. It would be a very important finding to be able to demonstrate the precision of such a judgement.

---

<sup>7</sup> Necking, in engineering or materials science, is a mode of tensile deformation where relatively large amounts of strain localize disproportionately in a small region of the material. The resulting prominent decrease in local cross-sectional area provides the basis for the name "neck". Because the local strains in the neck are large, necking is often closely associated with yielding, a form of plastic deformation associated with ductile materials, often metals or polymers.

## Chapter 5 Conclusion

If we are to concentrate on optimum parameters to run an appropriate and consistent V bend test, in the pursuit of neglecting crack occurrence, it is obvious that the bend speed and bend radius has to be kept as high as possible. Looking at Figure 3.18 and 3.19, it is understood that crack resistance is optimum for relatively high and low sample widths. The problem with using a narrow test piece would be a possible interaction of crack occurrence on the edge portion to that of the middle so small widths should be avoided and the width should be as close as possible to the length of the test piece.

High bend radii and bend speeds, as much as they are more likely to provide crack free surfaces, may be misleading in terms of representing the actual practice during the production process in the plant. Such an issue has to be neglected at this point since it's not possible to make a comparison of any sort between the test conditions and the actual ones.

Frankly, it is understood that keeping the bending speed as high as possible – within the range the press machine allows – would increase the material's crack resistance. When V bend testing is taken into consideration, this value is 400 mm/min, considering the range of the test machine. Likewise, the best results in terms of crack resistance are obtained using the highest bend radius which is 3.5 mm in our case.

Such parameters should be supported by the material dimensions and its preparation methods. The dimensions of the sample should be chosen in a way that the ratio of length and width of the sample is close to 1 and the edges should be grinded before the process.

How accuracy and consistency of these findings can be further improved is discussed in the following section and improvements for current situations - as well as future developments - that are thought to lead the investigation to the next step are proposed.

## Chapter 6 Future Suggestions

Despite the fact that macro findings of this investigation that are previously discussed and concluded have been quite satisfying in terms of leading results, there are some additional steps that might have been taken to enrich the outcomes.

To analyse the outcome of tensile stresses occurring along the surface, especially around the bent zone, tensile test is proposed to be performed under different speeds in order to catch a similar trend to that of the bending phenomenon occurring during v bend testing. The method doesn't fully satisfy the need to observe tension variations. Yet, it is the most promising method that is likely to have a similar trend in terms of crack behaviour comparison. Such a method wouldn't reveal much information on the behaviours demonstrated under different bend radii or varying sample dimensions and the finding would mainly concern the speed related changes. The problem lies beneath the application method and the instruments that need to be used to perform such test.

Previous studies regarding strain rates are referred in Toyota internal reports but the test were performed in external facilities and servo hydraulic high speed tensile testing machine is used to observe the dynamics. In that sense the technical capabilities of the instruments currently present don't allow a thorough investigation of this sort.

Evaluating the data obtained in hardness tests, it was possible to observe tension & compression zones and the neutral axis, schematically. Still, it was not possible to come up with some results that would enable us to suggest a comparison between the series. It is basically a matter of measurement sensitivity and microhardness (UMH) measurements performed following the same steps could be able to provide us with more promising results in that sense.

Previous studies on the internal stresses of dual phase steels have been found to be limited and, therefore, they were unable to be leading by means of proposing an appropriate investigation development and progress. The phenomenon, in theory, is able to reveal crucial information regarding the behaviours of dual phase steels under different bend speeds and radii. When bending radius is taken into consideration, it is possible, up to some extent, to come up with a conclusion analysing the data obtained throughout the relevant section of this study. Combining

our technical knowledge with initial residual stress measurements ensures a comparison for varying bend radii and the crack behaviour demonstrated, whereas, bending speed is yet an area rather mysterious when the internal stresses for single cases are in question.

To carry this investigation to a further step, one promising path to take would be to repeat the residual stress measurements performed for samples that are subject to different bending speeds. The difficulty of such a procedure is the high possibility of not being able to perform accurate and consistent measurements. The geometrical restrictions that are brought to attention and the time consuming nature of such measurements bring along the necessity to develop a testing method to come up with accurate and precise findings. Assuming that this is achieved, measurements should be repeated for test pieces bent under different parameters and the results should be evaluated in terms of compression and tension phenomena, as well as the positioning issues that point out the crack behaviour along the bending axis, on the surface.

In case residual stress measurements are not sufficient to reveal leading information on the outcome of further study, investigations may be focused on grain hardness measurements and hardness comparison of single ferritic and martensitic grains within the material as well as between materials bent under different conditions could be performed in order to have a better understanding on the dynamics driving the optimization phenomenon (ultramicrohardness).

Electrochemical corrosion measurements using the cell described in chapter 2 aren't done due to time restrictions. Such an analysis, as briefly mentioned in chapters 2 and 3, is capable of revealing leading information regarding the corrosion behaviours and active / passive zones of CR 980 DP. Materials bent under different parameters may be expected to demonstrate different crack behaviours and therefore their vulnerability to future complications such as corrosion would vary. Electrochemical corrosion tests are suggested to be performed to have better understanding of the concept and how the material faces with the phenomenon under different circumstances.

## References

- 1996 The IRON and STEEL INSTITUTE of JAPAN, "Cold Rolled Steel Sheets – Technology and Products in Japan", ISBN 4-930980-08-9 C3057, Tokyo, (Original Publication in Japanese Version) May 15, 1996.
- 1996 PREVEY P. S., "Current Applications of X-Ray Diffraction Residual Stress Measurement", Lambda Technologies, Ohio, 1996.
- 1997 LUNDTH H., BUSTAD P., CARLSSON B., ENGBERG G., GUSTAFSSON L., LINDGREN R., "Sheet Steel Forming Handbook", SSAB Tunntat AB, Borlange, October 1997
- 1997 GURAL A., ERDOGAN M., SEKER U., KORKUT I, "Cift Fazli Celiklerde Martensit Hacim Oranina Bagli Olarak Kesici Ucta Asinma ve Sivanma (Bue) Olusumu Egiliminin Kesme Kuvvetleri ve Yuzey Puruzlulugu Uzerine Etkisi", Gazi Universitesi Teknik Egitim Fakultesi, Zonguldak Karaelmas Universitesi Karabuk Teknik Egitim Fakultesi Makina Egitim Bolumu, Ankara, Karabuk, 1997.
- 2001 SCHAFER H., "Electrochemical Corrosion Analysis", Fraunhofer Institute for Manufacturing Technology and Applied Materials Research, Bremen, 2001.
- 2003 DEGARMO E. P., BLACK J. T., KOHSER R. A., "Materials and Processes in Manufacturing (9<sup>th</sup> ed.)", Wiley, ISBN 0-471-65653-4, 2003.
- 2003 CALLISTER W. D., Jr., "Material Science and Engineering: An Introduction (6<sup>th</sup> ed.)", John Wiley & Sons, Inc., New York, 2003.
- 2004 LOHRENGEL M.M., ROSENKRANZ C., KLUPPEL I., MOEHRING A., BETTERMANN H., VAN DEN BOSSCHE B., DECONINCK J., "A new microcell or microreactor for material investigations at large current densities", *Electrochimica Acta* 49 (2004) 2863-2870, Dusseldorf, Brussels, 2004.



- 2004 ASTAKHOV V. P., SHVETS S., “The Assessment of Plastic Deformation in Metal Cutting”, Journal of Materials Processing Technology 146 (2004) 193-202, 2004.
- 2004 CETINEL H., “Formability of Dual Phase Steel Sheets”, DEU Muhendislik Fakultesi Fen ve Muhendislik Dergisi Cilt: 6 Sayi: 2 s. 73-80, Izmir, 2004.
- 2005 FITZPATRICK M. E., FRY A. T., HOLDWAY P., KANDIL F. A., SHACKLETON J., SUOMINEN L., “Determination of Residual Stresses by X-ray Diffraction – Issue 2”, National Physics Laboratory, Middlesex, September 2005.
- 2005 BIRBILIS N., Padgett B.N., Buchheit R.G., “Limitations in microelectrochemical capillary cell testing and transformation of electrochemical transients for acquisition of microcell impedance data”, The Ohio State University, Ohio, 2005.
- 2005 UNITED STATES STEEL CORPORATION (USS), “DUAL-TEN® Steel”, [http://xnet3.uss.com/auto/tech/grades/dual\\_ten.htm](http://xnet3.uss.com/auto/tech/grades/dual_ten.htm), 2005.
- 2006 TSIPOURIDIS P., “Mechanical Properties of Dual Phase Steels”, Technischen Universitat Munchen, Munich, 2006.
- 2006 HAYASHI N., “Line spec for Press Dies”, TMMF Stamping Production Engineering Division, France, 2006.
- 2006 SMITH W. F., HASHEMI J., “Foundations of Material Science and Engineering (4<sup>th</sup> ed.)”, McGraw-Hill, ISBN 0-07-295358-6, 2006.
- 2006 KABAKCI F., “Cift Fazli Celiklerde Mikroyapinin Mekanik Ozelliklere Etkisi”, Zonguldak Karaelmas Universitesi Fen Bilimleri Enstitusu Metal Egitimi Anabilim Dalı, Karabuk, 2006.

- 2008 BANDIVADEKAR A., BODEK K., CHEAH L., EVANS C., GROODE T., HEYWOOD J., KASSERIS H., KROMER M., WEISS M., “On the Road in 2035: Reducing Transportation’s Petroleum Consumption and GHG Emissions”, MIT Laboratory for Energy and the Environment Report No. LFEE 2008-05 RP, Cambridge, Massachusetts, July 2008
- 2010 ArcelorMittal, “Dual Phase Steels”, <http://www.arcelormittal.com>, Last update October 1, 2010.
- 2010 DILLIEN S., “Bridging the Physics-Engineering Gap in Dual Phase Steel Formability”, Katholieke Universiteit Leuven Faculteit Ingenieurswetenschappen Departement Metaalkunde en Toegepaste Materiaalkunde (MIM), Leuven, 2010.
- 2010 METALLIC and INORGANIC MATERIALS DEPARTMENT, “Re:Standardisation of quality requirements and inspection operation for sheet materials (new-SPC980DU and SCGA980DU)”, Toyota Motor Europe NV/SA, Brussels, 2010.
- 2011 GAMRY Instruments, “Getting Started with Electrochemical Corrosion Measurements”, <http://www.gamry.com/assets/Application-Notes/Getting-Started-with-Electrochemical-Corrosion-Measurement.pdf>., Retrieval date September 8, 2011.
- 2011 Corrosion-club.com, “Electrochemical Corrosion Theory”, <http://www.corrosion-club.com/basictheory.htm>, Retrieval date September 23, 2011.
- 2011 MICHAELIS A., “Local electrochemistry with fast exchange of electrolytes – the micro electrochemical flow cell with  $\Theta$  capillary”, Fraunhofer Institute for Ceramic Technologies and Systems, Dresden, retrieval date September 2011.
- 2011 TANAHASHI K., ARMAN E. O., TUNA U., “V-Bend TESTER (INSTRON) USER MANUAL, Toyota Motor Europe NV/SA”, Brussels, 2011.
- 2011 AUTOLAB INSTRUMENTS, “Autolab Application Note 11”, Metrohm Autolab B.V., [www.metrohm-autolab.com](http://www.metrohm-autolab.com), Retrieval date 2011.

- 2011 AUTOLAB INSTRUMENTS, "Autolab Application Note 16", Metrohm Autolab B.V., [www.metrohm-autolab.com](http://www.metrohm-autolab.com), Retrieval date 2011.
- 2011 AUTOLAB INSTRUMENTS, "Autolab Application Note 17", Metrohm Autolab B.V., [www.metrohm-autolab.com](http://www.metrohm-autolab.com), Retrieval date 2011.
- 2011 WORLDAUTOSTEEL, "Dual Phase (DP) Steels", <http://www.worldautosteel.org/SteelBasics/Steel-Types/Dual-Phase.aspx>, Retrieval date 2011.